NOAA Grant NA90RAH00077, NA37J0202

National Oceanic and Atmospheric Administration

CONVECTION IN TOGA COARE: HORIZONTAL SCALE, MORPHOLOGY, AND RAINFALL PRODUCTION

by Thomas M. Rickenbach

Steven A. Rutledge, P.I.

Colorado State University

DEPARTMENT OF ATMOSPHERIC SCIENCE

PAPER NO. **630**

CONVECTION IN TOGA COARE: HORIZONTAL SCALE, MORPHOLOGY, AND RAINFALL PRODUCTION

by

Thomas M. Rickenbach

Department of Atmospheric Science

Colorado State University

Fort Collins, CO 80523-1371

Research Supported by

National Oceanic and Atmospheric Administration

under Grant NA90RAH00077 and NA37J0202

November 1996

Atmospheric Science Paper No. 630

ABSTRACT

CONVECTION IN TOGA COARE: HORIZONTAL SCALE, MORPHOLOGY, AND RAINFALL PRODUCTION

Shipboard radar data collected during the recent Tropical Oceans - Global Atmospheres Coupled Ocean - Atmosphere Response Experiment (TOGA COARE) provided an unprecedented view of convection in the western Pacific warm pool, a region of global climatological significance. Previous studies have shown that the vertical transport of heat and momentum by convection differs with the scale and organization of precipitating systems. The relative importance of these transports by mesoscale convective systems (MCS) versus smaller groups of convective clouds over the tropical oceans is not well understood. The goal of this study is to understand the variability of warm pool rainfall production in terms of the horizontal scale and morphology of convective systems. This variability is examined in the context of the kinematic and thermodynamic state of the environment. Furthermore, high frequency convective variability (1-5 days) is studied in detail.

It is found that although most of the rainfall is associated with MCS scale systems, unorganized isolated convection was most common and produces a significant fraction of the total rainfall. Although MCS scale heating dominated the COARE mean, distinct

sub-MCS scale events heating occurred more frequently. Environmental moisture profiles distinguished between modes of convective organization more clearly than wind profiles. Furthermore, the weak diurnal variation of rainfall was found to result from the superposition of stronger, distinct diurnal rainfall variability associated with each mode of organization. These results are important to the refinement of convective parameterizations in global climate models.

Thomas M. Rickenbach
Department of Atmospheric Science
Colorado State University
Fort Collins, CO 80523
Fall 1996

ACKNOWLEDGEMENTS

I would like to express my sincere appreciation to my advisor, Prof. Steven A. Rutledge, for his consistent guidance and advice throughout the course of this research, and for the opportunity to take part in field programs in northern Australia (Down Under Doppler and Electrification Experiment) and the western Pacific warm pool region (Tropical Ocean-Global Atmosphere Coupled Ocean-Atmosphere Response Experiment). Further thanks goes to my graduate committee members, Profs. Richard Johnson, Wayne Schubert, and Viswanathan Bringi for valuable advice and criticism. Paul Hein and Doug Burks are acknowledged for their indispensable computing guidance. Discussions with Charlotte Demott, Rob Cifelli, and Walt Petersen were instrumental in focusing many aspects of this work. I would further like to acknowledge innumerable discussions with many scientists at the International TOGA COARE Data Workshop in Toulouse, France (1994) which helped to define the direction of this research. Finally, I want to express my thanks to my parents, brothers and sisters without whom I would not be writing these words, and to my wife Rosana Nieto Ferreira for her unwavering support and love. This research was funded by the National Oceanic and Atmospheric Administration Grant NA90RAH00077 and Grant NA37RJ0202.

TABLE OF CONTENTS

CHAPTER 1

INTRODUCTION

Precipitating cumulus convection in the tropics is manifested over a large span of spatial scales. Individual convective cells occur on the micro-α scale (several hundred meters to a few kilometers; Orlanski 1975), while the merged anvils of mesoscale regions of precipitation can form meso-α scale super cloud clusters several thousand kilometers in length (Nakazawa 1988). On the meso-β scale (20 km - 200 km), a common mode of convective organization is the mesoscale convective system (MCS). An MCS is defined as a group of thunderstorms with a contiguous precipitation area of at least 100 km (this length scale is herein referred to as *MCS scale*), often with an extensive precipitating anvil cloud which can reach several hundred kilometers in horizontal extent (Cotton and Anthes 1991, Houze 1993). MCSs have been shown to contain both regions of convective cells which produce heavy rainfall, and stratiform precipitation where local rainfall rates are typically much less. These regions are linked dynamically and microphysically through momentum and condensate transport by mesoscale flow features and energy transport by gravity waves (Leary and Houze 1979, Zipser et al. 1981, LeMone 1983, Churchill and Houze 1984, Rutledge and Houze 1987, Schmidt and

Cotton 1989, Biggerstaff and Houze 1991).

Previous studies of convection on the meso-β scale have focused on the importance of the scale and morphology of convective organization to the vertical transports of moist static energy and momentum, and the subsequent modification of the environment within which the convection occurs. Riehl and Malkus (1958) hypothesized that vertical energy transport occurs on the scale of the convective cell, in the undilute cores of convective "hot towers". More recently, Houze (1982) suggested that the effect of convection on large scale circulations may be viewed with the mesoscale convective system (MCS) as the fundamental unit of vertical energy transport. For convective organization with a contiguous precipitation area less than 100 km (herein referred to as *sub-MCS scale*), these transports are controlled more by randomly colliding dry, cool outflow boundaries near the surface than by mesoscale flow features. These gust fronts are initiated by downdrafts associated with individual convective cells, resulting in a downgradient momentum flux for the cumulus population as a whole (LeMone et al. 1984).

Although transports associated with MCS scale convective organization are also controlled by downdrafts, the magnitude and spatial scale of these drafts (and the resulting transports) differ greatly between convective and non-convective[1] components of the system (Zipser 1977, Houze 1989). LeMone (1983) concluded that the momentum flux in a tropical squall line system was initiated in the convective region at the leading edge of the line, with little contribution from the trailing stratiform region. Furthermore, momentum flux in MCS scale squall lines may be either upgradient or downgradient

[1] The terms "non-convective" and "stratiform" are synonymous at this point. These terms will be defined precisely in Chapter 2, Section 4.

(LeMone et al. 1984). Similarly, the vertical distribution of heating is distinct for the convective and non-convective components of an MCS. Heating in the convective region is strongest at lower levels, while upper level heating and lower level cooling characterizes the anvil region (Houze 1982, Johnson 1984). Moreover, the horizontal scale over which MCS heating is distributed occurs on the scale of the local Rossby radius of deformation, a meso-α length scale in near-equatorial regions (Cotton et al. 1989, Mapes 1993). Hartmann et al. (1984) showed from a numerical simulation that the heating profile associated with a "mature cloud cluster" (Houze 1982) produced a more realistic Walker circulation compared to the circulation produced with a convective cell heating profile. That result suggests that the effects of MCS heating on large scale circulations may dominate over heating from individual convective towers in producing the net tropospheric heating in the tropics. Yet, the relative importance of heating from both sub-MCS scale and MCS scale systems has not been quantified.

In terms of morphology, the organization of convection into lines (on both the sub-MCS scale and the MCS scale) determines the nature of the vertical momentum transports. The system relative ascending front to rear and descending rear to front flow features associated with many organized squall lines tend to increase line-rearward momentum at upper levels and increase line-forward momentum at low levels (LeMone et al. 1984). Convection without linear organization does not show consistent momentum transport properties (ibid.).

The recent Tropical Oceans - Global Atmospheres Coupled Ocean - Atmosphere Response Experiment (TOGA COARE; Webster and Lukas 1992) resulted in an

unprecedented multiscale view of tropical oceanic convection. The shipboard radar component of COARE provided a nearly continuous three month Eulerian meso-β scale sample of the precipitation structure of tropical oceanic convection. *The aim of this study is to examine convective organization and rainfall in the context of the scale (sub-MCS vs. MCS scale) and morphology (linear vs. non-linear organization) of contiguous precipitation features.* First, the notion of what defines a "convective event" in this study is developed. The frequency of occurrence, rainfall production, and vertical depth of convection is then diagnosed within this context. The occurrence and rainfall production of convection organized on the sub-MCS scale has not been previously compared to that of MCS scale systems. Furthermore, the thermodynamic and kinematic state of the local and synoptic scale environment is studied for each mode of scale and morphology. Fundamentally contrasting environmental regimes were observed during COARE, modulated on the time scale of the experiment (1 - 2 months) by the tropical intraseasonal oscillation. The heating and moistening composite profiles associated with each mode of organization is also discussed.

Based on these results, extensive analyses of higher frequency (of order 1 - 5 days) variability of convection are given. First, a detailed study of the diurnal variation of rainfall from each organizational mode is presented. By isolating the diurnal rainfall signal by the scale and organization of convection, valuable insight is gained not only to the mechanisms which produce the net diurnal rainfall variation, but also to the evolution of individual convective events. Next, rainfall variability associated with westward propagating equatorial wind oscillations (4 - 5 day period) is discussed.

Results from this dissertation may ultimately aid in the refinement of cumulus parameterizations of the interaction of the synoptic scale environment with unresolved convection in large scale models.

CHAPTER 2

DATA AND METHODOLOGY

This chapter first provides a description of the radar reflectivity and sounding data used in this study. Next, a background of previous studies of convective organization is given, leading to a development of the basis of the present partition of convective organization. This is followed by a discussion of the importance of isolating convective from stratiform[1] reflectivity regions, along with the procedure to accomplish this. This forms the basis for a quantitative estimation of rainfall rate.

2.1 Data platforms

Radar reflectivity data were collected with the Massachusetts Institute of Technology (MIT) C-band Doppler radar, deployed aboard the R/V Vickers (Rutledge et al. 1993). The radar operated during three cruises of the Vickers, between November 1992 and February 1993, as part of the COARE intensive observation period (IOP). For each cruise, the ship maintained a nearly fixed position at approximately 2° S, 156° E for

[1] A precise definition of stratiform rain is discussed in Section 2.4. Since the technique used herein to distinguish between convective and stratiform reflectivity regions identifies convective reflectivities, the term "non-convective" will be introduced in that section to refer to stratiform rain.

nearly thirty days, with a nearly ten day interruption in data collection between cruises. Data was collected nearly continuously while the ship was on station, for a total of about ninety days. The MIT radar data collection periods are summarized in Table 2.1.

Reflectivity volume scans were analyzed at twenty minute intervals for the ninety days of data collection, or just over 6000 volumes. The reflectivity data were interpolated from polar to Cartesian coordinates to a 2 km horizontal, 0.5 km vertical grid[2]. The grid origin was fixed in space at the ship's nominal position to correct the echo locations for ship motion. Only reflectivity data within 120 km of the radar were used for this study, since beam broadening beyond this range smooths convective cell spatial structures in the reflectivity field below acceptable limits. All subsequent analysis was performed at a constant altitude of 2 km MSL[3]. This value was chosen as a compromise between the need to produce rainfall estimates close to the surface and the increase in horizontal reflectivity data coverage with height. The reflectivity values at each gridpoint in the volume were then increased by 2.4 dBZ to account for a correction to the antenna gain, and for a missing bandwidth term in the radar equation.

Radiosonde data during COARE were obtained every six hours from three nested sounding arrays in the Western Pacific warm pool region. These arrays spanned both meso-α (Large Scale Array, Outer Sounding Array; LSA and OSA respectively) and meso-β scales (Intensive Flux Array; IFA), with the R/V Vickers located near the center

---

[2] The REORDER software package developed at the National Center for Atmospheric Research was used for this purpose.

[3] Volume scans during periods of extensive sea clutter were analyzed at a height of 3 km; c.f. Section 2.2.

Table 2.1. Time periods corresponding to each cruise of the R/V Vickers. Radar reflectivity data were collected nearly continuously during each cruise.

Cruise	Time Period
1	10 Nov 92 - 10 Dec 92
2	21 Dec 92 - 19 Jan 93
3	29 Jan 93 - 25 Feb 93

of the array. The location of the sounding array and the MIT radar sampling area is shown in Fig. 2.1. Data used in this study were taken from a six hourly gridded analysis (Lin and Johnson 1996a) and interpolated to a point representative of the nominal location of the R/V Vickers near the center of the IFA (2° S, 156° E; c.f. Fig. 2.1). In this way, the profiles of thermodynamic and kinematic variables used represent a spatially weighted sample of both the near and far field with respect to the radar location. That is, the combined effects of local convection and the meso-α scale environment are included at each sounding grid point (see Chapter 3 Section 3 for a further discussion of this issue).

2.2 Convective organization: background

Many previous studies have classified the convective organization of radar echoes to understand the observed variability in the horizontal precipitation morphology of MCSs. Each of these studies developed distinct classification schemes, designed to study specific hypotheses and reflect recurrent trends in the data. Accordingly, differences in the bases of classification reflected both what the investigator viewed as the important attributes which characterized the range of structural variability, and the system properties under investigation.

In a summary of GARP Atlantic Tropical Experiment (GATE) observational studies, Houze and Betts (1981) characterized convection in the tropical eastern Atlantic Ocean as being associated with squall clusters and non-squall clusters, delineated by differences

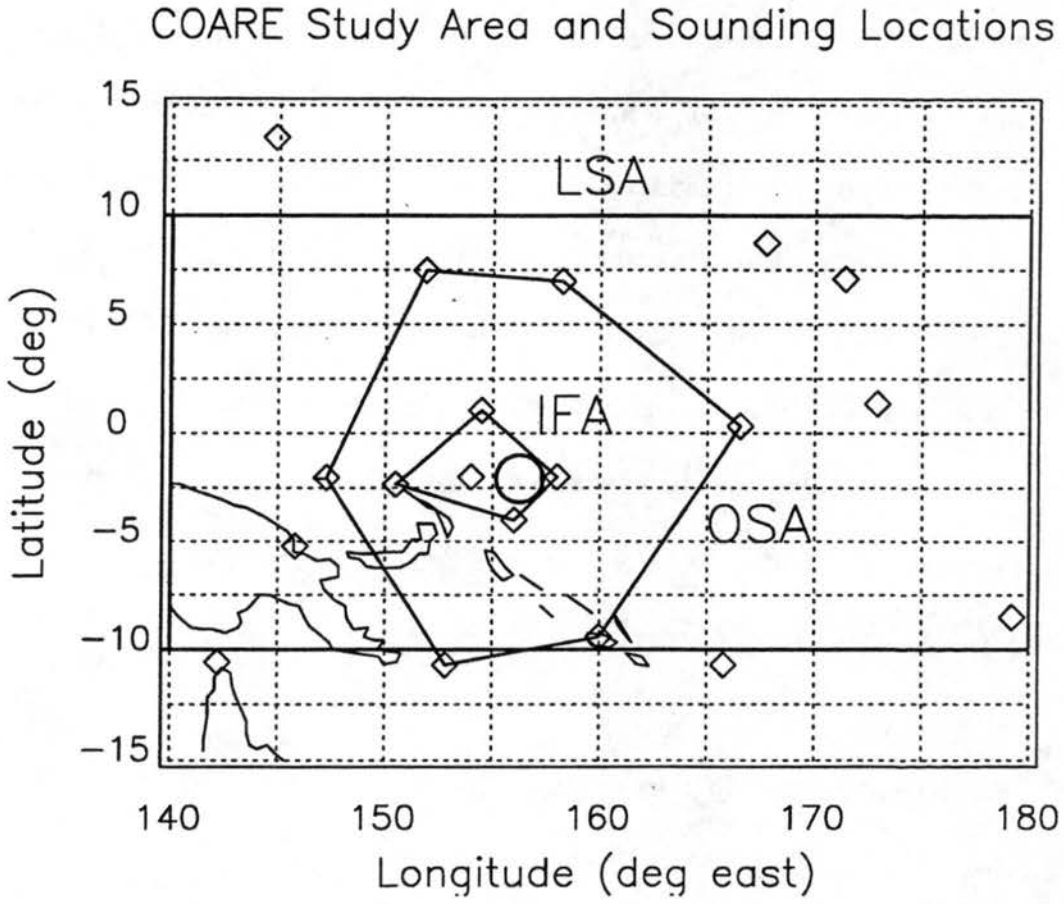

Figure 2.1. Location of the radar study area (circle of 120 km radius) relative to the TOGA COARE Large Scale Array (LSA), Outer Sounding Array (OSA), and the Intensive Flux Array (IFA). Sounding sites are indicated by open diamonds.

in propagation speed and downdraft intensity. These differences were attributed to the strength of the vertical wind shear. Bluestein and Jain (1985) studied the formation of lines of convective cells in the southern plains of the U.S. They developed a four category classification to identify the horizontal patterns of precipitation associated with the formative stage of convective lines, determined from radar reflectivity data. Each category was characterized in terms of the convective available potential energy (CAPE) and vertical wind shear of the formation environment. Using satellite and radar data from the Amazon Boundary Layer Experiment (ABLE) in the Amazon Basin, Greco et al. (1990) adopted a different approach, classifying convection by region of origin relative to significant topography or proximity to coastal areas affected by the land - sea breeze circulation. They discussed differences in morphology and propagation in terms of convective initiation mechanisms specific to each region. Houze et al. (1990) examined the morphological characteristics of the significant rain producing systems during three spring seasons in Oklahoma. They described systems in terms of their degree of conformity to an idealized squall line with a broad region of trailing stratiform rain, as well as to what degree systems contained a spatially symmetric leading convective line and trailing stratiform region. The resulting classification was interpreted in terms of CAPE and vertical wind shear. Keenan and Carbone (1992) used the same CAPE - shear parameter space to study differences in break vs. monsoon convection in the vicinity of Darwin, N.T., Australia. They categorized convective systems based on the dominant flow regime within which each system formed, discussing similarities and differences in oceanic monsoon systems (northwest flow from the ocean) and continental

"break period" systems (southeast flow from the continent). More recently, Loehrer and Johnson (1995) examined the morphology of convective systems in the central plains of the U.S. in the context of the symmetric versus asymmetric structure classification discussed by Houze et al. (1990). They concluded that these two organizational modes were not distinct system types, but represented different stages in the life cycle of a general class of squall line MCSs.

During COARE a broad spectrum of convective organization spatial scale and morphology was observed by shipboard radar. The variety, complexity and persistence of COARE convection presented a challenge to not only account for this diversity, but to interpret it in terms of the limited spatial sample provided by a stationary platform. The spatial scale of the sample area (circular area of radius 120 km) was large enough to observe a significant portion of an MCS, yet small enough not to sample several MCSs at the same time. Moreover, the areal coverage of the radar limited the temporal sample to the time required for systems to propagate across the sample area (typically six to eight hours, hereafter referred to as the *advective timescale*). The goals of this study and the analysis techniques used are intimately tied to these scale considerations.

The two general goals of the present classification were to distinguish between convection which attained the spatial scale of an MCS (> 100 km) from that which did not, and to distinguish between systems which attained linear organization from those which did not. The basic approach to stratifying the ubiquitous convection was to first isolate (in time) rainfall "events" and then to assess the scale and morphology attained by each event, in a meaningful, consistent and objective manner. The first step was to

examine low level maps of radar reflectivity[4]. The ninety day data set was then manually divided into 215 discrete periods (events) within which convection reached a *maximum level of organization* (hereafter abbreviated "MLO"), before either decaying or advecting out of the study area. The MLO was defined as the horizontal reflectivity morphology of the spatially largest contiguous convective echo pattern attained during each event. With the MLO as a basis, each event was categorized by whether or not the MLO attained the minimum spatial scale of an MCS (100 km; c.f. Chapter 1), and by whether or not the MLO displayed linear organization (i.e. convective cells arranged in lines). The assessment of the scale and morphology at the MLO was done manually. The horizontal scale and linear structure at the MLO had to be maintained for at least twenty minutes (time between successive radar scans in the animation) to be considered characteristic of the event. Event duration ranged from several hours to 1.5 days.

The MLO established a simple and objective basis to account for system evolution when characterizing the system's organization. However, care had to be used to interpret the stage of evolution of the observed event. Since the advective timescale of reflectivity features across the radar sample area (6-8 hours) was often smaller than lifetimes of many MCS scale systems (e.g. McAnelly and Cotton 1989), the full lifecycles of such systems could not always be observed. In addition, the spatial scale of the sample area was less than the scale of many previously studied MCSs (ibid.). On the other hand, sub-MCS scale system evolution timescales (minutes to hours) were well within the advective timescale, and the sub-MCS scale spatial dimensions were smaller than the sample area.

---

[4] This was accomplished by animation of a time series of low level reflectivity images on a workstation.

With this in mind, the MLO was assumed to coincide with an approximate measure of the system's mature stage. In so doing, the characterization of an event's morphology was not influenced by an *a priori* or subjective notion of what the reflectivity patterns at event maturity should look like. For example, the mature stage of a commonly studied type of MCS (squall line with associated stratiform rain) has been defined by Leary and Houze (1979) as the stage of the system's life cycle at which extensive stratiform precipitation appears to the rear of the leading convective region. Yet, applying this definition to a diverse sample of convection would bias the characterization of that sample. That is, a stratification scheme must have the capacity to consider a field of isolated convective cells as a mature convective event as well as a squall line with trailing stratiform rain.

2.3 Event classification

Two general categories were defined based on the spatial scale of the contiguous convective echo pattern at the MLO. Events with an MLO spatial scale < 100 km were termed *sub-MCS scale* events, while those with an MLO spatial scale of $\geq$ 100 km were denoted as *MCS scale* events. The spatial scale of 100 km refers to the MCS definition (Houze, 1993) given in Chapter 1. Within these categories, events were further separated as to whether or not the convective echo pattern at the MLO displayed linear organization, as discussed below. The resulting four category classification scheme is summarized in Table 2.2, and discussed in detail below.

Table 2.2. Summary of the definition of each event type at the maximum level of organization (MLO): Sub-MCS scale non-linear, sub-MCS scale linear, MCS scale non-linear, and MCS scale linear.

Category	Description
Sub-MCS scale non-linear	*No linear organization, < 100 km in scale.* Population of isolated convective cells.
Sub-MCS scale linear	*Linear organization, < 100 km in scale.* Lines of convective cells, often in groups.
MCS scale non-linear	*No linear organization, $\geq$ 100 km in scale.* Contiguous group of convective cells, embedded in non-convective rain.
MCS scale linear	*Linear organization, $\geq$ 100 km in scale.* Line of convective cells with associated non-convective rain.

Sub-MCS scale events which did not display linear organization at the MLO were termed *sub-MCS non-linear events*. Typically, a group of isolated convective cells either formed within the radar sample area or was advected into the sample area, following the decay or advection of the previous event. At times, individual cells merged, forming small conglomerates of individual cells which were generally 10 km - 50 km in scale. These merged groups of cells characterize the MLO in this category. Although events containing groups of contiguous cells of up to 100 km in horizontal dimension were included in this category, contiguous convection of spatial scale greater than about 50 km was uncommon on the sub-MCS scale. Thus, organization of this scale and morphology may be characterized by a field of isolated convective cells or small groups of cells. An example of a sub-MCS scale non-linear event is shown in Fig. 2.2. This figure shows hourly maps of radar reflectivity over four hours of an event in early December 1992, encompassing the time of the MLO for that event.

A sub-MCS scale non-linear event was defined as having ended when one of two scenarios occur. The most common ending scenario occurred when convection of another organizational mode (sub-MCS scale linear or an MCS scale system) was advected into or formed within the sample area. The spatial scale of the encroaching system had to be larger than the scale of the largest contiguous convective echo feature[5] of the first event for that event to be terminated. The event was furthermore defined to end if the convection decayed or moved out of the sample area.

---

[5] Refer to Sec. 2.5 for a discussion of contiguous convective echo.

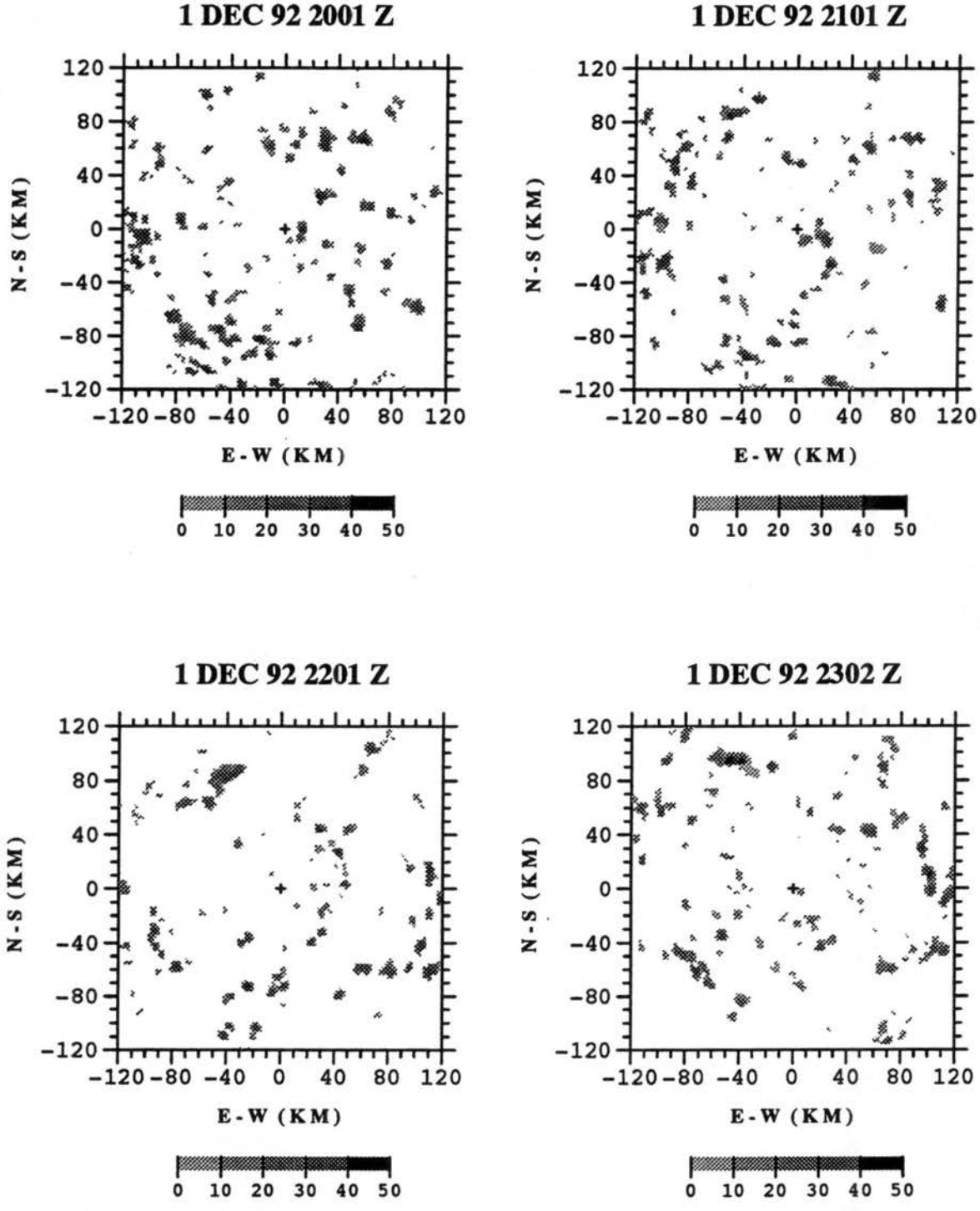

Figure 2.2. Hourly maps of radar reflectivity (units of dBZ) at a height of 2 km for a sub-MCS scale non-linear event on 1 December 1992. The time period shown encompasses the maximum level of organization (MLO) for this event.

Sub-MCS scale systems which had linear structure at the MLO were called *sub-MCS scale linear events*. By definition, sub-MCS scale linear events were limited to between 50 km and 100 km in maximum length. The lower length scale limit of 50 km was used by Bluestein and Jain (1987) as the smallest length scale of a convective line. These events began when a sub-MCS scale linear event either formed within the sample area or was advected into the area, provided that the line did not then evolve into a system of MCS scale while within the radar's view. Sub-MCS scale linear systems generally consisted of the convective cells which formed the line with little attendant stratiform precipitation, though the presence of stratiform echo was not tied to the definition of a sub-MCS scale linear (or any other) event. More than one sub-MCS scale line may appear within a particular event, with two or more lines often coexisting within the sample area (an example is given in Fig. 2.3). The event was defined as having ended when either a system of MCS scale or an sub-MCS scale non-linear convective feature spatially larger than the sub-MCS scale linear event was advected into or formed within the sample area, even if the sub-MCS scale linear event was still present. Also, if the sub-MCS scale linear event decayed or moved out of the study area, the event was ended.

MCS scale events which contained no linear organization of convective features at the MLO were termed *MCS scale non-linear events*. These events were characterized by a large convective region comprised of convective cells, appearing in a random, clustered pattern. These events generally formed from the merger of isolated cells and groups of cells, which connected to form a single broad convective region. The convective region was generally embedded in stratiform precipitation, which formed and expanded where

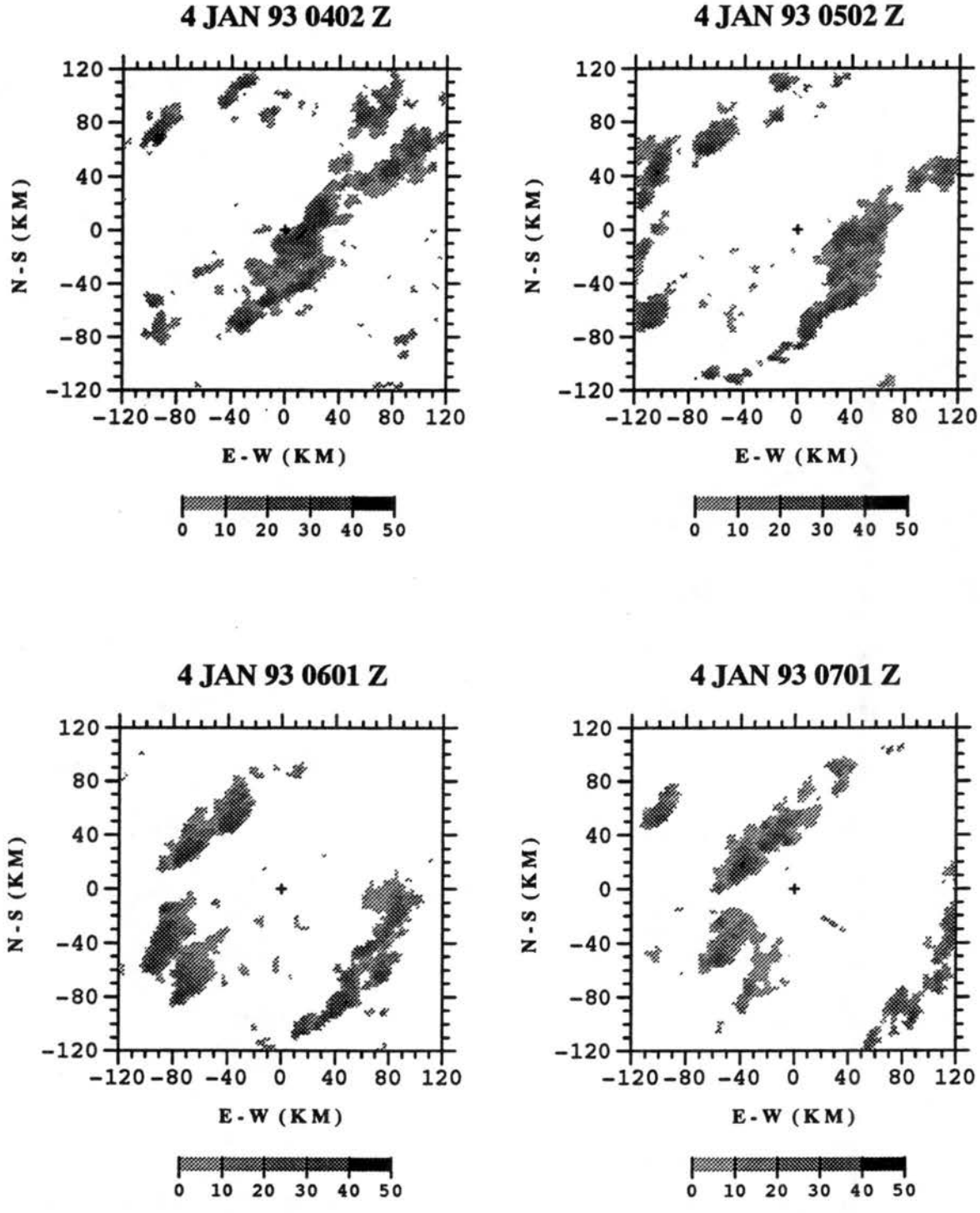

Figure 2.3. As in Figure 2.2, but for a sub-MCS scale linear event on 4 January 1993.

previously collocated convective cells had collapsed and decayed (an example is presented in Fig. 2.4). The stratiform rain region persisted following the decay of the convective cells and slowly dissipated with time. An MCS scale non-linear event was defined to end when the convective region and the associated stratiform rain either decayed or moved out of the sample area. The advection of another MCS scale system into the sample area marked the end of the MCS scale non-linear event only if the contiguous convective echo of the new system was spatially larger than that of the MCS scale non-linear event at the MLO of both systems.

MCS scale events which exhibited linear organization of convective echo at the MLO were denoted as *MCS scale linear events*. These events commenced as a line of convective cells forming within or being advected into the radar sample area (Fig. 2.5). Often, stratiform precipitation formed rearward of the propagating line. However, the presence of a large region of stratiform rain was not linked to the definition of this event type. The convective line had to remain coherent and greater than 100 km in length for at least twenty minutes (time between successive reflectivity volumes used in this study) for the event to be characterized as a MCS scale linear event. The event was defined to terminate after both the convective line and the associated stratiform precipitation region decayed or moved out of the radar sample area.

2.4 Convective vs. stratiform (non-convective) partitioning and rainfall estimation

Previous case studies of MCSs have discussed fundamental distinctions between

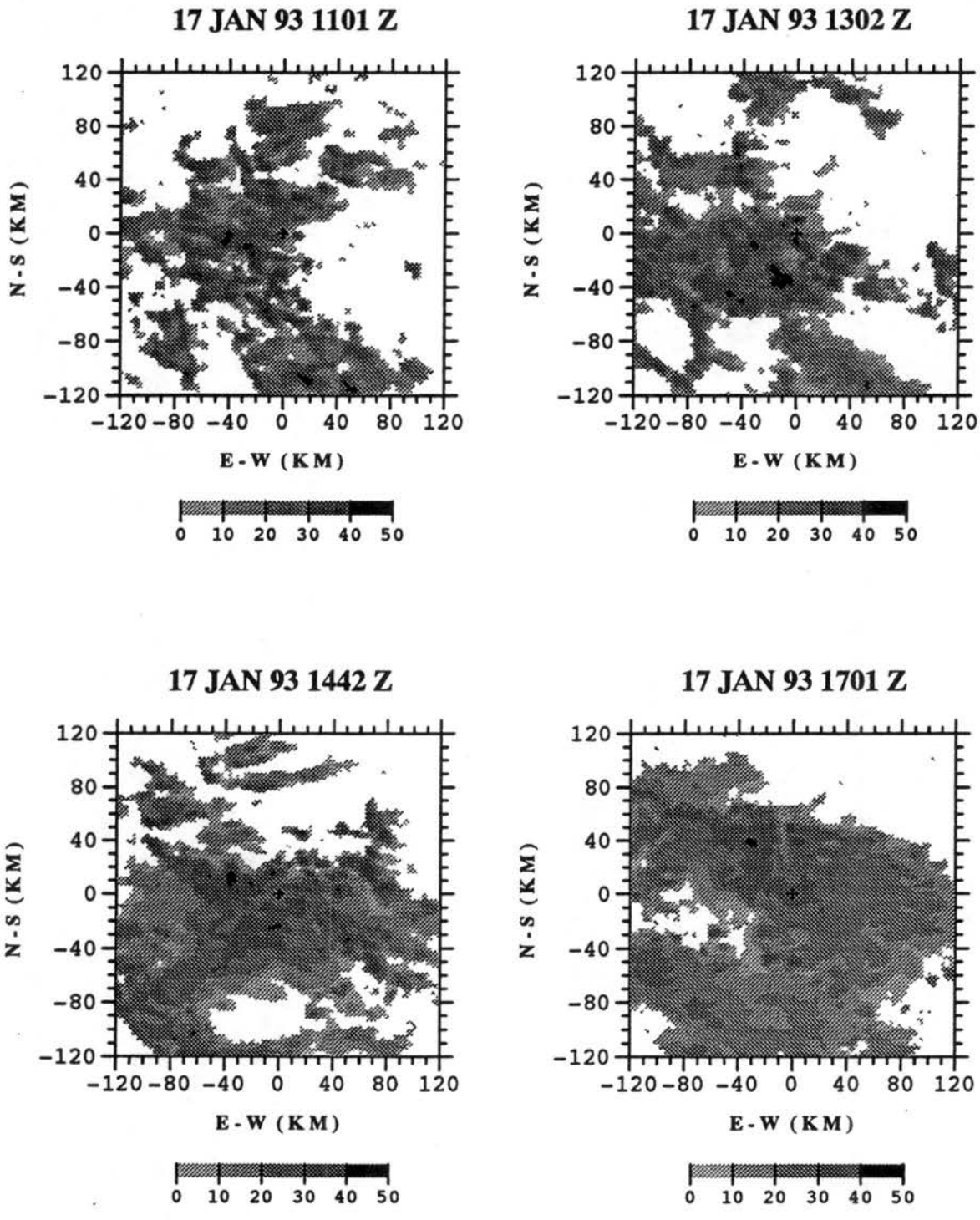

Figure 2.4. As in Figure 2.2, but for two-hourly maps of an MCS scale non-linear event on 17 January 1993. Two-hourly maps are shown to cover most of the life cycle of this event.

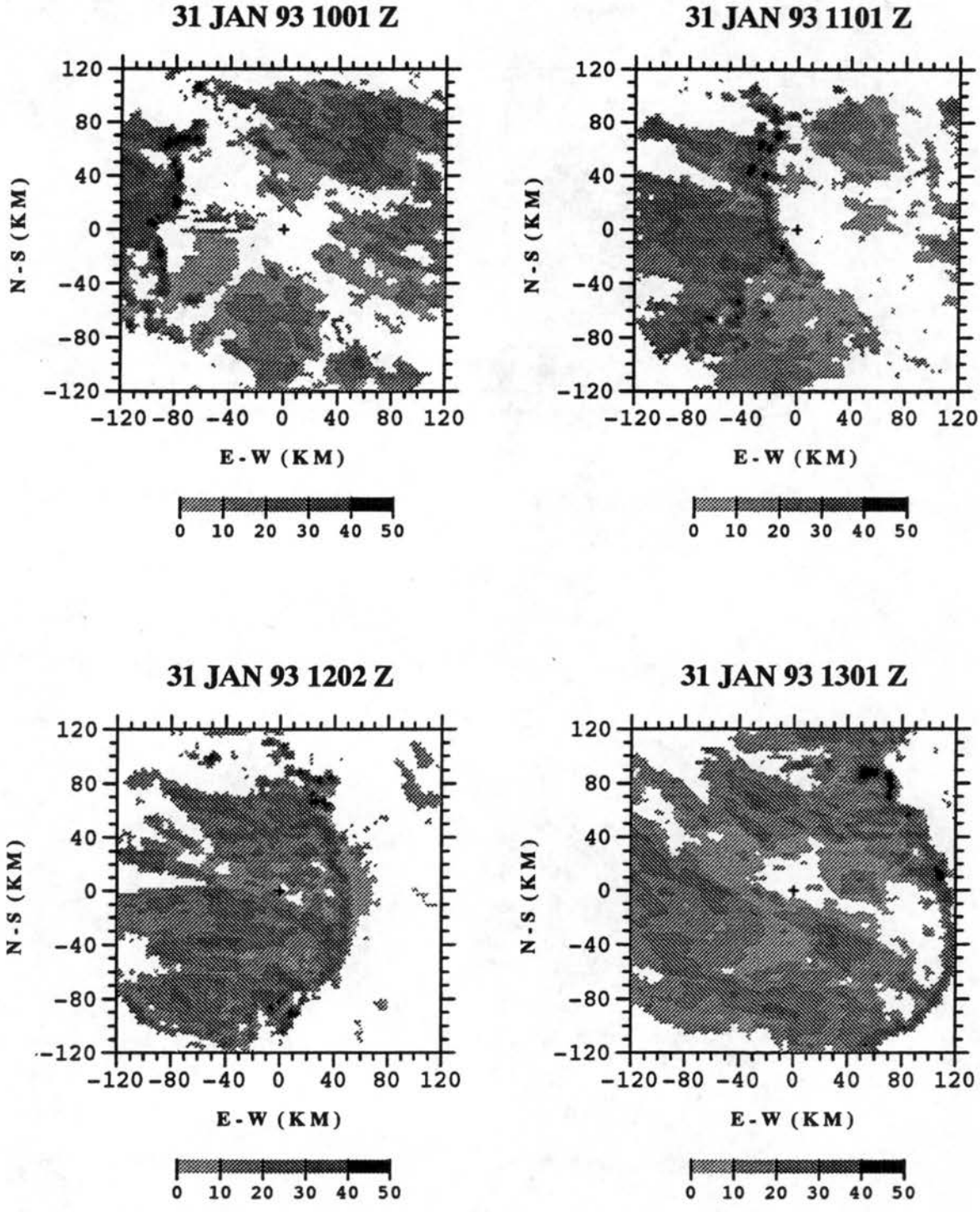

Figure 2.5. As in Figure 2.2, but for an MCS scale linear event on 31 January 1993.

convective and stratiform precipitation in terms of dynamical and microphysical processes, and the resulting vertical profile of heating associated with both precipitation types (c.f. Chapter 1). The relative amount of convective versus stratiform rain produced by a precipitating system provides insight as to the dominant microphysical processes which produce the precipitation in MCSs, and how the resultant latent heating of the atmosphere is distributed vertically (Houze 1989). It is thus important to estimate the relative amount of convective and stratiform rain associated with each event.

Tokay and Short (1996) analyzed raindrop size distribution data from surface disdrometers on Kapingamarangi Atoll during COARE. They found distinct size spectra, attributable to unique drop size distributions in convective and stratiform rain. This observation led them to derive separate reflectivity - rainfall rate (Z-R) relations for each rain type:

$$Z = 139\ R^{1.43}\ \text{(convective)} \tag{2.1}$$

$$Z = 367\ R^{1.30}\ \text{(stratiform)} \tag{2.2}$$

Equations 2.1 and 2.2 illustrate the conclusion of Tokay and Short (1996) that for COARE, a stratiform raindrop population produced roughly half the rainfall rate compared to that of convective regions for a given reflectivity value. This is because the presence of a few relatively large drops (formed from the melting of large aggregates) in the stratiform drop spectra increases the radar reflectivity much more than the

corresponding increase in rain volume[6]. It is therefore necessary to distinguish between convective and stratiform rain when making a quantitative estimate of rainfall rates in the COARE region.

The basis for distinguishing between convective and stratiform precipitation is formulated in terms of the magnitude of vertical air motions ($|w|$) relative to ice hydrometeor fallspeeds (V_{ice}) above the 0° C level. Stratiform rain is defined as rainfall resulting from microphysical processes occurring in clouds where the magnitude of the vertical air velocity is less than ice hydrometeor fallspeeds (Houze 1993, Ch. 6):

$$|w| < V_{ice} \tag{2.3}$$

The ideal approach to distinguishing between convective and stratiform precipitation regions is to identify by direct measurements areas where Eq. 2.3 is satisfied, i.e. where ice particles fall relative to the surrounding air (e.g. Willis et al. 1995). Unfortunately, measurements of vertical motion coincident with particle fallspeeds are rare, and are not generally available for COARE systems sampled by the ship radars.

Accordingly, indirect methods for identifying regions where particle fallspeeds exceed the vertical air speed must be used. These techniques necessarily involve identifying convective rain regions rather than stratiform rain regions, because the vertical resolution of the Cartesian reflectivity data is often too coarse to resolve the

[6] Drop volume is proportional to the third power of the drop radius, while radar reflectivity is proportional to the sixth power of the drop radius.

stratiform radar bright band[7]. The most common approach is to examine spatial gradients of radar reflectivity to isolate regions of more intense, horizontally variable precipitation indicative of convective rain from regions of weaker, widespread precipitation associated with stratiform rain (Churchill and Houze 1984, Steiner et al. 1995). This technique examines the low level horizontal radar reflectivity field for two criteria related to the spatial uniformity of rainfall: *intensity* and *peakedness*. The intensity criterion for convective rain is satisfied wherever reflectivity exceeds 40 dBZ, accounting for observations that stratiform reflectivities do not generally exceed this value 2 km above the surface (Steiner et al. 1995). Alternately, a reflectivity value may be considered convective if it exceeds the mean "background"[8] reflectivity of a surrounding region by a threshold value (the peakedness criterion of Steiner et al. 1995). Once a reflectivity value is denoted as convective, a circular "convective cell" with a radius dependent on the mean background reflectivity is also considered convective. All other reflectivity values are considered stratiform. The method used herein follows that of Steiner et al. (1995), except for a difference in how the peakedness criterion was applied (see Appendix A).

It is important to note that this technique cannot distinguish precipitation associated with decaying convective updrafts from stratiform rain resulting from melting hydrometeors which grew by vapor deposition in a mesoscale updraft. Though both of these rain scenarios are considered stratiform by Eq. 2.3, each would have a distinct

---

[7] Rosenfeld et al. 1995 discuss a technique to identify stratiform rain regions using higher resolution polar reflectivity data

[8] The background area is defined in Steiner et al. 1995 as a circular area with an 11 km radius surrounding the point in question.

vertical profile of latent heating associated with it. For this reason, the term *non-convective* rain will be used in this paper rather than stratiform rain to identify rain which has not been categorized as convective by the above technique. In this way, it is not implied that such rain necessarily results in heating aloft and cooling at low levels (c. f. Chapter 1). It will later be argued that non-convective rain associated with MCS scale events likely has the aforementioned heating profile, and that such rain associated with sub-MCS scale events does not.

The appropriate Z-R relation was applied to convective and non-convective reflectivity values in order to calculate rainfall rates. These rainfall rates were then corrected for attenuation by intervening precipitation, which can be significant at C-band, following Patterson et al. (1979). The attenuation correction was therefore dependent on the convective - non-convective rainfall partition, since the correction was applied to the rainfall rate fields. This correction increased the mean ninety day total rainfall rate by about 10%. No other correction was applied to the reflectivity values (e. g. removal of anomalous propagation, manual editing of sea clutter) because of the large number of data volumes used. For these reasons, relative rainfall amounts between modes of convective organization are given more emphasis than absolute rainfall amounts.

2.5 Convective feature identification

Once the convective vs. non-convective status of the horizontal reflectivity field was determined, convective grid points were grouped into *convective features*. A convective

feature was defined as a group of horizontally contiguous convective grid points, isolated from other such groups by non-convective grid points or by reflectivity-free regions. As such, a single convective feature may contain one or more individual convective cells. The area of a convective feature was thus a measure of the degree to which individual convective cells were contiguously clustered in space. For each reflectivity volume, all convective features were uniquely identified, and the maximum height, maximum length, area, and rainfall rate were calculated for each feature. In this way, the variation with scale and morphology in the size distribution of merged convective elements could be studied. Convective feature statistics were related to the time integration of the instantaneous echo population, rather than to the time history of individual features. The convective feature identification algorithm was based on a similar algorithm developed for satellite observations of cumulus clouds by Wielicki and Welch (1986).

CHAPTER 3

RAINFALL AND ENVIRONMENTAL CHARACTERISTICS BY CONVECTIVE ORGANIZATION

This chapter provides an analysis of rainfall production partitioned by each mode of convective organization discussed in Chapter 2. Features of the composite wind and humidity environment of each mode are presented. Finally, composite heating profiles for each mode are given and related to system morphology.

3.1 Overview of ninety day rainfall time series

Shown in Fig. 3.1a-c are time series of the areally integrated rainfall rate (total, convective, and non-convective) for each cruise, along with the time series of the mode of convection present. Rainfall was nearly continuous, punctuated by local maxima ranging from 10 mm d^{-1} to 60 mm d^{-1}. These maxima corresponded both to the formation and growth of precipitation events within the radar sample area and to the propagation of events across the sample area. Rainfall rate maxima above about 20 mm d^{-1} are consistently associated with MCS scale events. In addition, the occurrence of non-convective rainfall rates above ~ 10 mm d^{-1} were exclusively found during MCS scale

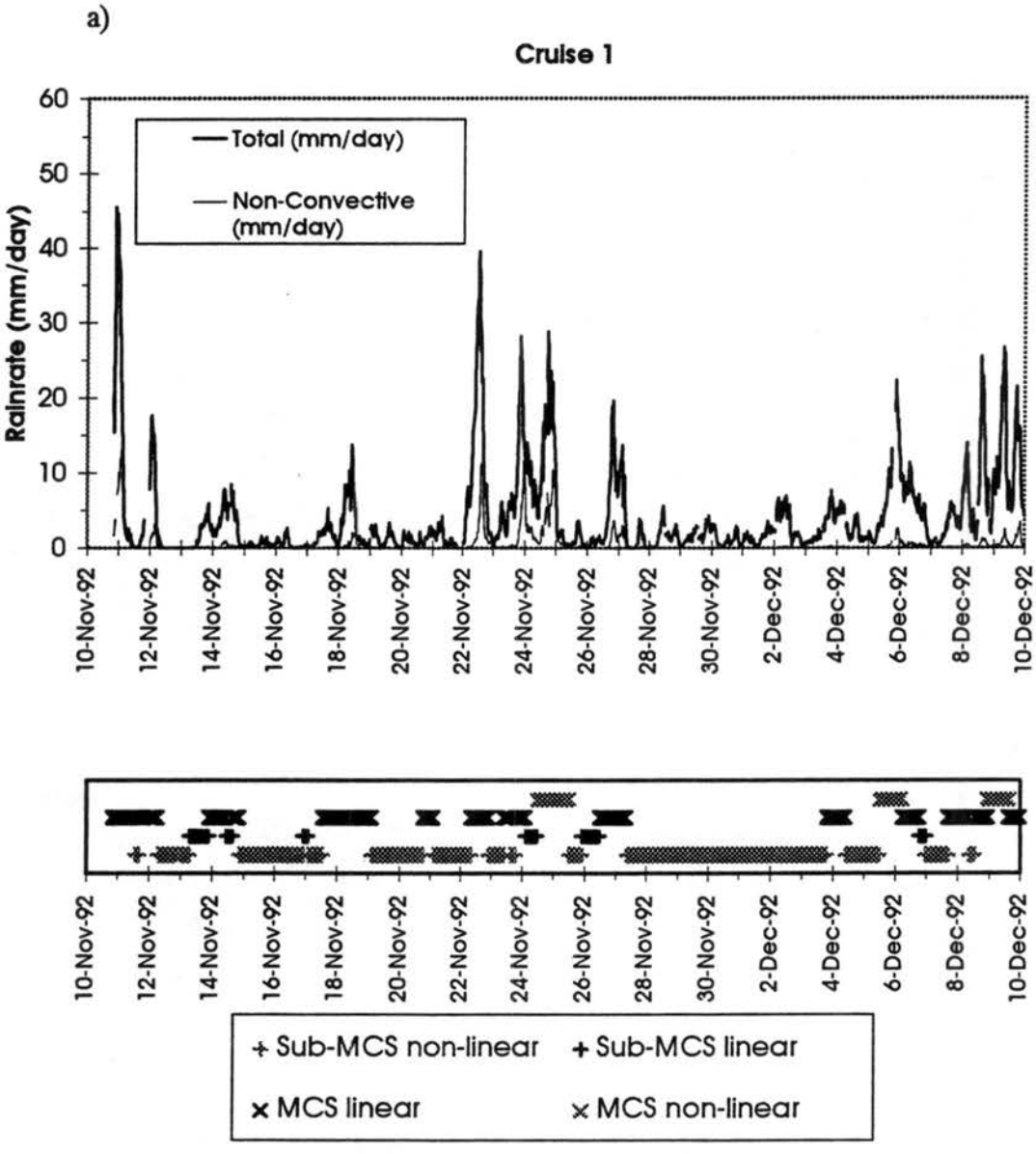

Figure 3.1. Time series of total rainrate (thick solid line) and non-convective rainrate (thin solid line) in mm day^{-1} for a) Cruise 1. The time intervals when events of each type were present are also shown. Convective rain time series are not shown because of their similarity to the total rain time series.

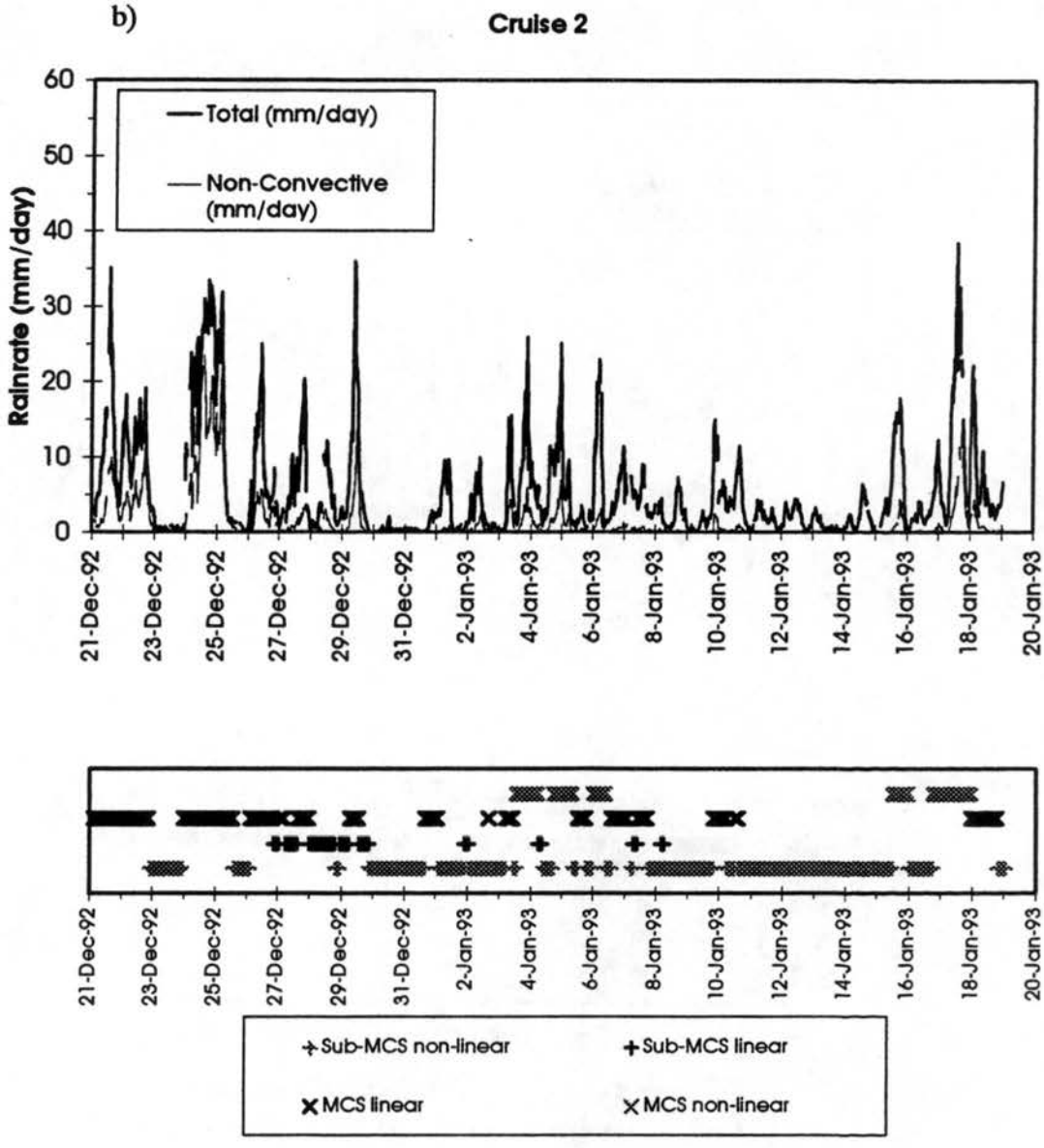

Figure 3.1. (continued) Time series of total rainrate (thick solid line) and non-convective rainrate (thin solid line) in mm day^{-1} for b) Cruise 2. The time intervals when events of each type were present are also shown. Convective rain time series are not shown because of their similarity to the total rain time series.

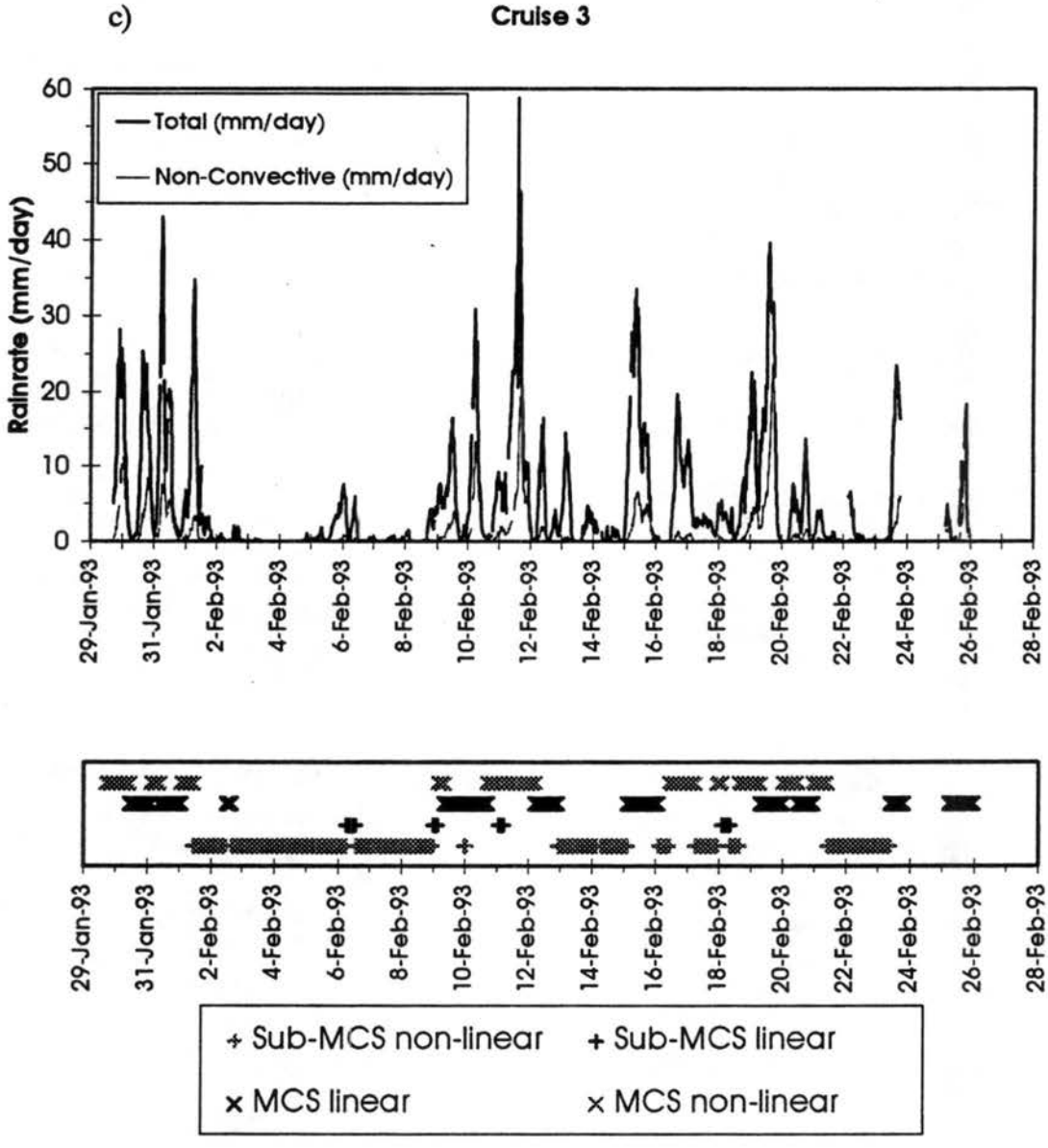

Figure 3.1. (continued) Time series of total rainrate (thick solid line) and non-convective rainrate (thin solid line) in mm day^{-1} for c) Cruise 3. The time intervals when events of each type were present are also shown. Convective rain time series are not shown because of their similarity to the total rain time series.

events. For these events, the peak non-convective rainrate was often observed to lag the peak convective rainrate by several hours. This may be attributable to the evolution of MCS scale events, with the peak in non-convective rain associated with the later stages of the system's lifecycle (Leary and Houze 1979, McAnelly and Cotton 1989). The duration of these MCS rainfall periods (comprised of one or more events) varied from several hours to about 1.5 days. A striking feature of the rainfall time series was the almost complete lack of non-raining periods, except for two 24 hour periods centered on 13 November and 4 February.

3.2 Ninety day mean rainfall statistics

The ninety day mean rainfall rate and convective rainfall fraction were 4.5 mm d^{-1} and 69% respectively. The mean convective rain fraction of 69% was higher than previous estimates from squall line case studies (50% - 60%; Houze 1977, Gamache and Houze 1983, McAnelly and Cotton 1989). This was in part due to the inclusion in this study of all convection, not only MCS scale systems with broad non-convective regions, into the estimate of convective rain fraction. Rosenfeld et al. (1995) estimated a convective rain fraction of 78% from raingauge data for maritime ITCZ convection. They suggested that previous radar case studies underestimated the convective rain fraction by not accounting for the distinct drop size distributions (and thus reflectivity - rainfall relations) in convective vs. non-convective rain (i.e. Waldvogel 1974, Tokay and Short 1996). Since the latter study established this distinction for the COARE region,

this factor was accounted for in the present study.

The ninety day total rainfall production and event occurrence frequency partitioned by scale and morphology are given in Fig. 3.2. Although sub-MCS scale rainfall was present nearly 60% of the time, the total rain volume associated with sub-MCS scale events comprised only one-fifth of the total ninety day rain volume. The mean MCS scale rainfall rate of 8.8 mm d^{-1} was six times greater than the mean sub-MCS scale rain rate. Sub-MCS scale non-linear events were present just over one-half of the time and produced nearly 15% of the total ninety day rain volume. As a comparison, Simpson et al. (1993) found that, for island convection in the southern maritime continent region near Darwin, less than 10% of the observed precipitation was associated with isolated convective cells.

Since MCS scale events were less common than sub-MCS scale events, two factors may account for the higher mean rainfall rate of MCS scale events: greater rainfall intensity, and greater areal coverage. For both scales there was a similar range of normalized areal coverage of "intense" (> 40 dBZ) low level reflectivity (a measure of rainfall intensity), illustrating that intense local rainfall occurred on both scales of precipitation organization (Fig. 3.3) at the time of maximum rainfall for each event. However, the broader distribution of MCS scale rainfall intensity suggests that intense rainfall was more common on that scale compared to the sub-MCS scale. MCS scale event-mean rainfall rates were generally higher than those on the sub-MCS scale for a given intensity value, suggesting the importance of large areal coverage in producing greater MCS scale rainfall rates. The large event-mean MCS scale rainfall rates shown in

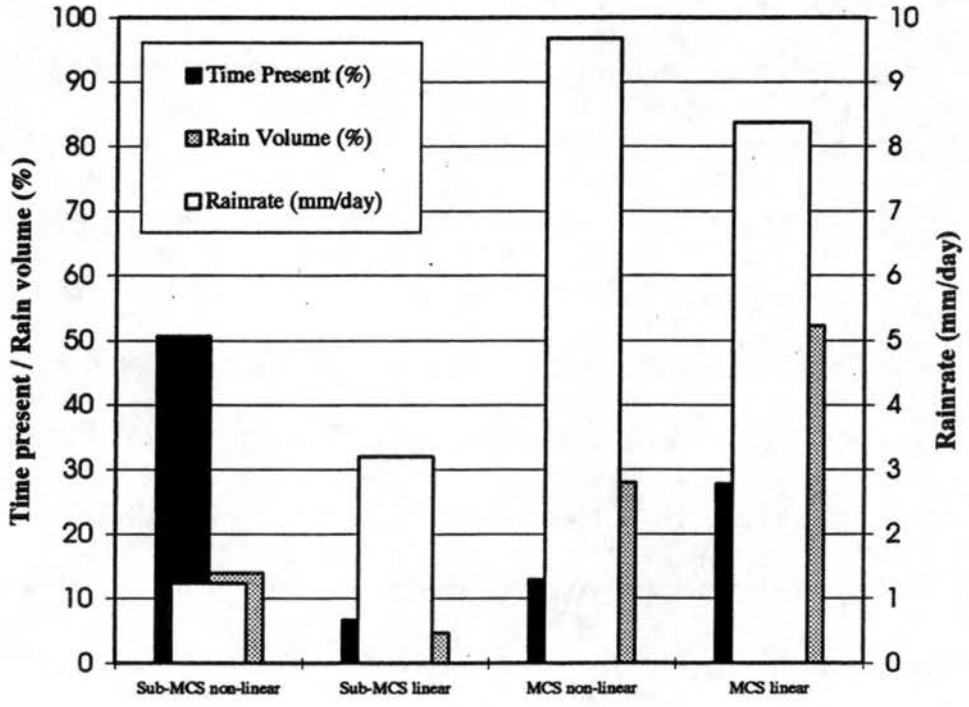

Figure 3.2. The time present (black), rain volume (gray), and mean rainfall rate (white, mm day^{-1}) for each event type for all three cruises combined. Time present and rain volume are expressed as fractions of the three cruise totals.

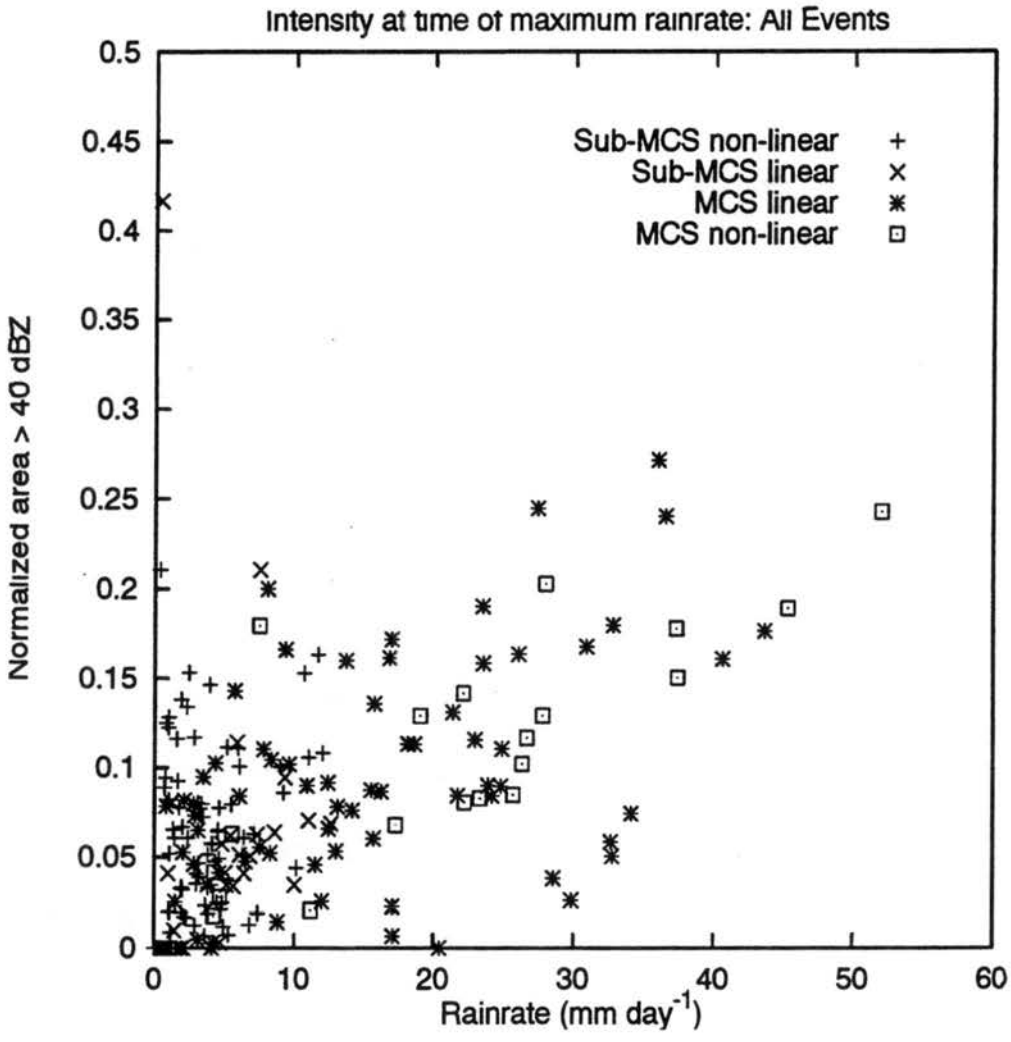

Figure 3.3. Scatterplot of the instantaneous rainfall rate (mm day^{-1}) and the area covered by reflectivities > 40 dBZ (normalized by the convective area) for all 215 events. Each point represent the time of the highest instantaneous rainfall rate for that event.

Figs. 3.2 and 3.3 were therefore associated with both the larger areal coverage of precipitation and the occurrence of locally intense rainfall rates, though the difference in the areal coverage was the dominant factor.

The mean convective rainfall fraction separated by scale and morphology is shown in Table 3.1. The convective rainfall fraction associated with MCS scale events was lower compared to sub-MCS scale events. This observation is consistent with previous case studies documenting significant fractions of non-convective rainfall associated with MCSs (see discussion below). Within each scale, events with linear organization had a lower mean convective rainfall fraction than events without linear organization, with the largest difference occurring on the MCS scale. In previous case studies, the horizontal flow branches associated with MCS scale squall lines have been shown to play an important role in the enhancement of non-convective precipitation (Houze 1989). In those systems, the front-to-rear flow branch provided a condensate transport mechanism at upper levels into the stratiform region. The convergence at the interface between the front-to-rear and rear-to-front flow branches augmented the mesoscale updraft at mid and upper levels in the stratiform region, enhancing depositional growth of ice particles. These flow structures may be absent or less well organized in MCS scale non-linear events, which might account for the higher convective rainfall fractions in those events (73%) compared to MCS scale linear events (64%). Detailed case studies of the flow features of individual systems are required to test this hypothesis.

The mean convective rainfall fractions compared well to previous studies of tropical and middle latitude convection, considering the range of techniques used to produce the

Table 3.1. Mean convective rain fraction for each event type, averaged over all three cruises.

Category	Mean Convective Rain Fraction
Sub-MCS scale non-linear	81%
Sub-MCS scale linear	76%
MCS scale non-linear	73%
MCS scale linear	64%

estimates. For the three phases of GATE combined, Cheng and Houze (1979) estimated a convective rainfall fraction of 60% from all scales of radar echo. This can be compared with the present estimate for the ninety day mean convective fraction of 69% for both scales of organization combined. In a climatology of MCCs over the central U.S., McAnelly and Cotton (1989) found a range of convective rainfall fraction between 55% and 64%. Since it was not known whether the largest mesoscale precipitation features within each MCC in that study contained linear organization, this result is best compared with the convective rain fraction for all MCS scale events (67%). The mean convective rainfall fraction for MCS scale linear events (64%) was quite similar to several case studies of tropical squall lines over the entire system lifetime (Houze 1977, 60%; Gamache and Houze 1983, 51%; Houze and Rappaport 1984, 58%). Studies of tropical squall lines over a portion of the system lifetime produced a broader range of results (Leary 1984, 70%; Zipser et al. 1981, 45%-50%), within which the current estimate of the MCS scale linear event convective rain fraction falls.

The rainfall contribution from convective features of various heights by scale, morphology, and for all events combined is shown in Fig. 3.4. The distribution for all events showed two distinct maxima, with a primary rainfall maximum at the 14-15 km feature height bin and a secondary peak at 9-10 km. The rainfall distribution from both MCS scale event types were quite similar. Both show a dominant peak between 14-16 km. This result is generally consistent with an analysis of a group of mesoscale precipitation features over a 24 hour period during the GARP Atlantic Tropical Experiment (Leary 1984). However, a secondary maximum in rainfall from convective

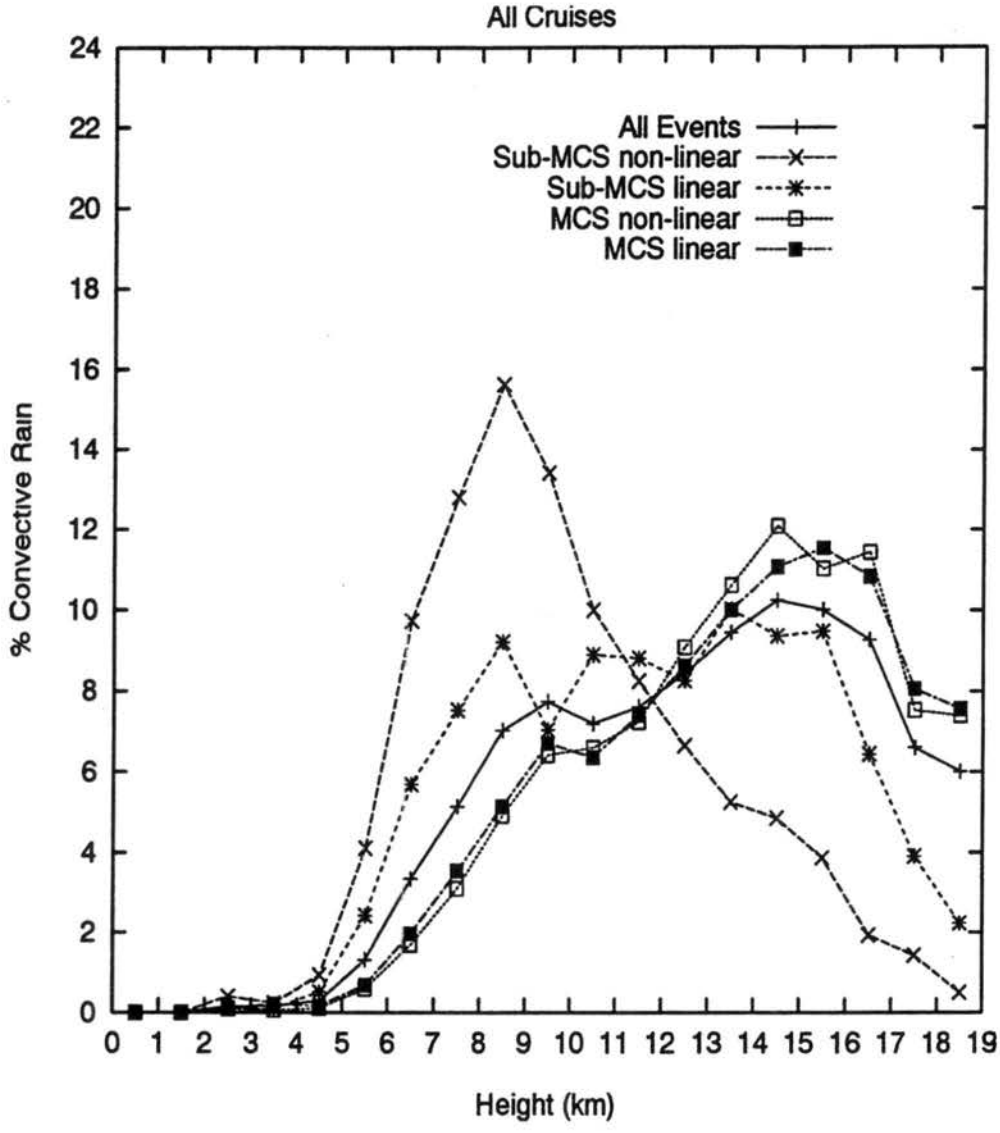

Figure 3.4. Histograms of the fraction of convective rain produced by convective features of various heights (1 km bins), for each event type and for all events combined. Each histogram represents the fraction of convective rain produced by that event type. Convective feature height represent the maximum height attained by the feature.

features of 9-10 km height was unique to COARE. This robust feature may relate to the presence of stable layers near the 0°C level (~5.5 km) as discussed in Johnson et al. (1996). These layers may attenuate the upward momentum of buoyant parcels ascending from the boundary layer, limiting the vertical development of convection.

Fig. 3.4 suggests that while cloud populations associated with MCS scale events may have been slightly influenced by this stable layer, clouds within sub-MCS non-linear events were dominated by it. The distribution of sub-MCS scale non-linear events was clearly centered at 8-9 km. Sub-MCS scale linear events showed a broad distribution, with rainfall distributed rather uniformly from the 8-9 km to 14-15 km feature heights. Therefore, most sub-MCS scale non-linear rainfall was produced by shallower convective features, while sub-MCS scale linear events produced significant rainfall from both shallow and deep features. The contribution of sub-MCS scale rain to the lower "all event" peak was not large, since 80% of total rainfall occurs with MCS scale events (c.f. Fig. 3.2). Nevertheless, it was enough to enhance the lower maximum in the "all event" distribution. Above the 14-15 km height bin, the "all event" distribution was dominated by MCS scale features. Thus the bimodal structure for all events combined appeared to be related to distinct convective feature height populations associated with sub-MCS scale and MCS scale events.

In order to understand this distribution further, the number distribution of convective features over the spectrum of observed feature heights is shown in Fig. 3.5. The most common height for convective features (all events) was 6-7 km, with a decrease in number frequency with height above that level. This trend was preserved for both scales.

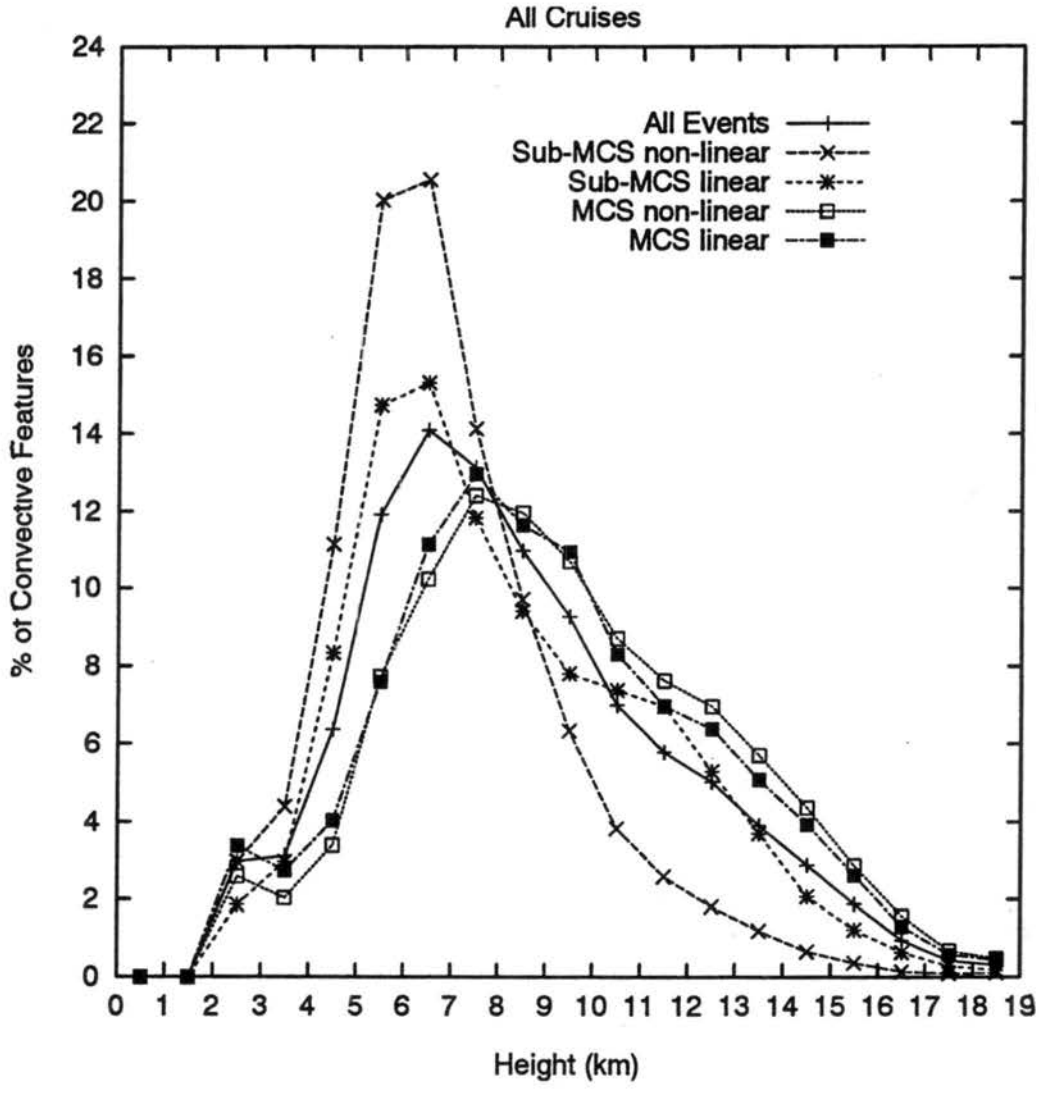

Figure 3.5. Histograms of the number fraction of convective features occurring in 1 km convective feature height bins, for each event type and for all events combined.

Houze and Cheng (1977) showed a similar decrease in number frequency with height, although the echo frequency was highest for the 2-3 km height category in that study. A comparison with Fig. 3.4 shows that the rainfall peak at 15-16 km for MCS scale events was associated with only 2% - 4% of the total features. Since feature height increased with feature area (not shown), the upper height peak in the rainfall - feature height distribution was associated with the large flux of rain from a few large features. Therefore, the lack of an upper level height peak in rainfall from sub-MCS scale non-linear events was due to the rarity of deep convective features from those events.

The rainfall distribution shown in Fig. 3.4 provided a lower limit estimate of rainfall produced by isolated shallow convection where only collision and coalescence processes were active ("warm rain" clouds). Since the 0°C level was generally located near 5.5 km (Johnson et al. 1996), convective features with echo top heights at or below this level were likely dominated by warm rain processes. For all events combined, nearly 2% of the total rainfall was associated with echo tops below 5.5 km. For sub-MCS scale non-linear events, this value increased to just over 5%. However, these are lower limit estimates, since warm rain processes were most likely active below the 0°C level even within deep convection.

3.3 The environment associated with event scale and morphology

An examination of several environmental variables provided insight as to the interpretation of the rainfall statistics presented in the previous section. As a preface, a

discussion of what is meant by "environment" in the context of this study is needed. In Chapter 2, the multi-scale nature of the sounding array was discussed. It was surmised that by interpolating the gridded sounding analysis to a point collocated with the MIT radar, the point represented a combination of the meso-α scale environment and the local meso-β environment. It was not possible, and arguably not meaningful, to separate the effects of meso-β scale convection from the meso-α scale synoptic background state of the environment. For example, a meso-α scale areal mean measure of upward vertical motion in the tropics reflects the ensemble influence of cumulonimbus vertical drafts (Riehl and Malkus 1958, Emanuel et al. 1994). Similar measurements of wind speed and relative humidity also include this blending of the background synoptic state and the local effects of convection. It is this amalgam of scale to which the term "environment" refers in this section. Therefore, the relationship of cause and effect between convection and the surrounding environment cannot be established.

Shown in Figs. 3.6-3.7 are the mean vertical profiles of divergence and vertical motion for MCS scale, sub-MCS scale, and all events combined. The "all events" divergence profile indicated convergence below 400 mb and divergence above, which implied mean tropospheric ascent. This was consistent with the ubiquitous presence of rain near the radar during COARE, as well as the location of the IFA in a region of climatological upward motion during the southern hemisphere summer (Peixoto and Oort 1992).

On the MCS scale, a consistent feature of both linear and non-linear event types was the strong divergence near the tropopause (250 mb - 150 mb), implying strong upper

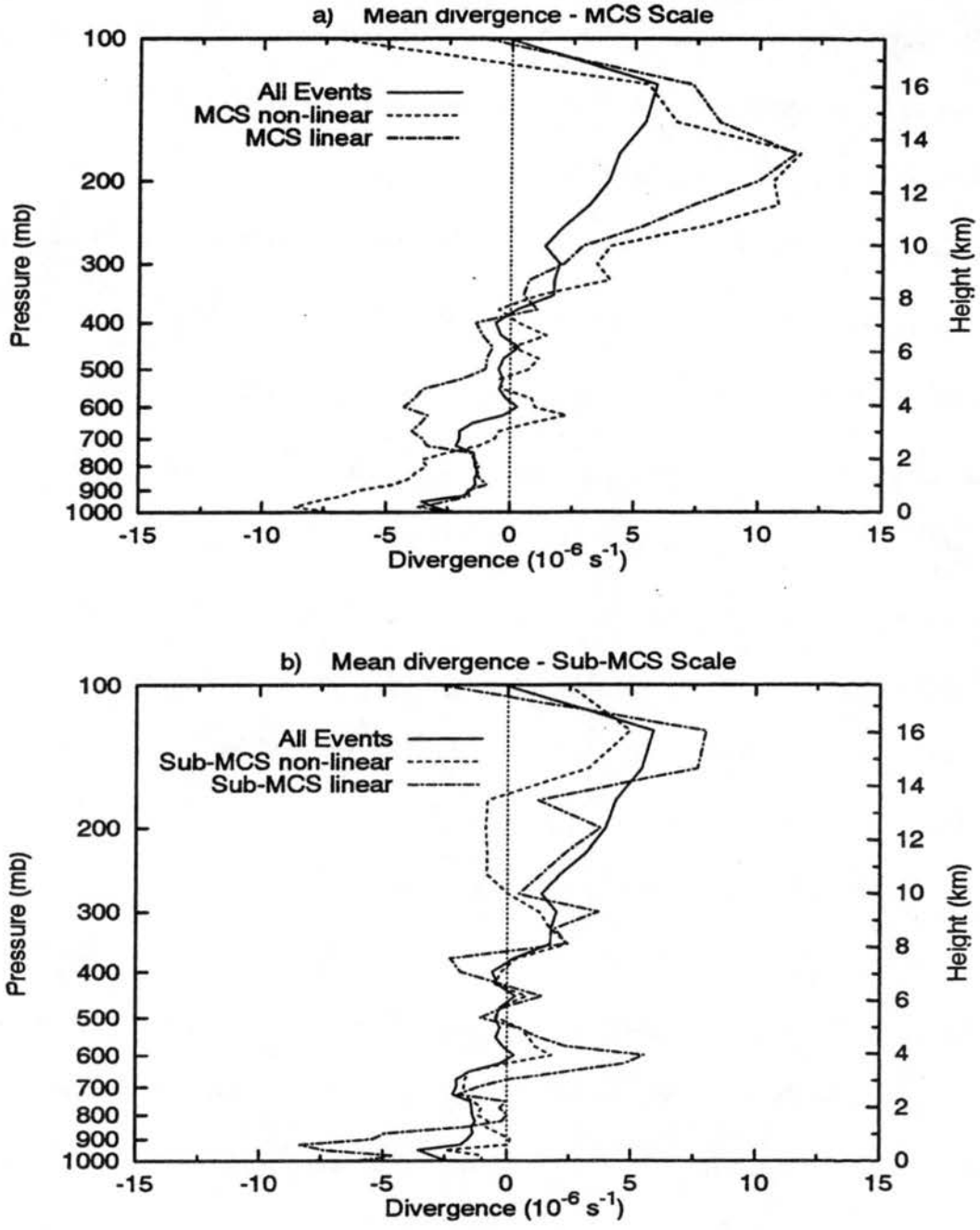

Figure 3.6. The mean vertical profile of divergence (10^{-6} s^{-1}) for a) MCS scale events, and b) sub-MCS scale events. The three cruise mean profile is also shown. Divergence was interpolated from the six closest sounding sites to the nominal position of the R/V Vickers.

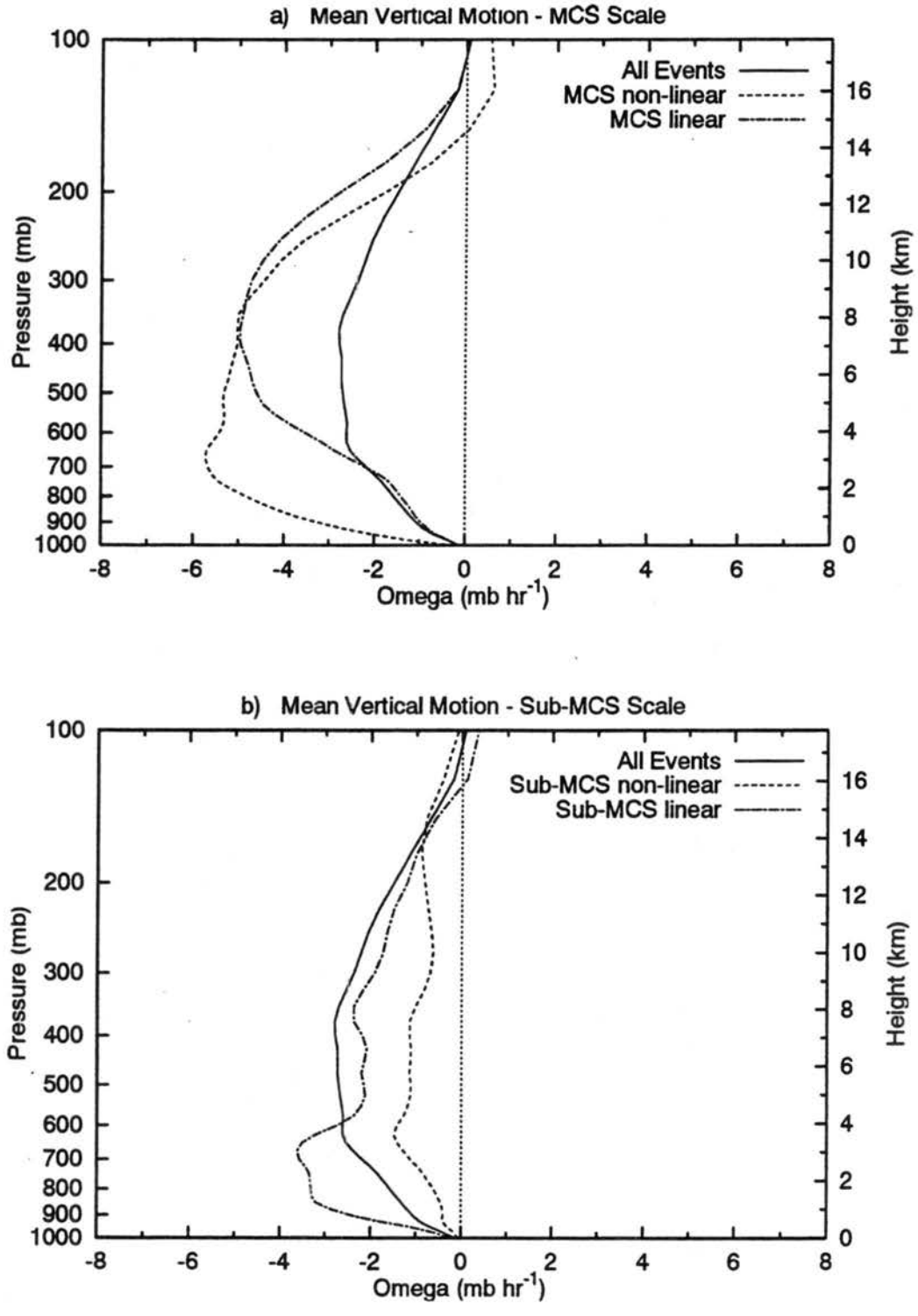

Figure 3.7. As in Figure 3.6, but for vertical motion (mb hr^{-1}) for a) MCS scale events, and b) sub-MCS scale events.

level upward motion. This may be associated with a population of deep convective features for events of this scale (c.f. Fig. 3.4). Yet, significant differences were evident between the composite divergence profiles of MCS scale linear and MCS scale non-linear events (Fig. 3.6a). The most important difference was at mid-levels: the MCS scale linear event composite showed strong convergence near 600 mb, while MCS scale non-linear events were characterized by weak divergence at that level. This may be evidence for the presence of mesoscale flow features associated with MCS scale linear events. The convergent front-to-rear and rear-to-front flow features at mid-levels in non-convective regions associated with many squall lines may reinforce the mesoscale vertical drafts above and below the interface of the horizontal drafts, augmenting depositional growth of ice particles in the mesoscale updraft (Smull and Houze 1987, Rutledge et al. 1988). Strong divergence near the tropopause was also consistent with previous squall line studies. Upward vertical motion (Fig. 3.7) was strongest at mid and upper levels for MCS scale linear events, while strong mean upward motion was present throughout the troposphere for MCS scale non-linear events.

Sub-MCS scale event divergence and vertical motion profiles were quite distinct from those of MCS scale events. The sub-MCS scale event vertical motion profiles were several mb hr^{-1} weaker than the corresponding MCS scale profiles, particularly at mid-to-upper levels. This suggests the absence of organized mesoscale ascent in sub-MCS scale events[1]. Furthermore, sub-MCS scale linear events had a mean divergence profile quite different from that of MCS scale linear events, with strong low-level convergence and

[1] Since this was anticipated, this result lends credence to the characterization of the environment discussed in Chapter 2.

strong mid-level divergence. Strong divergence at 4 km for sub-MCS scale linear events was consistent with the presence of a corresponding maximum in the feature number distribution at a feature height of 6-7 km, allowing for echo top to extend somewhat above the divergence layer (c.f. Fig. 3.5). A maximum in divergence at 350 mb corresponds to the height (8-9 km) of the population of convective features which produce most of the rainfall for this event type. Sub-MCS scale non-linear event mean vertical motion was upward but weak throughout the troposphere.

In contrast, the composite zonal component of the wind (Fig. 3.8) was quite similar for MCS and sub-MCS scale events. Both showed a layer of deep westerly winds from the surface to 400 mb, with easterlies in the upper troposphere. However, sub-MCS scale linear events were associated with strong mean tropospheric easterly shear compared to the other organizational modes. Since most of the variance in the total wind was in the zonal component, the meridional wind composites are not shown. The wind speed profile composites for MCS and sub-MCS scale events (not shown) were also quite similar, with the exception of strong windspeed at 650 mb for sub-MCS scale linear events. This maximum corresponded to the position of the low level westerly jet in the zonal wind composites. These results suggest that there were no distinct wind profiles associated with the different organizational modes, with the exception of stronger tropospheric shear for sub-MCS scale linear events.

The mean profiles of relative humidity (with respect to water for $T > 0°C$ and ice for $T \leq 0°C$) composited by event scale and morphology are presented in Fig. 3.9. The "all events" profile was characterized by a moist boundary layer, a secondary moisture

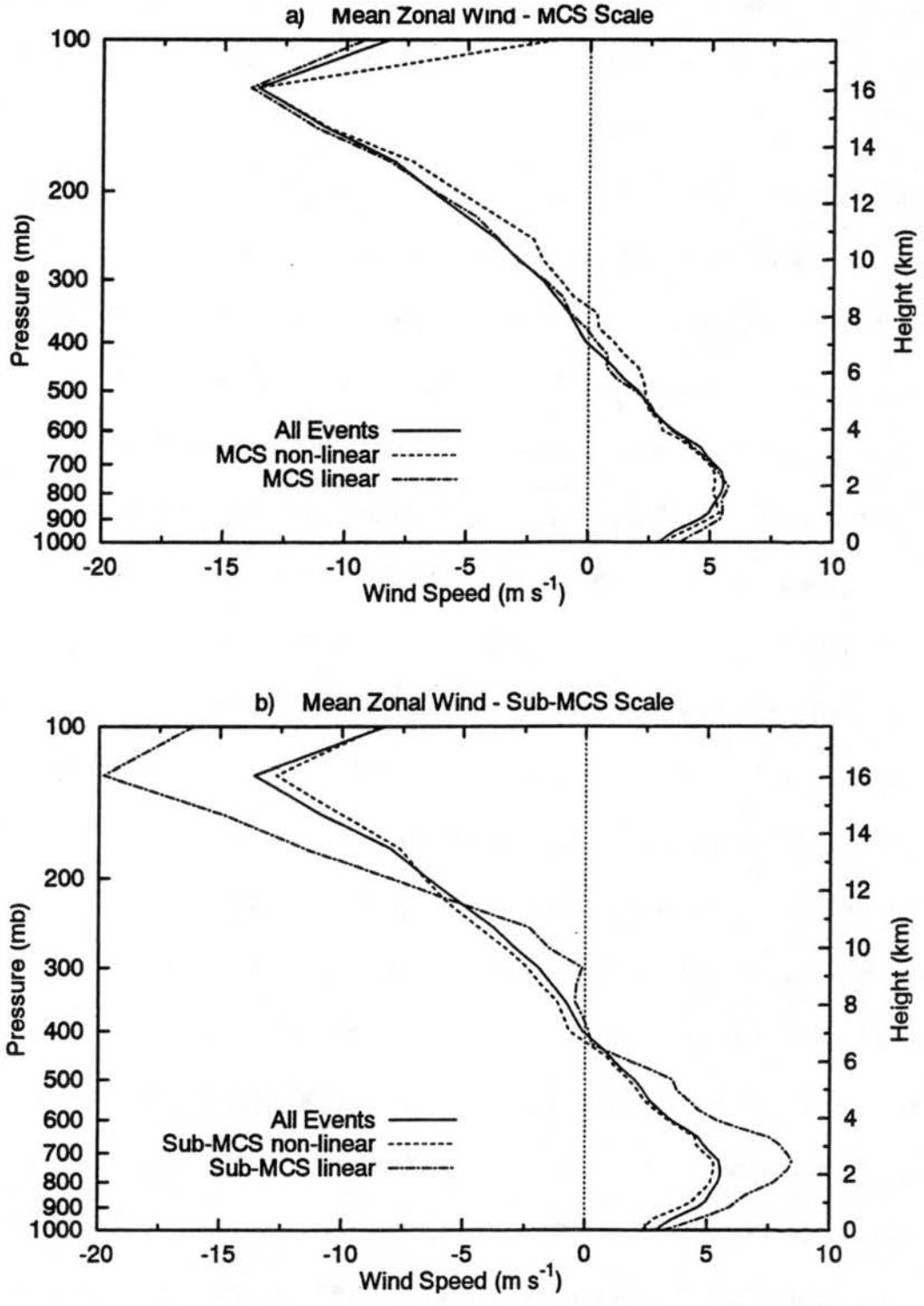

Figure 3.8. As in Figure 3.6, but for zonal wind (m s^{-1}) for a) MCS scale events, and b) sub-MCS scale events.

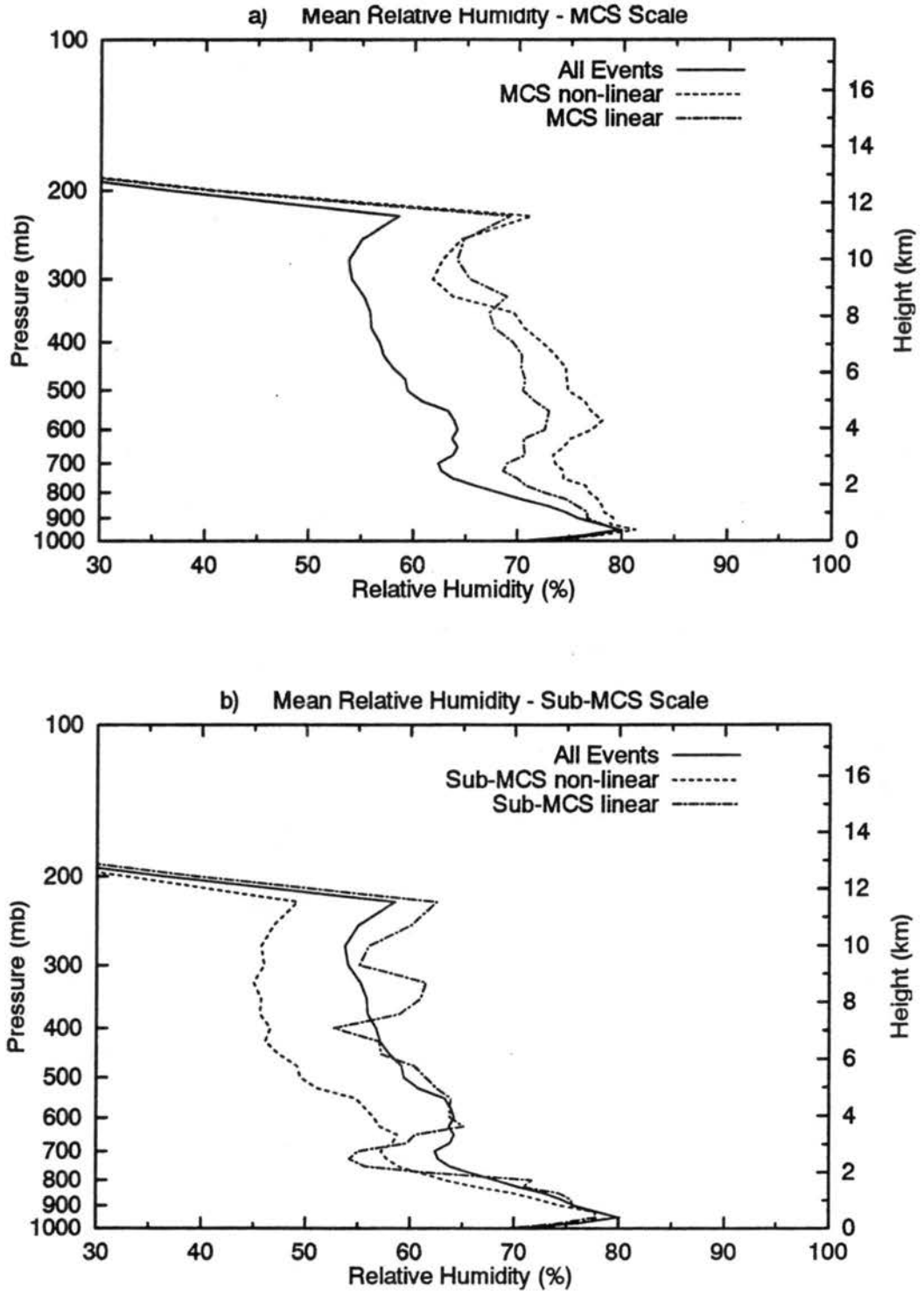

Figure 3.9. As in Figure 3.6, but for relative humidity (%) for a) MCS scale events, and b) sub-MCS scale events. The sharp decrease in relative humidity above 200 mb is due to ice covering the water vapor sensor.

inversion at mid-levels (700 mb - 500 mb), and a decrease in relative humidity with height above that layer. The rapid drop in relative humidity above 200 mb was caused by ice covering the humidity sensors at upper levels (Lin and Johnson 1996a). These general characteristics of the mean relative humidity profile were common to each composite, yet important distinctions are present. The sub-MCS scale non-linear composite was below the mean at all levels. A distinguishing feature of the sub-MCS scale linear event composite is a strong dry layer at 725 mb, capped by a sharp increase in relative humidity. This feature was situated just below a strong divergent layer (c.f. Fig. 3.6b), consistent with moisture detrainment at that level. The MCS scale composites both had relative humidity values greater than the mean above the boundary layer. The MCS scale non-linear event profile was more humid below 300 mb compared to the MCS scale linear event profile, and the level of the mid level moisture inversion was nearly 100 mb higher. Furthermore, the mid-level moisture inversion commences at 700 mb for both scales, but extends about 100 mb heigher for the MCS scale events compared to the sub-MCS scale events. This suggests the presence of more vertically developed convection associated with MCS scale non-linear events compared to MCS scale linear events.

3.4 Heating and moistening profiles

Lin and Johnson (1996b) presented mean profiles of the apparent heat source (Q_1) and the apparent moisture sink (Q_2) derived from sounding data for the COARE IOP,

following the technique of Yanai et al. (1973). They showed that the IFA was characterized by heating throughout the troposphere with a maximum near 400 mb as shown by the Q_1 profile, consistent with the ubiquitious presence of convection in the warm pool. In addition to showing the drying effects of convection at mid levels, the mean Q_2 profile indicated moistening below 700 mb. Lin and Johnson (1996b) attributed this low level moistening to the presence of shallow non-precipitating cumulus clouds which moistened the lowest several kilometers by the evaporation of detrained cloud water. Uncertainties in moisture measurements above 200 mb rendered these profiles suspect near the tropopause.

The heating and moistening associated with each organizational mode were estimated from composite vertical profiles of Q_1 and Q_2, using the data of Lin and Johnson (1996b). The composite Q_1 profiles for the MCS scale events are shown in Fig. 3.10a, along with the mean profile for all events combined. Both MCS scale events showed a maximum heating peak between 400 mb and 300 mb of more than twice the magnitude of the "all events" maximum. Heating maxima at this height for tropical cloud systems have been attributed by Johnson (1984) to mesoscale heating associated with latent heat release associated with depositional growth of ice particles in mesoscale upward motion. Thus, both MCS scale modes appeared to contain upper level mesoscale ascent and heating. This heating peak was elevated for MCS scale linear events by 2 km relative to MCS scale non-linear events, suggesting that latent heat release in upper level mesoscale ascent for MCS scale linear events was concentrated at a higher level than for MCS scale non-linear events.

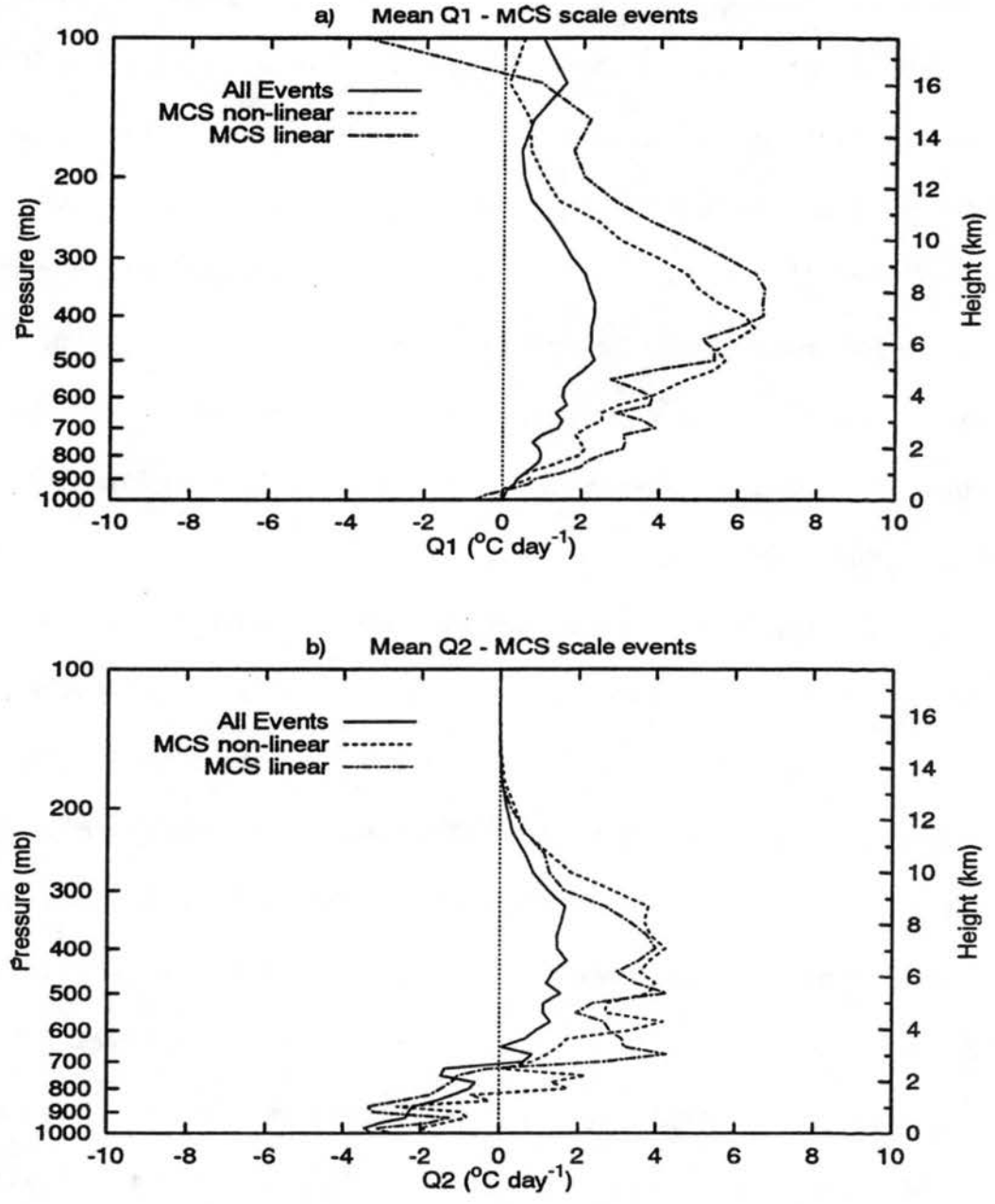

Figure 3.10. As in Figure 3.6, but for a) the apparent heat source (Q_1, °C day^{-1}) and b) the apparent moisture sink (Q_2, °C day^{-1}) for MCS scale events.

The MCS scale Q_2 profiles (Fig. 3.10b) showed a maximum in drying between 500 mb and 300 mb for both MCS scale modes, again related to mesoscale ascent (ibid.). Below 500 mb, the profiles were more complex. The MCS scale linear event composite showed a secondary drying peak near 700 mb, a feature discussed by Johnson (1984) as being linked to convective drying. Below 700 mb, the linear event Q_2 composite indicated moistening. This feature was more likely associated with the evaporation of non-convective rain for MCS scale events rather than the presence of shallow cumulus. For the non-linear event composite, a weaker drying peak occurred at a slightly lower level (750 mb), while the low level moistening was confined to below 800 mb. The low level moistening layer was shallower and weaker for the non-linear event composite compared to the linear event composite. This was consistent with the higher mean convective rainfall fraction for non linear events, which implied less evaporation (moistening) from non-convective rainfall compared to linear events.

The sub-MCS scale event composite heating and moistening profiles (Fig. 3.11) were fundamentally different than the MCS scale event profiles. The only significant heating was confined to below 650 mb, associated with sub-MCS scale linear events. The sub-MCS scale non-linear event composite showed weak heating (< 1 °C day^{-1}) between 700 mb and 450 mb (2 km - 6 km). Both of these heating features were most likely convective in origin because they peaked at low levels. Therefore, there was no significant mesoscale heating produced on the sub-MCS scale. This is strong evidence for the origin of non-convective rain on this scale as simply collapsed convective cells, rather than associated with a mesoscale updraft. An unusual feature of the sub-MCS

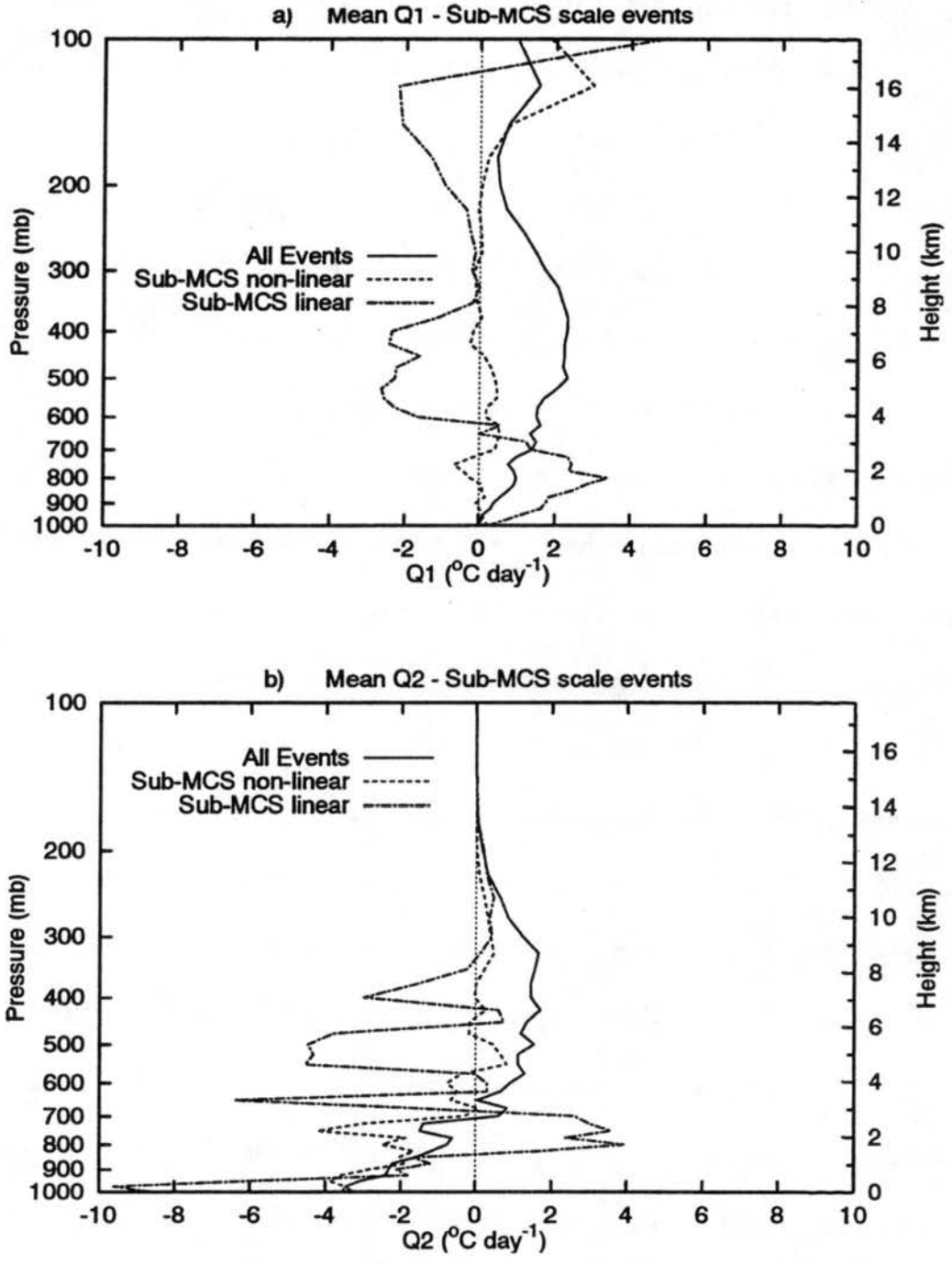

Figure 3.11. As in Figure 3.6, but for a) the apparent heat source (Q_1, °C day^{-1}) and b) the apparent moisture sink (Q_2, °C day^{-1}) for sub-MCS scale events.

scale linear event composite was the strong cooling and moistening centered at 500 mb. This may be related to evaporation of condensate in the dry air found below that level, though the dry air is located 2 km lower (700 mb). The sharp moistening peak near the surface may be related to boundary layer surface moisture flux from the strong low level winds associated with sub-MCS scale linear events. A layer of strong moistening was centered near 750 mb for the non-linear event composite. This was likely a signature of shallow cumulus associated with a population of convective cells, as suggested by Lin and Johnson (1996b).

3.5 Rainfall statistics in distinct environmental regimes

It was shown in Section 3.3 that the mean profiles of divergence (and thus vertical motion) and relative humidity varied significantly with the scale and morphology of precipitation events. This variation was less apparent in profiles of wind speed and the zonal wind component, with the exception of strong mid-level winds with sub-MCS scale linear events. This section examines how the composite rainfall rates and convective rainfall fractions of each organizational mode vary with changes in the profiles of wind and relative humidity. Significant vertical levels (or range of levels) of these composite profiles were chosen to reflect important features of each profile. Then, the lowest and highest quartile at the chosen levels were used to characterize the extrema in the space of each parameter.

Variation in the low level zonal wind in the tropical western Pacific has been shown

to have a correlation with precipitation over a large range of frequencies. Deep convection was observed to lead eastward moving low level westerly wind maxima by one or two weeks (Lau et al. 1989, Lin and Johnson 1996a). These "westerly wind bursts" occurred with a frequency of 30 - 60 days, related to the eastward migration of convection from the Indian Ocean to the western and central Pacific Ocean associated with the interseasonal oscillation (Madden and Julian 1994). Analyses of IFA mean zonal winds (Lin and Johnson 1996a) suggested that the strongest variability in the zonal wind at this frequency was near 750 mb. Furthermore, the magnitude of the upper tropospheric easterlies increased as the low level westerlies increased, so that the strength of the low level zonal flow was directly proportional to the tropospheric shear (ibid.). Latent heat flux driven by strong low level winds have been hypothesized to provide kinetic energy to large scale cloud clusters associated with the intraseasonal oscillation (Emanuel 1987). To examine the association of convection with wind speed, the first and last quartile of wind speed and zonal wind at 750 mb are used to isolate wind regimes in terms of both the magnitude of the low level wind vector and the direction of the low level zonal flow.

The intrusion of low and mid level subtropical air into the warm pool region during COARE appeared to suppress widespread convection (Yoneyama and Fujitani 1995). A relative minimum in the composite vertical profile of relative humidity near 700 mb (Lin and Johnson 1996a; also Sec. 3.3) may reflect these subtropical dry air intrusions. Moreover, the relative humidity increase above this level to 575 mb may reflect moisture evaporation and detrainment due to the effects of the dry stable layer. To examine the

effects of this feature on the rainfall statistics, the first and last quartiles of the mean relative humidity between 700 mb and 575 mb were used to isolate dry and moist mid level regimes.

Shown in Fig. 3.12 is the composite convective rain fraction during the first quartile (weak/dry) and last quartile (strong/moist) low level wind and mid level relative humidity periods (as discussed above). Each MCS scale event convective rain fraction was 10% - 20% greater than the average during periods of weak low level winds and dry mid level air compared to strong low level wind and moist mid level air periods. In addition, this difference was 5% - 10% greater for MCS scale linear events than for MCS scale non-linear events. These observations suggest that the convective rainfall fraction of MCS scale events, particularly linear events, was much more sensitive to changes in the strength of the low level wind and the mid level relative humidity than that of sub-MCS scale events. The convective rainfall fraction of sub-MCS scale linear events increased by 5% during dry mid level air periods (with a similar decrease for moist mid level air), consistent with the higher mid-level relative humidities expected while more non-convective rain is present. This trend was reversed for sub-MCS scale non-linear events, which is somewhat more difficult to explain. The heating profiles (Sec. 3.4) suggested that for these events, non-convective rain production was linked more to decaying convective cells than to depositional growth in a mesoscale updraft. The presence of dry mid-level air during sub-MCS scale non-linear events may actually augment non-convective rain production because of a larger population of decaying

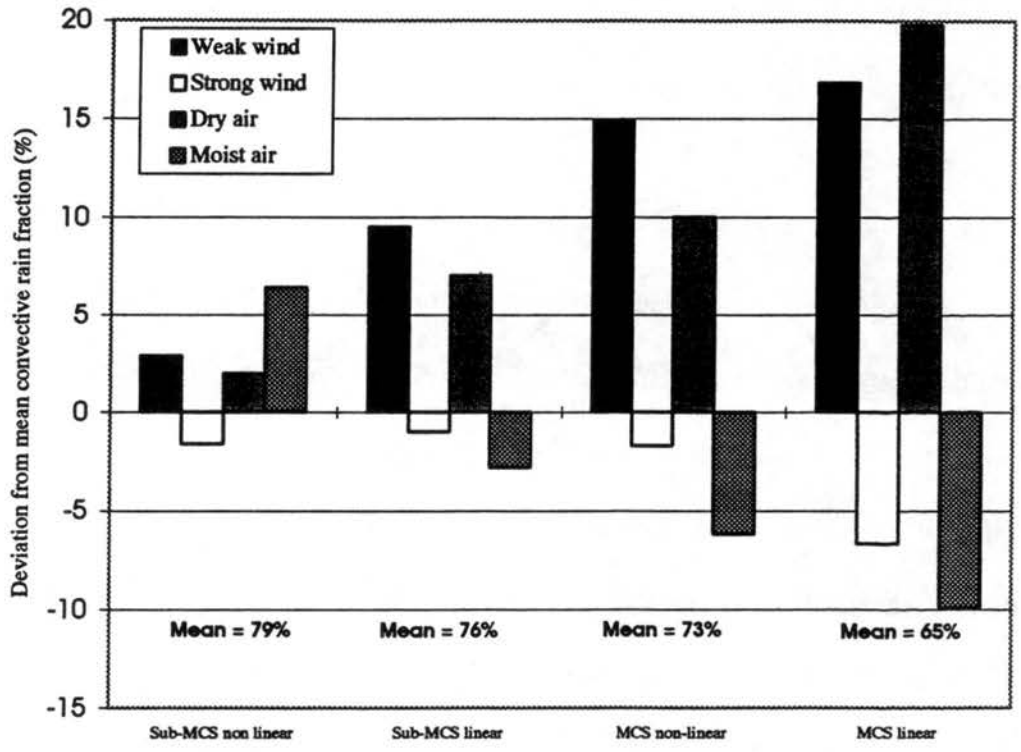

Figure 3.12. The deviation from the three cruise mean convective rainfall fraction for each event, during periods of weak and strong low level wind, and dry and moist mid level air (as discussed in the text). The three cruise mean convective rainfall fraction for each event type is indicated.

convective clouds which do not last long or penetrate deeply due to the dry mid level air[2]. Visual observations from the R/V Vickers of detached mid-level anvils atop weak collapsing convection were common during periods of dry mid level air.

Shown in Fig. 3.13 are the integrated rainfall rates for each mode of organization, separated by wind and relative humidity regime. Rainfall rates of linear events *for both scales* were lower by nearly a factor of two during the weak low level wind and dry mid level air periods. Rainfall was diminished despite the fact that convective rain fractions for linear events were higher during those periods. This implies that non-convective rain areal coverage was small for linear events for periods of weak wind and dry mid-level air. In contrast, rainfall rates for non-linear events on both scales remained near their respective mean values for all wind and relative humidity regimes. For MCS scale non-linear events, the high convective rainfall fractions for weak wind and dry mid level air periods were not associated with lower rainfall rates as they are in MCS scale linear events. This suggests that the convective rainfall associated with MCS scale non-linear events was more intense than for MCS scale linear events, consistent with Fig. 3.3.

The distribution of rainfall from convective features of different heights is shown in Fig. 3.14 for periods of strong and weak low level windspeed. Clear distinctions from the ninety day mean distribution are evident (c.f. Fig. 3.4). The peak at 8 - 9 km seen in the ninety day mean was absent in the strong wind composite for all modes combined and for both MCS scale events (Fig. 3.14a). Sub-MCS scale event distributions retained a weak local maximum at 8 - 9 km for both wind regimes. The rainfall distribution from

---

[2] The presence of a larger population of shallower precipitation features during dry mid level air periods is shown in Fig. 3.14.

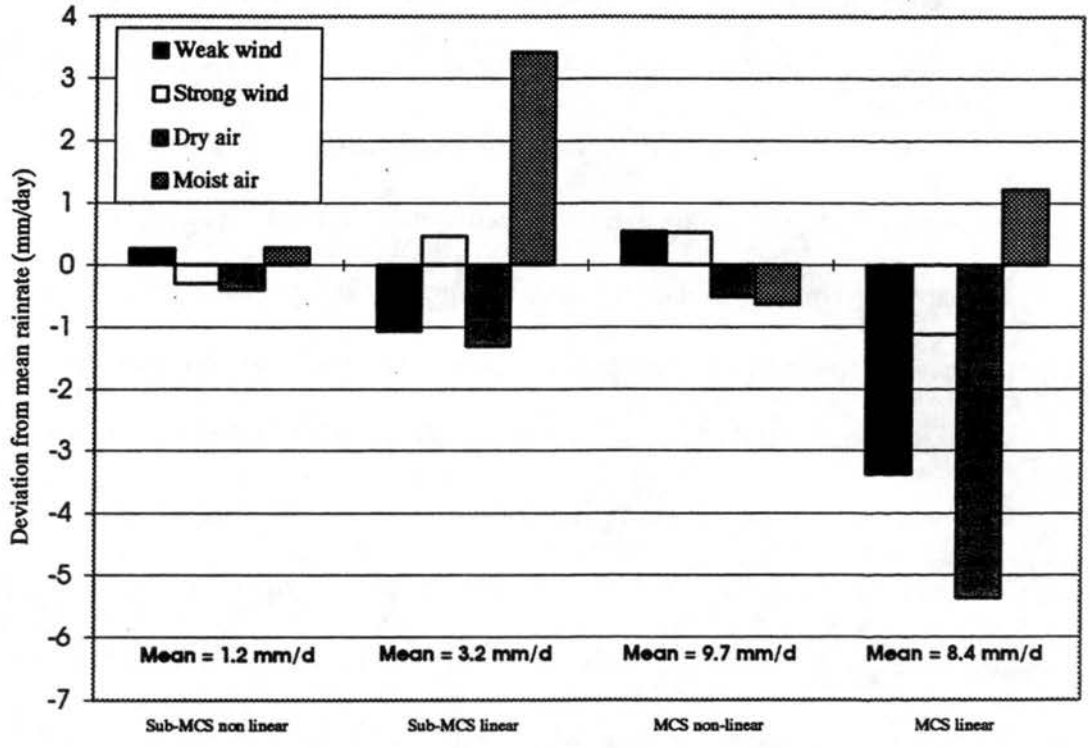

Figure 3.13. As in Figure 3.12, but for mean rainfall rate (mm day^{-1}).

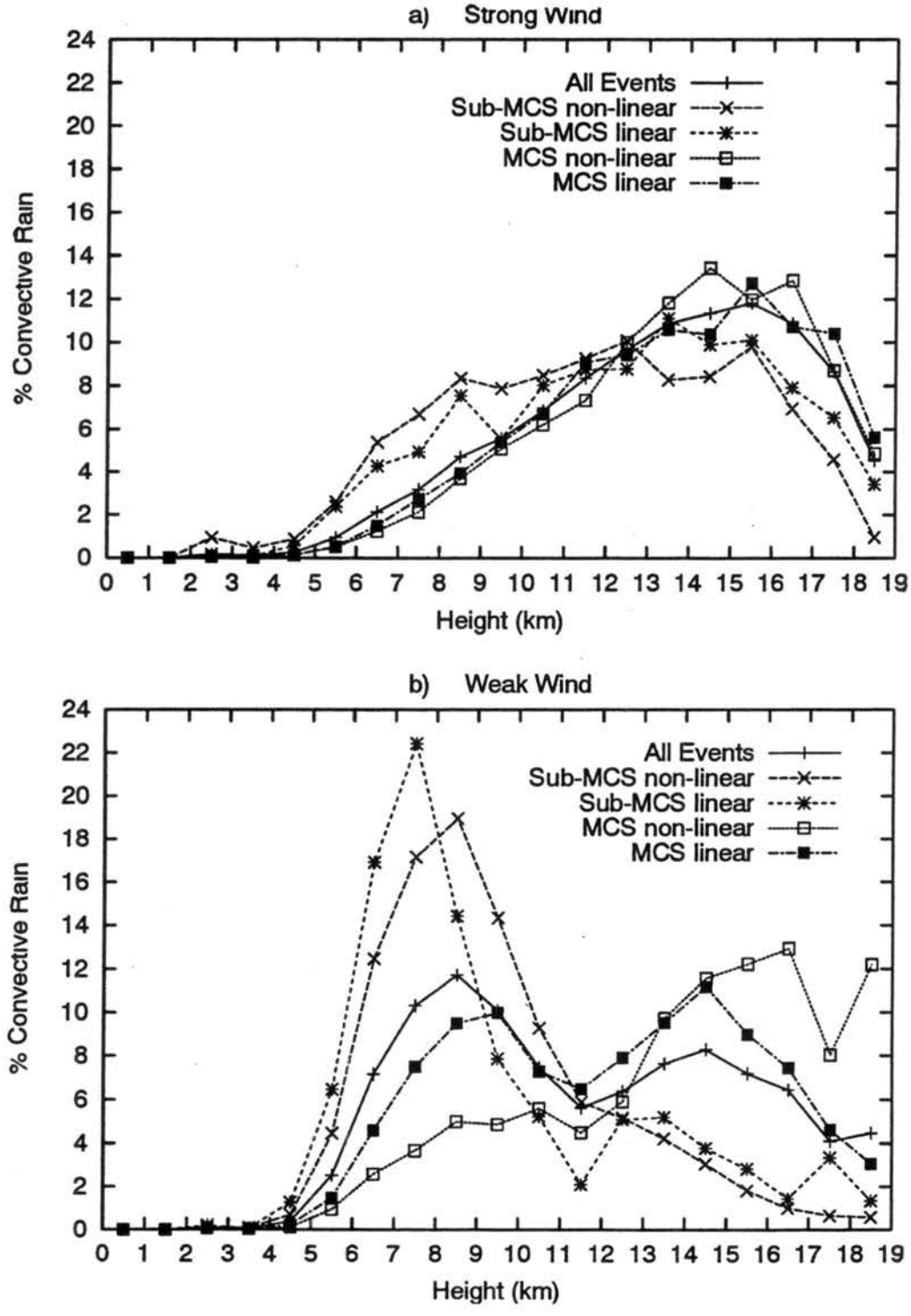

Figure 3.14. As in Figure 3.4, but for the periods of a) strong low level wind, and b) weak low level wind, as discussed in the text.

the deeper convective features for the MCS scale events was similar to the ninety day mean, but there was a significant shift to more rainfall production from deeper features from sub-MCS scale non-linear events. In contrast, rainfall was shifted to the shallower convective feature heights during the weak windspeed periods for the sub-MCS scale events, and to a small degree for MCS scale linear events. The MCS scale non-linear event rainfall distribution was nearly the same for both wind regimes. A very similar dichotomy was seen in the moist vs. dry mid level air MCS scale event composites (Fig. 3.15), with the single rainfall peak at deep feature heights during the moist mid level period, and the bimodal distribution for the dry mid level period. Dry air entrainment at mid levels combined with weak low level forcing from colliding outflows may limit the depth of sub-MCS scale convection during weak wind and dry mid level air periods. On the MCS scale, the presence of system-internal mesoscale circulations may mitigate this effect, such as mid level convergence with MCS scale linear events which may contribute to non-convective rain production. In addition, spatially large outflow boundaries may augment low level mechanical forcing on that scale. Such forcing by outflow boundary interaction may be strong enough for MCS scale non-linear events that the convective feature depths were not nearly as sensitive to the wind and moisture characteristics of their environment.

As discussed earlier in this Chapter, previous studies suggested that the occurrence of large scale convective cloudiness may be influenced by not only windspeed but also wind direction. Rainfall statistics were thus determined for periods of easterly and westerly low level (750 mb) winds. In order to further isolate the effects of wind direction from

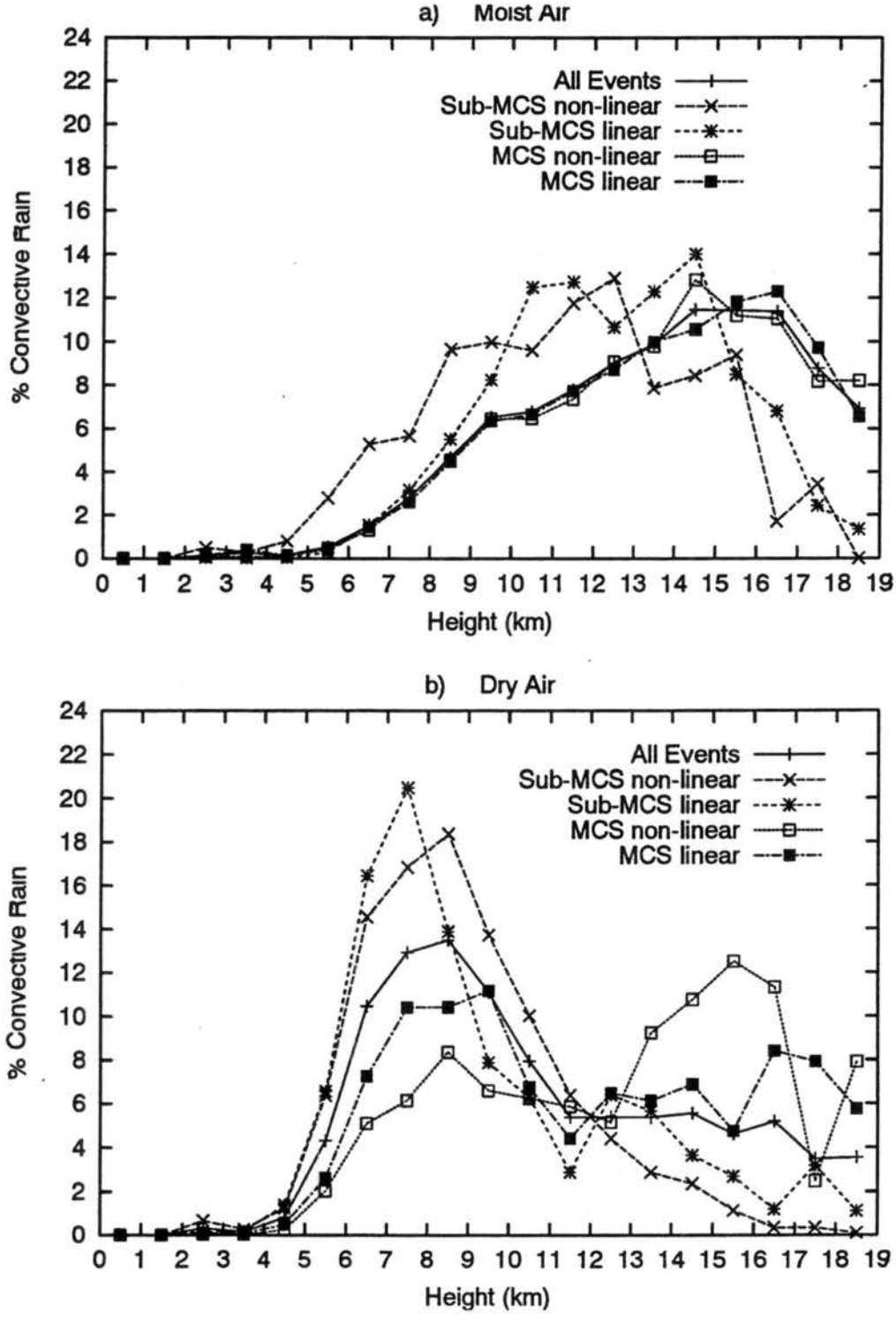

Figure 3.15. As in Figure 3.4, but for the periods of a) moist mid level air, and b) dry mid level air, as discussed in the text.

that of wind speed[3], the periods of event mean westerly wind speed less than or equal to the maximum event mean easterly wind (9 m s^{-1}) were also examined. Shown in Fig. 3.16 is the convective rainfall fraction by event scale and morphology divided into periods of westerly and easterly low level wind direction. The effect of wind direction on convective rainfall fraction was most apparent for linear events on both scales. The convective rainfall fraction was 10% - 15% higher during low level easterly winds for those events, while the corresponding rainfall rates (Fig. 3.17) were 1-2 mm d^{-1} lower. These observations suggest that non-convective rain production and areal coverage was diminished for linear events during low level easterly winds. Furthermore, the fraction for weak westerly winds (equal or lesser magnitude compared to easterlies) was quite similar to that of the westerly wind periods on both scales, suggesting that the increased convective rainfall fraction in easterlies was related to wind direction, not wind speed. Since upper tropospheric easterlies were always present over the IFA during COARE (Lin and Johnson 1996a), the tropospheric shear was stronger in the presence of low level westerly winds. This increased shear may have provided a more favorable environment for the production of non-convective rain in linear events. The enhanced easterly shear resulted in stronger system relative upper level flow, which would distribute condensate from the convective region over a wider area and produce higher areal mean non-convective rainfall rates. Neither wind direction nor wind speed had an appreciable effect on the rainfall distribution by convective feature height (not shown).

---

[3] The COARE-mean westerly wind speed was considerably higher than the mean easterly wind speed because of the influence of westerly wind bursts (Lin and Johnson 1996a).

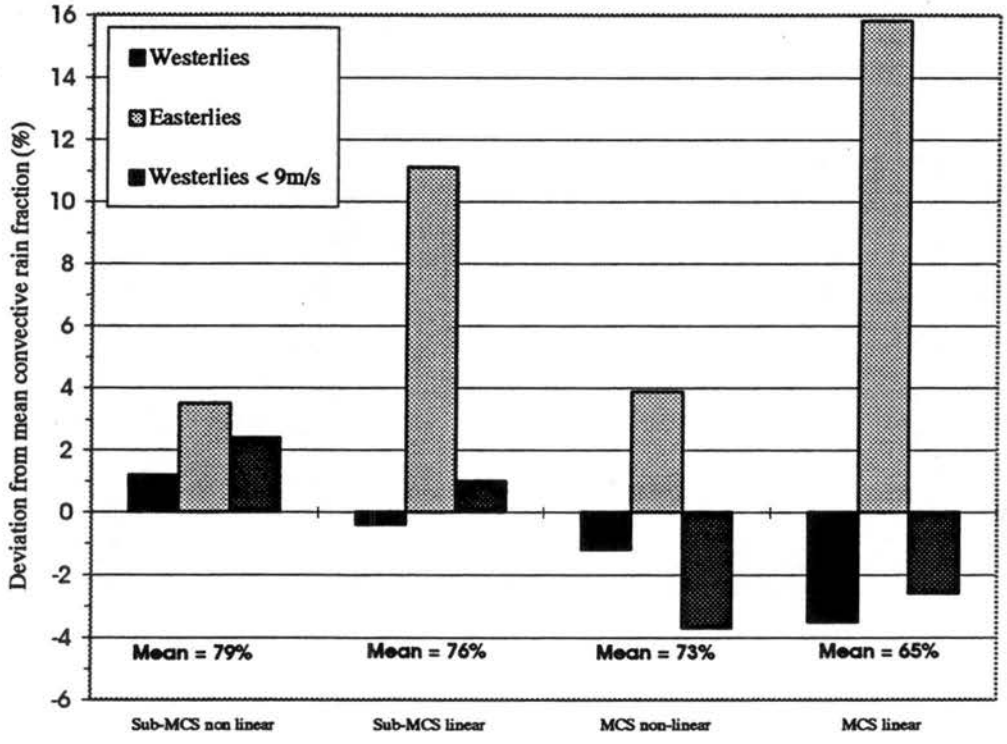

Figure 3.16. As in Figure 3.12, but for periods of low level westerly wind, low level easterly wind, and low level westerly wind weaker than the strongest event mean low level easterlies (< 9 m s^{-1}).

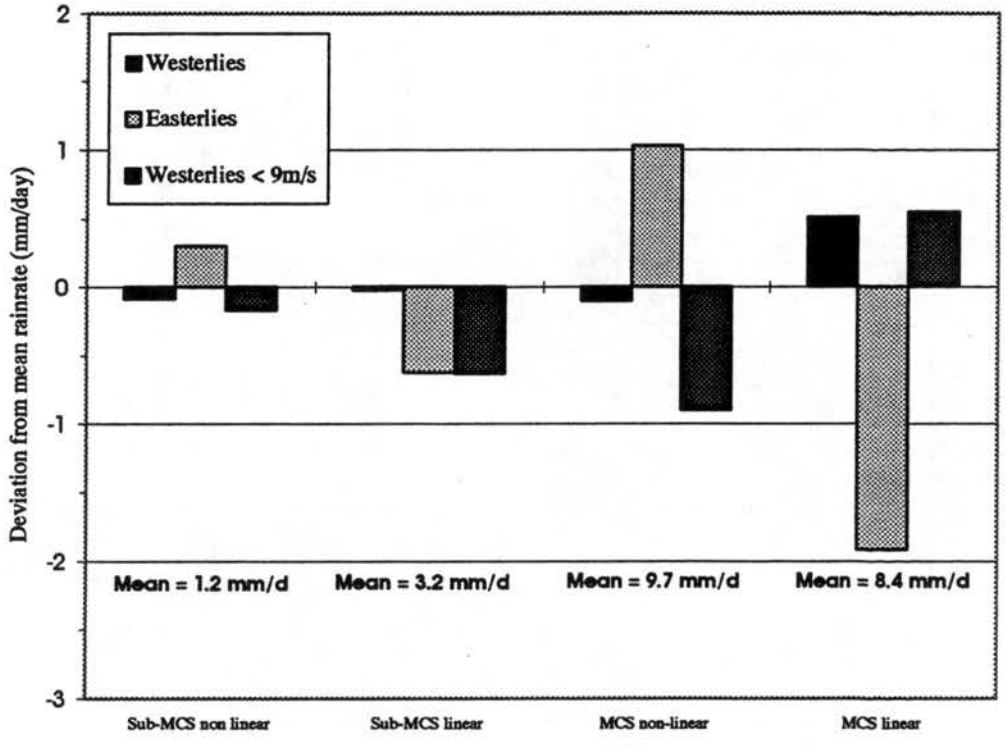

Figure 3.17. As in Figure 3.12, but for mean rainfall rate (mm day^{-1}) during periods of low level westerly wind, low level easterly wind, and low level westerly wind weaker than the strongest event mean low level easterlies (< 9 m s^{-1}).

3.6 Summary of each mode of convective organization

It has been shown that fundamental differences exist in the occurrence frequency, rainfall, and convective echo population in MCS vs. sub-MCS scale of convective organization. Sub-MCS scale events were present 60% of the time, but 80% of the total rainfall was associated with the spatially larger and locally more intense MCS scale events. Rainfall on the sub-MCS scale was associated with a large number of relatively small, shallower convective rainfall features. In contrast, MCS scale rainfall was produced by fewer, larger, and deeper features. Furthermore, the mean sub-MCS scale convective rainfall fraction was 10% higher than that for the MCS scale. These general observations provide the context for a discussion of each organizational mode.

3.6.1 Sub-MCS scale non-linear events

Sub-MCS scale non-linear events were the most common mode of convective organization. Despite the limited spatial coverage of precipitation, these events produced a non-negligible fraction (16%) of the total sampled rainfall. Rainfall from this event type had the highest mean convective rainfall fraction of any organizational mode. Heating was very weak compared to MCS scale events, and is mainly confined to mid levels (650 mb - 400 mb). Heating and moistening were very weak above 450 mb, suggesting the absence of non-convective rain production mechanisms beyond the decay of convective cells. The moistening which occurred below 650 mb (3 km) was likely

associated with the presence of shallow non-precipitating cumulus clouds (Lin and Johnson 1996b).

The environment of sub-MCS scale non-linear events appeared to be most easily distinguished by the tropospheric relative humidity. The mean relative humidity profile showed substantially lower values at all levels compared to the other organizational modes, while the mid level relative humidity inversion was shallow and weak. Interestingly, mean convective rainfall fractions were lower during periods containing the driest mid level air, while for the same periods rainfall was nearly absent from deep convection. These observations suggested that the mid level dry air may cause convective cells to cease vertical development and to collapse. The prevalence of a large population of collapsing convection may account for the increased fraction of non-convective rainfall for those periods. The lower convective rainfall fraction associated with periods of stronger mid level convergence and low level divergence (which are consistent with the presence of widespread decaying convection) supports this hypothesis. Total rainfall production was slightly increased during periods of high mid level relative humidity, as was rainfall from deeper convective features. The presence of greater amounts of mid level moisture may allow deeper and larger convective features to persist. This moisture may further be augmented by condensate detrainment from deep convection.

The occurrence of sub-MCS scale non-linear events spanned periods of strong and weak low level winds, occurring only slightly more often during weak winds. This suggests that windspeed was not tied to the presence of sub-MCS scale non-linear events;

rather, the presence of this event type was linked more closely to profiles of tropospheric relative humidity.

3.6.2 Sub-MCS scale linear events

Sub-MCS scale linear events produced the lowest amount of rainfall compared to the other organizational modes, because linear organization rarely occurred on the sub-MCS scale. Their presence was most common during periods of both strong low level winds and dry mid level air[4]. However, the greatest rainfall occurred during periods of strong wind and moist mid level air, while the highest convective fractions were observed during dry mid level air periods. Strong low level convergence may act to mechanically force rising parcels through this dry layer to sustain convection. These observations imply that the environment of sub-MCS scale linear events was not conducive to non-convective rain production, even though the mean relative humidity profile and visual observations suggest the presence of a non precipitating upper level cloud deck was often present during these events[5]. The presence of mid level cooling and moistening suggested the presence of virga evaporating into the dry mid-level air. Intense moisture flux from the ocean surface due to the strong low level winds could account for a shallow layer (< 1 km) of strong moistening near the surface.

Two factors may account for the high convective rain fraction associated with sub-

---

[4] Both conditions were dominant during the last week of Dec. 1992 (Lin and Johnson 1996a), when sub-MCS scale linear events were most common.

[5] Veldon and Young (1994) discuss the westward advection of extensive cirrus clouds toward the IFA from cloud clusters located thousands of kilometers east of the Vickers during late December 1992.

MCS scale linear events. The first was the presence of an extremely dry layer of mid level air, which could cause the evaporation of non-convective condensate. This may prevent the formation of broad regions of non-convective precipitation. The second was the presence of mean mid level divergence, suggesting that convergent mid level flow features (often associated with stratiform rain regions) were absent. Furthermore, the strong tropospheric shear present during the strong wind periods (Lin and Johnson 1996a) appeared to be associated with the occurrence of sub-MCS scale linear events. The shear at low levels may have been too strong to maintain a balance with the vorticity associated with propagating cold pools (Rotunno et al. 1988), so that lines that managed to form in this environment were small and short-lived. It is therefore hypothesized that the presence of dry mid level air and strong tropospheric shear may have inhibited the upscale growth of these lines to the MCS scale.

3.6.3 MCS scale non-linear events

MCS scale events with no linear organization produced the highest mean rainfall rates of any organizational mode. The high mean rainfall rate results from broad areal coverage of precipitation combined with a mean convective rainfall fraction higher than that of MCS scale linear events. Although strong low level convergence and upper level divergence are present consistent with widespread strong convection, weak divergence exists at mid levels. This observation suggests that these events may lack the mid level mesoscale convergence associated with colliding mid level horizontal flow features (e.g.

Smull and Houze 1987). The lack of mid level convergence may thus account for the higher mean convective rain fraction for MCS scale non-linear events compared to linear events. The weaker vertical motion at mid levels for non-linear events may be related to the absence of mid level convergence. However, the presence of strong mid level heating and drying near 400 mb is consistent with latent heat release in a mesoscale updraft. It is suggested that residual upper level upward motion from decaying convection may be sufficiently strong that depositional growth of detrained upper level condensate could occur in the moist environment.

MCS scale non-linear events had a mean relative humidity profile of greater magnitude at all vertical levels than the other organizational modes, associated with the presence of strong upward motion throughout the troposphere and the presence of deep convection. Deep convective reflectivity features (15-16 km) dominated the rainfall production, with a secondary rainfall maximum from mid level (8-9 km) features. The mid level moisture inversion extended much deeper than that of sub-MCS scale perhaps associated with the presence of the population of deeper clouds. Furthermore, deep convection may have been favored because it was embedded within non-convective rain, since the air entraining into convective cells is moist due to to the surrounding evaporating non-convective rain.

3.6.4 MCS scale linear events

MCS scale events with linear organization produced the lowest mean convective rainfall fraction of any mode. The key difference in the environment for these events compared to the non linear MCS scale mode was that MCS scale linear events contained strong mid level convergence. The strong mid level convergence associated with MCS scale linear events was a common feature of the non-convective portion of previously studied squall lines (Houze 1989, Mapes and Houze 1993). This feature was evidence for the presence of convergent horizontal flow features, which have been shown to play a crucial role in augmenting non-convective rain production by generation of mesoscale ascent and by upper level condensate advection (i.e. Rutledge and Houze 1987). The strong heating and drying near 400 mb may have resulted from depositional growth of condensate and subsequent latent heat release in a mesoscale updraft. The composite vertical motion profile showed upward motion at upper levels, consistent with the presence of mesoscale ascent. Mesoscale upward motion in the non-convective regions associated with MCS scale squall lines has been commonly observed (e.g. Gamache and Houze 1983, Houze 1989). Moreover, the mean convective rainfall fraction (64%) was within the range of values from previous case studies of MCS scale squall lines, as discussed in Sec. 3.2. Observations point to the relation of strong low level winds (and thus deep shear), high mid level relative humidity, and mid level convergence to the production of widespread non-convective rain.

The effect of wind direction on the rainfall was significant in MCS scale linear

events, with higher convective rain fractions and lower rainfall rates during easterly winds. This was not observed for MCS scale non-linear events. The wind direction dependence on linear event rainfall may underscore the importance of deep shear on augmenting mesoscale flow features (and thus non-convective rain) in MCS scale linear events, because the tropospheric shear was weakest during low level easterly winds (Lin and Johnson 1996a).

CHAPTER 4

DEPENDENCE OF THE DIURNAL VARIATION OF RAINFALL ON CONVECTIVE ORGANIZATION

In this chapter, the diurnal variation of rainfall measured by shipboard radar is examined in the context of the modes of convective organization discussed in chapter 2. These observations are compared to the diurnal changes in vertical profiles of several environmental variables in order to study the physical mechanisms which affect the rainfall variability.

4.1 Previous studies of diurnal rainfall variability

The daily oscillation in solar insolation may be thought of as a recurring natural experiment to observe the atmosphere's response to regular variations of its most fundamental forcing source. Yet after decades of study, the question of how the diurnal variation in land, ocean and atmospheric heating results in a daily rainfall variation is not well understood, particularly over the tropical oceans. A robust conceptual model of the links between the daily cycle of solar insolation and rainfall over the oceans has proved

elusive. In part, this reflects the historic scarcity of direct rainfall measurements over the tropical oceans.

Observations from raingauge data in the mid-latitude oceans (Krause 1963) and small tropical islands (Finkelstein 1964), as well as from ship radar reflectivity data in the tropics (Holle 1968) suggested that oceanic rainfall was more intense and more frequent at night. Gray and Jacobsen (1977) used atoll and small island raingauge data in the tropical western Pacific to show that the largest amplitude in the diurnal rainfall variation was associated with large disturbances, again with a nocturnal maximum. They hypothesized that nocturnal subsidence associated with radiational cooling in the cloud free regions surrounding a cloud cluster would induce low level convergence into the cloudy region, augmenting the upward motion and rainfall in the pre-existing disturbance. Although not ruling out this mechanism, Randall et al. (1991) used a general circulation model to show that daytime stabilization of the lapse rate by solar absorption at cloud top can by itself explain the nocturnal maximum of rainfall over the tropical oceans. Xu and Randall (1995) produced a similar result with a cumulus ensemble model.

Other observations revealed further complexity in the phase of the oceanic rainfall diurnal variation. An early afternoon maximum in rainfall was observed 500 km from the west African coast during the GARP Atlantic Tropical Experiment (GATE; McGarry and Reed 1978). This result was hypothesized to reflect a time delay of disturbance propagation from the genesis region over the African continent to the GATE array off of the coast. In a study of oceanic convection near the coast of Borneo, Houze et al. (1981)

found a large amplitude mid-morning maximum in rainfall, which they attributed to the life cycle of individual mesoscale convective systems (MCSs). Convective cells were initiated near midnight in the convergence region associated with the nocturnal offshore flow and the monsoonal flow, evolving into a mature MCS after sunrise. Thus, both the proximity to land and the evolution of convective systems influenced the daily rainfall variability, because the typical life cycle time scale of MCSs and the seabreeze circulation time scale were a significant fraction of a day.

More recent studies have used satellite measurements of outgoing longwave radiation (OLR) from cloud tops to infer the variation of rainfall associated with deep convection. Although instantaneous satellite observations can cover an entire ocean basin, they do not measure rainfall directly but rather the radiation from upper level cloudy regions associated with groups of convective systems. The assumption is generally made that the lower the OLR at cloud top, the more intense the underlying convection and the higher the rainfall rate[1]. In the south Pacific convergence zone, Albright et al. (1981) found that the coldest (deepest) cloud areas peaked near sunrise, while the warmer (lower) cloud areas peaked in the afternoon. They hypothesized that this observation represented the evolution of individual MCSs from the more vertically developed clouds of the mature stage to the mid-level anvil clouds of the decaying stage (c.f. Leary and Houze 1979). Chen and Houze (1996) hypothesized that the evolution of convection from scattered afternoon cells to a mature nocturnal MCS explained the diurnal variation of cloudiness over the equatorial western Pacific ocean. Hendon and Woodberry (1993) reached a

[1] Clouds with very low values of OLR are sometimes generically referred to as "cold cloud" because of the low brightness temperature associated with the cloud tops.

similar conclusion for cloudiness in the ITCZ regions. For tropical Atlantic cloudiness, Machado et al. (1993) came to a different conclusion from a similar observation. They interpreted the phase difference between diurnal variations in colder vs. warmer clouds as intensity differences between day and night systems, not the evolution of convective cells into MCSs at a preferred time of day. The larger cloudy regions exhibited the highest amplitude diurnal variation, a result corroborated by Mapes and Houze (1993) for the western Pacific ocean, and consistent with the mechanism of Gray and Jacobsen (1977).

This chapter explores the question of how the diurnal rainfall variation differs with the structure and organization of convection. This can provide insight as to the mechanisms which produce not only diurnal rainfall variability but convective variability in general. The main goal of the present chapter is to assess the roles of precipitation organization and system evolution in producing the observed diurnal variation of rainfall in the western Pacific warm pool region, using rainfall estimates from shipboard radar. Moreover, it is instructive to consider the relationship of the environment to the occurrence and organization of precipitating clouds in order to interpret the daily variability of rainfall. The radiosonde network characterized the local and synoptic scale environment in the vicinity of the ship radars as discussed in Chapter 2 (Lin and Johnson 1996). These data were used to characterize the diurnal variation in rainfall in terms of the scale and morphology of convective organization, and the environment within which the convection occurred.

Diurnal composites of the convective, non-convective, and total rainfall rate for the ninety day time series were produced by calculating the average deviation at each hour of

the day from the three month mean. The same was done for rainfall from the integrated periods that each event type was present. Thus, a total of fifteen diurnal rainfall rate composites were constructed, representing the diurnal variation of convective, non-convective, and total rainfall for linear and non linear sub-MCS scale events, linear and non linear MCS scale events, and the combination of all events. Harmonic analysis (e.g. Panofsky and Brier 1968) was then applied to each diurnal composite. The first 35 harmonics were calculated and the fraction of each composite's variability explained by each harmonic was determined. The phase and amplitude of each harmonic were also calculated.

The environmental variables examined were divergence, vertical motion, temperature, specific humidity, and relative humidity. Composite vertical profiles of these parameters were constructed from these data at 10LT (0000 UTC), 16LT (0600 UTC), 22LT (1200 UTC) and 04LT (1800 UTC) to estimate their diurnal variability. As with rainfall, composites of these variables were also produced for the periods when each of the four categories of convective organization were present.

4.2 COARE-mean diurnal rainfall variation

The "all event" diurnal composites for total, convective, and non-convective rain are shown in Fig. 4.1. These composites represent the daily variation of rainfall for all of COARE, not partitioned by convective organization. The peak values for each rain composite occurred between midnight and 03LT. This was generally consistent with

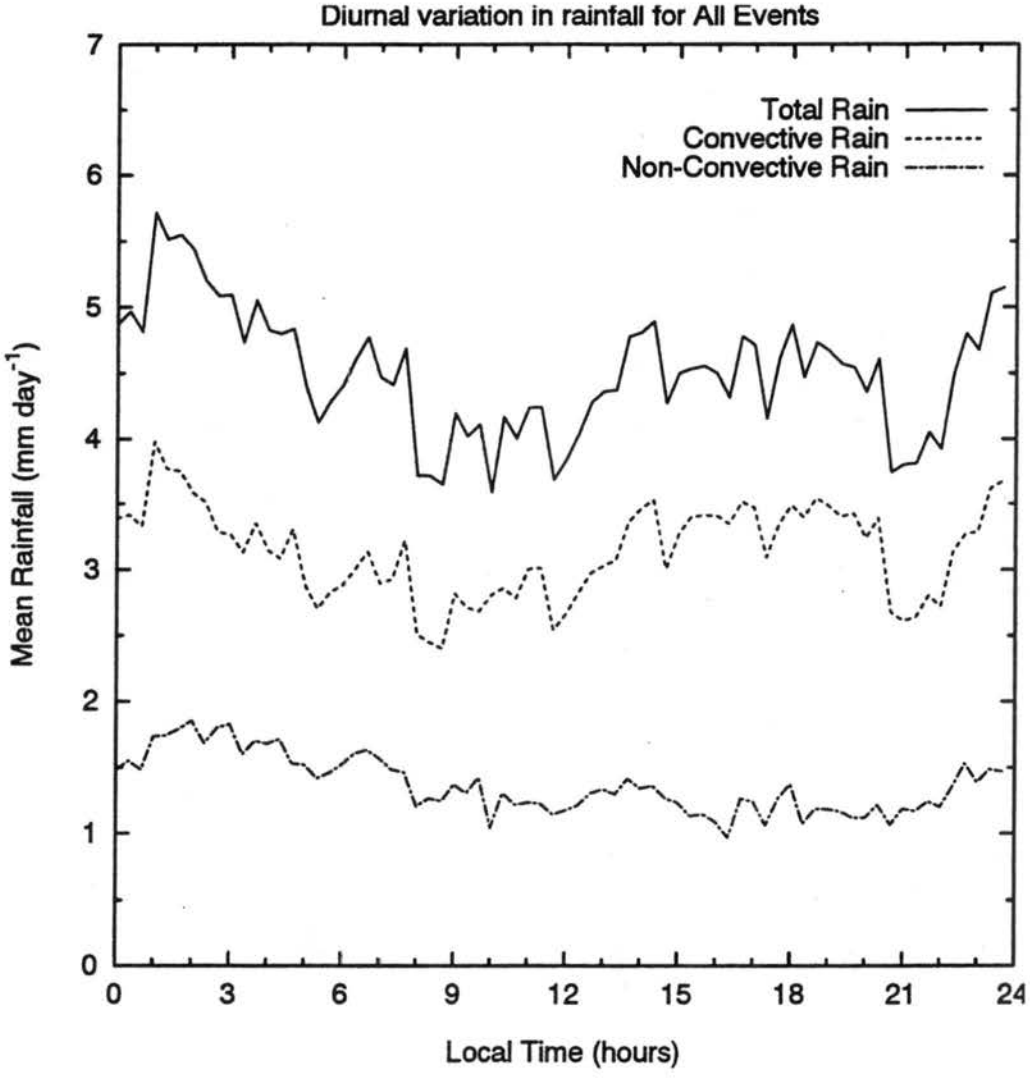

Figure 4.1. Diurnal composites of total rain, convective rain, and non-convective rain (mm day^{-1}) for all event types combined.

results from direct rainfall measurements from gauges. Janowiak et al. (1994) found the highest frequency of heavy rain events at 03LT from optical rain gauge data during COARE. The convective rain composite was quite similar to the total rain composite since 69% of the total rainfall was convective (Chapter 3). The total rain and convective rain composites displayed a weaker and broader secondary maximum in the mid to late afternoon, which is not present in the non-convective rain composite. However, the amplitude and phase of the daily variation were not at all obvious.

Given the high degree of variability in the diurnal composites, it was important to assess what portion of each composite was associated with true diurnal variation. The first (diurnal) and second (semi-diurnal) harmonics[2] of the total rain composite are shown in Fig. 4.2. Only 27% of the variance in the total rain diurnal composite (Fig. 4.1) was explained by the first harmonic. The diurnal harmonic of total rain indicated a maximum at 01LT, with an amplitude of 0.37 mm day^{-1} (8% of the mean of 4.5 mm day^{-1}). This suggested that although there is diurnal variability in the total rainfall, it is weak. In fact, more variance was explained by the semi-diurnal harmonic (33%), with maxima at 03LT and 15LT and amplitude of 0.40 mm day^{-1}. Therefore, the three month total rainfall in COARE contains weak yet significant[3] diurnal and semi-diurnal variations of equal importance.

The diurnal and semi-diurnal harmonics of the "all event" convective and non-convective rain composites are shown in Fig. 4.3. As for total rain, the diurnal amplitude

[2] Only the first two harmonics (diurnal and semi-diurnal) are discussed in this chapter, since no more that 8% of the variance is explained by any other individual harmonic for each diurnal composite shown.
[3] In this context, the term "significant" describes a harmonic which explains at least one-fourth of the variance of a diurnal composite.

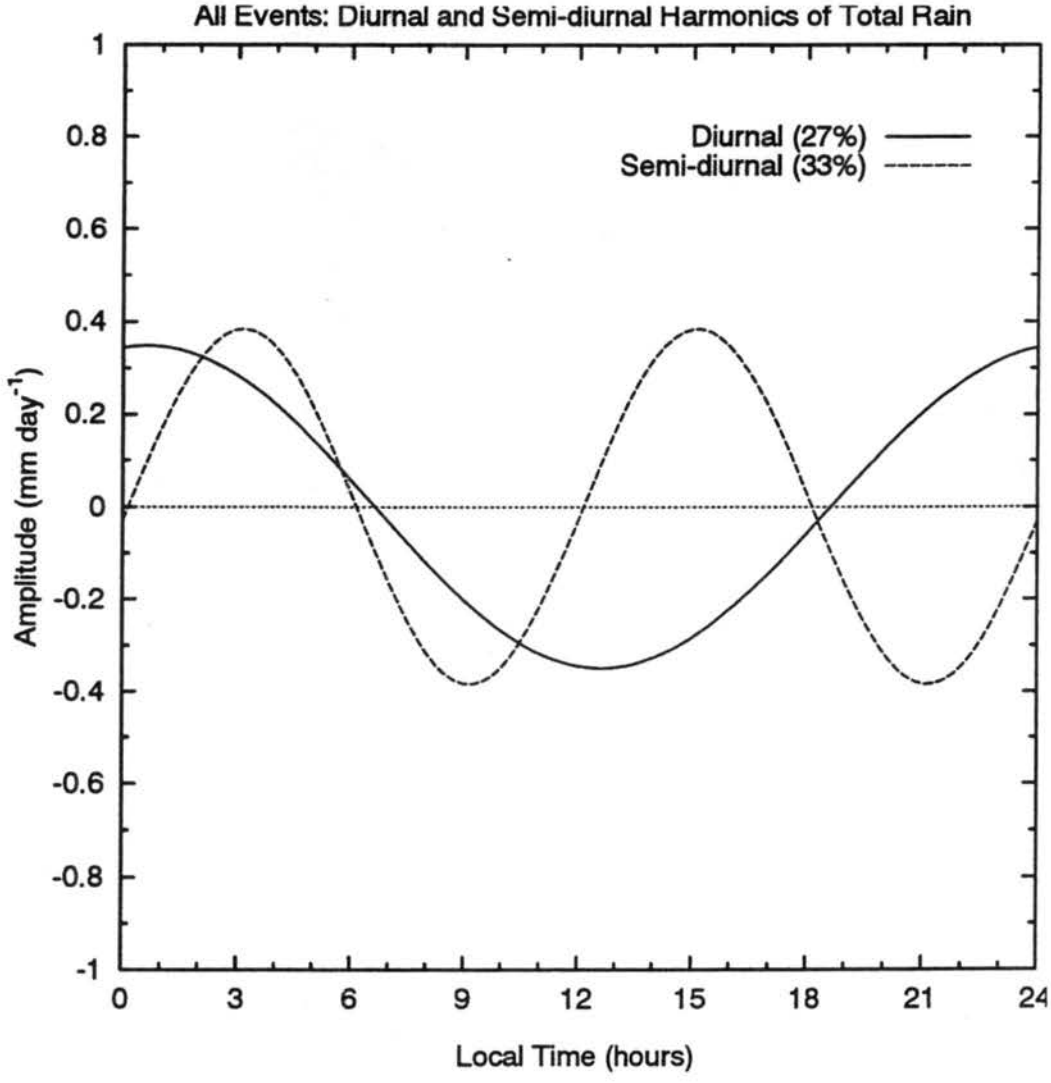

Figure 4.2. The first two harmonics (diurnal and semi-diurnal) of the diurnal composite of total rain for all event types combined. The fraction of the variance in the diurnal composite explained by each harmonic is indicated in the legend.

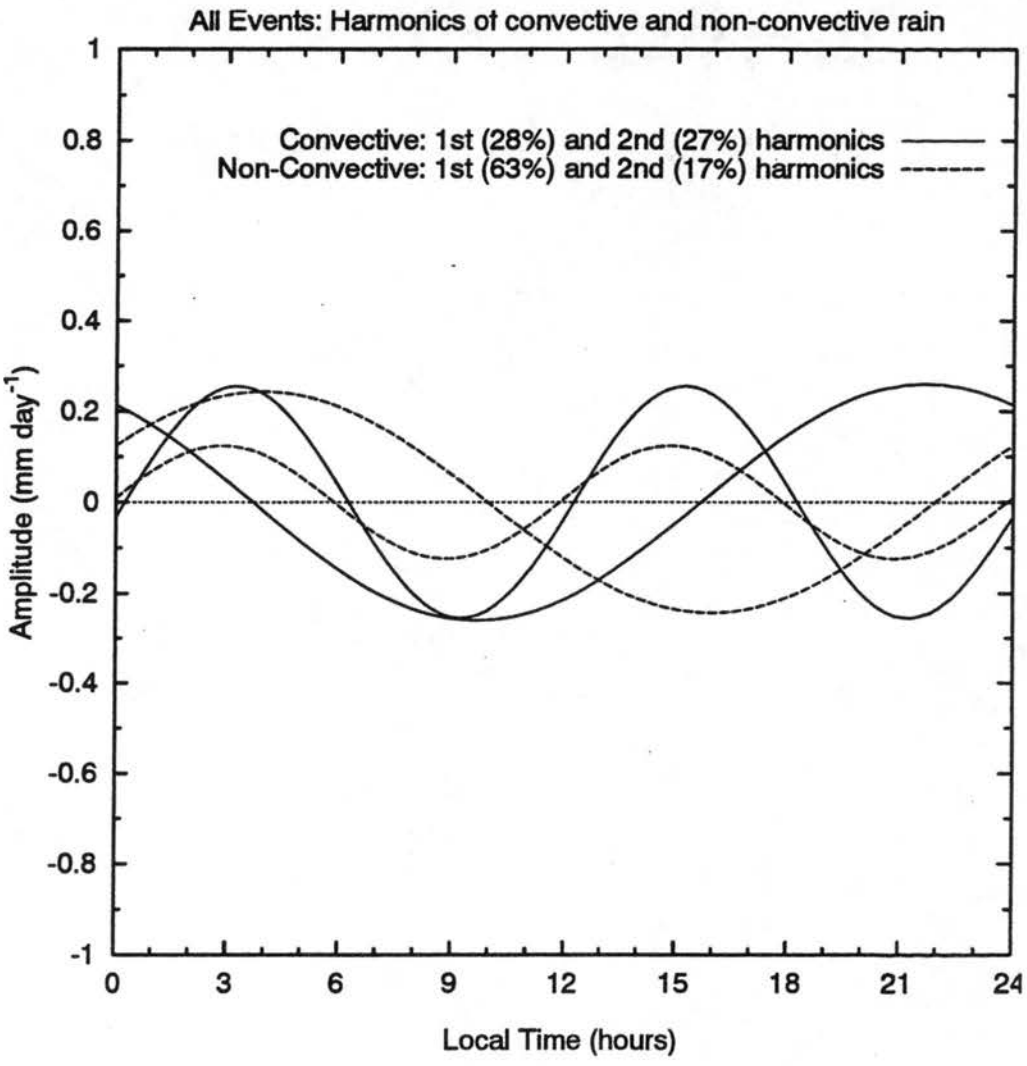

Figure 4.3. As in Figure 4.2, but for convective and non-convective rain.

of convective rain was about the same as the semi-diurnal amplitude, with just over one-fourth of the variance explained by each harmonic. However, the non-convective rain diurnal harmonic explained 63% of the total variance, and just 17% for the semi-diurnal harmonic. Furthermore, the amplitude of the non-convective diurnal harmonic is 19% of the mean value.

These observations suggested that the diurnal variation of non-convective rain is greater than convective (or total) rain. One hypothesis to account for this was that nocturnal destabilization of cloud tops has a much stronger effect on the broad, uniform regions of non-convective rain than on groups of convective cells because vertical motion in anvil clouds is weak. Another hypothesis was that nocturnal convection during COARE was more vertically developed as evidenced by lightning flash rates (Petersen et al. 1996). This implies that more upper level condensate may be available for non-convective rain production at night. Furthermore, the peak in the convective rain diurnal harmonic (22LT) led that of the non-convective rain (04LT) by six hours (Fig. 4.3). Previous case studies of MCSs (Leary and Houze 1979, McAnelly and Cotton 1989) have shown that the peak convective rainfall leads the non-convective rain peak by several hours for individual systems, associated with the time delay of ice particle advection from the convective region into the adjacent non-convective region and subsequent fallout as surface rain. Whether the observed phase lag of the convective and non-convective diurnal harmonics may be related to the life cycle of MCS scale events will be discussed later in this chapter.

4.3 Diurnal variation by convective organization: overview

The diurnal variation of rainfall had different characteristics depending on the scale and morphology of convective organization. These differences provided insight as to the weak diurnal variation for the COARE-mean total rainfall discussed in section 4.1. Shown in Fig. 4.4 are the diurnal harmonics of the total rain composites for each mode of organization (c. f. Table 2.2). The spatially larger (MCS scale) events had a larger diurnal amplitude than the smaller (sub-MCS scale) events. This result was consistent with previous studies indicating that diurnal rainfall amplitude increased with increasing system area (Gray and Jacobsen 1977, McGarry and Reed 1978, Machado et al. 1993, Mapes and Houze 1993, Chen and Houze 1996). The diurnal harmonic explained nearly half of the variance for each mode, with the exception of about one-third for sub-MCS scale non-linear events. The phase of the diurnal variation differed between organizational modes. Rainfall from sub-MCS scale events was greatest in the early evening: at 20LT for non-linear events and at 22LT for linear events. There was a much larger difference between MCS scale events: linear event rainfall peaks at 19LT, while non-linear event rainfall peaks at 0230LT. These observations highlighted fundamental differences in the diurnal character of rainfall by the scale and organization of convection. Furthermore, this suggested that *the weak diurnal variation in the COARE mean total rainfall was composed of stronger, out-of-phase diurnal rainfall variations associated with each mode of organization.*

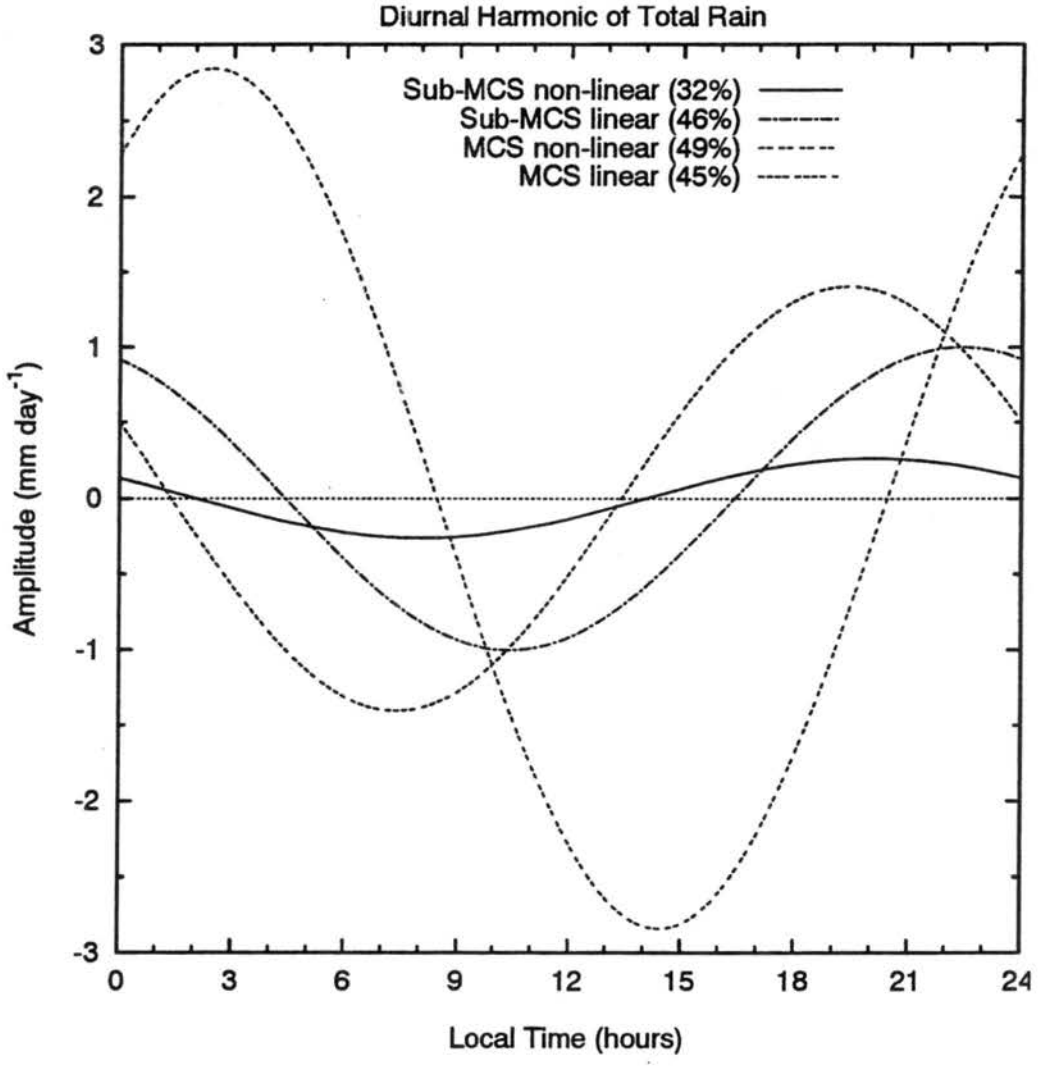

Figure 4.4. The first (diurnal) harmonic of the total rain diurnal composite for each mode of convective organization. The fraction of the variance in the diurnal composite explained by the first harmonic is indicated in the legend.

Chen and Houze (1996) concluded that the evolution of scattered convection in the afternoon into a mature MCS at night accounted for the observed diurnal variation of cloudiness in COARE. This hypothesis implied that there should be a tendency for MCS scale events to have peak rainfall rates at night. However, as shown in Fig. 4.5, there was no preferred time of day for the maximum rainfall of any event type to occur[4]. This observation suggested that the diurnal variation in rainfall may be linked to differences in the size, intensity and duration of daytime versus nighttime convective events, not the evolution of individual events throughout the day. That is, convective events which occur in the early to late evening produced more rainfall than those which occurred during the daytime. This is consistent with the conclusion of Machado et al. (1993) that the diurnal variation of oceanic convection was mainly a day versus night modulation of existing cloud clusters, rather than the evolution of scattered convection into organized large systems at a preferred time of day. Chen and Cotton (1988) found that radiative cooling of MCS cloud tops (which is enhanced at night) resulted in stronger horizontal flow features and mesoscale vertical motion within the system. This provided further evidence that nocturnal MCSs may differ in intensity compared to daytime MCSs.

The semi-diurnal harmonic of the total rainfall diurnal composites for each organizational mode is shown in Fig. 4.6. The sub-MCS scale non-linear event

[4] Note that the evolution of sub-MCS scale events into MCS scale events is not considered, since a precondition for a sub-MCS scale event to be defined as such is that it does not evolve into an MCS scale event (Chapter 2).

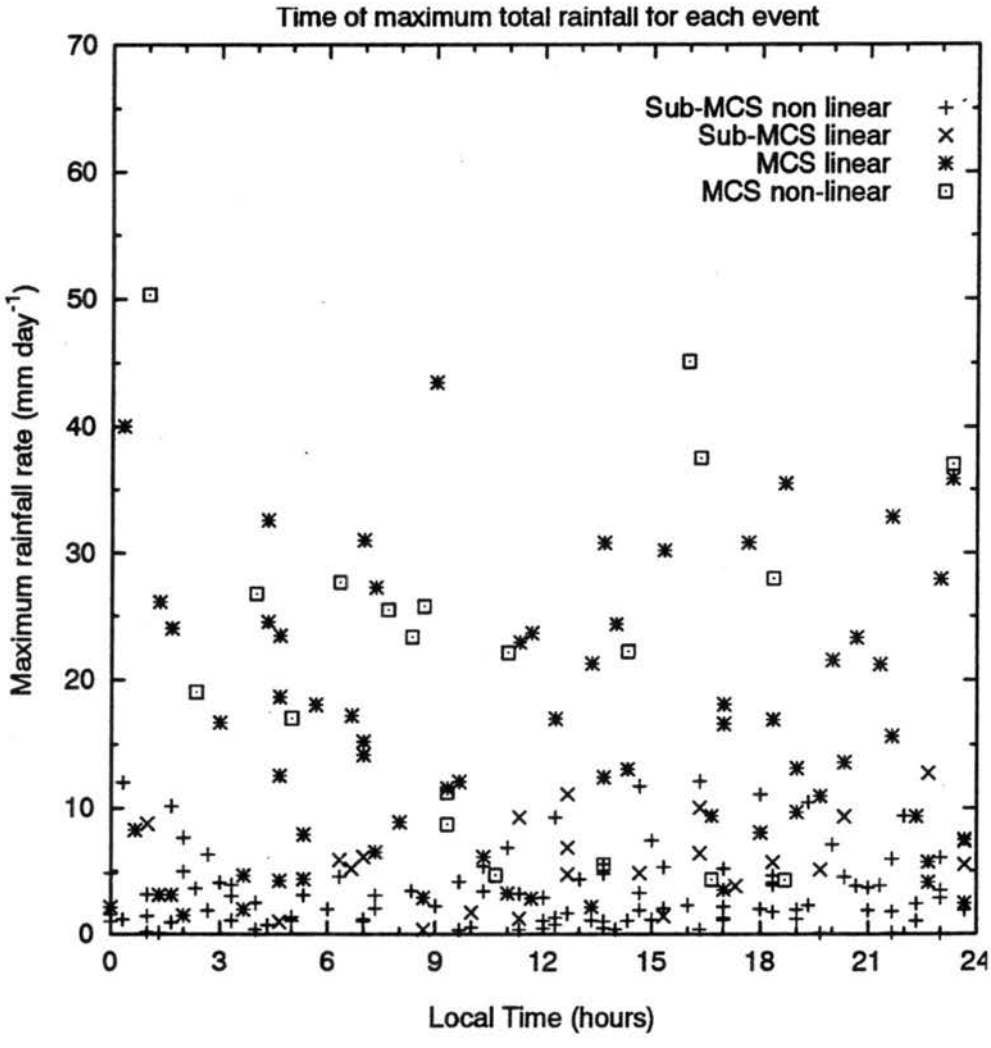

Figure 4.5. The time of day of the maximum total rainrate for each event.

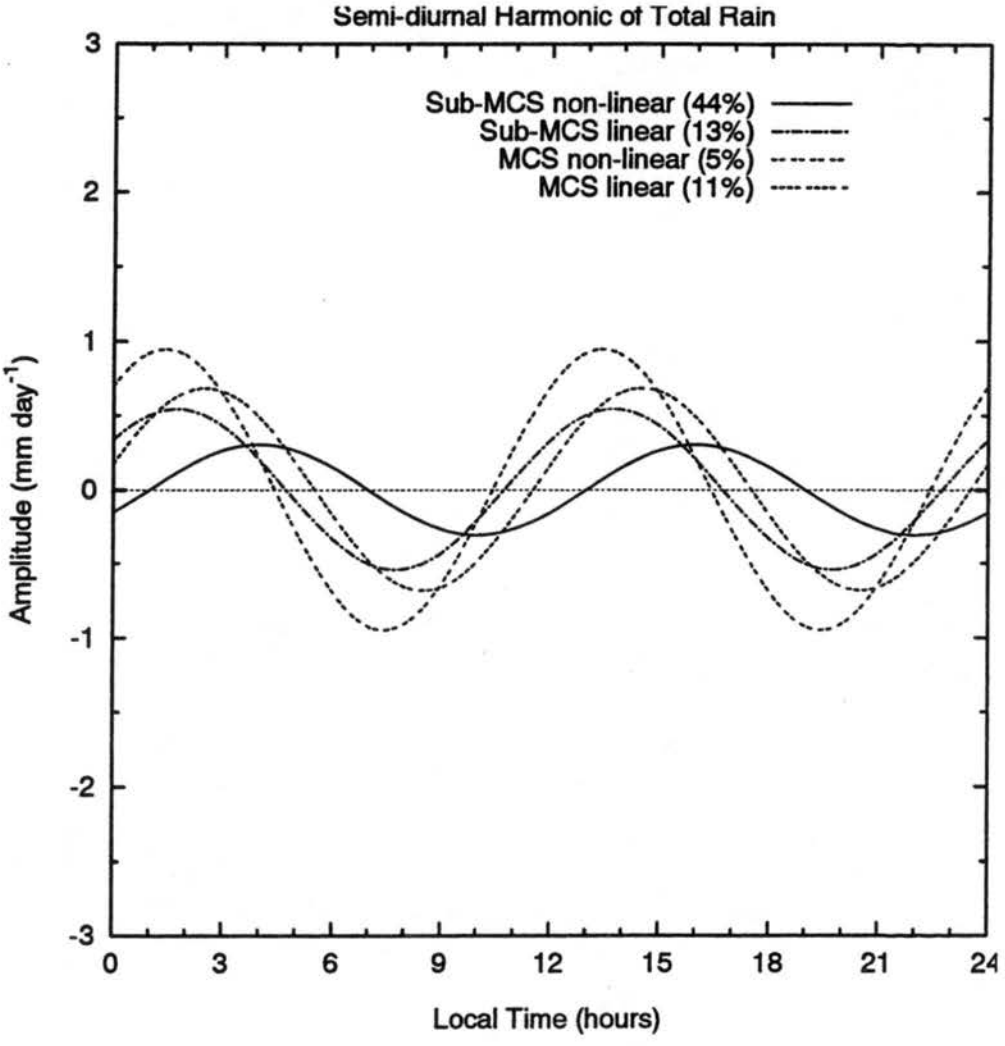

Figure 4.6. As in Figure 4.4, but for the second (semi-diurnal) harmonic.

composite had more variance explained by the semi-diurnal harmonic (44%) than by any other harmonic, with maxima at 04LT and 16LT. The semi-diurnal harmonic of all other organizational modes was very small compared to their respective diurnal harmonics[5]. Thus, the semi-diurnal rainfall variation was only significant in sub-MCS scale non-linear events, where it was actually the dominant harmonic. The hypothesis that the semi-diurnal pressure tide may have had a measurable effect on rainfall from this organizational mode is discussed later in this chapter.

The diurnal variation of convective and non-convective rainfall partitioned by convective organization provided further insight into the mechanisms which produce the diurnal cycle of rain. It should be kept in mind that non-convective rain production mechanisms differed for MCS versus sub-MCS scale events (Chapter 3). Non-convective condensate was likely augmented by growth in a mesoscale updraft for MCS scale events. On the sub-MCS scale, non-convective rain was composed simply of condensate fallout associated with decaying convective cells. Shown in Fig. 4.7a-b are the time of occurrence for the maximum convective and non-convective rainfall for each individual event. There was no tendency for either rain type to peak more frequently at a certain time of day (the same is true for total rain; c.f. Fig. 4.5). However, there was a tendency for the highest convective rain peaks to occur between 16LT and 00LT. The highest non-convective rain peaks generally occurred between 00LT and 07LT. These tendencies were most pronounced for MCS scale non-linear events. Thus, there was a mean phase lag of peak non-convective rain relative to convective rain of several hours

[5] The large semi-diurnal amplitude of the MCS scale modes explains very little of the total variance of the diurnal composite and thus is not significant.

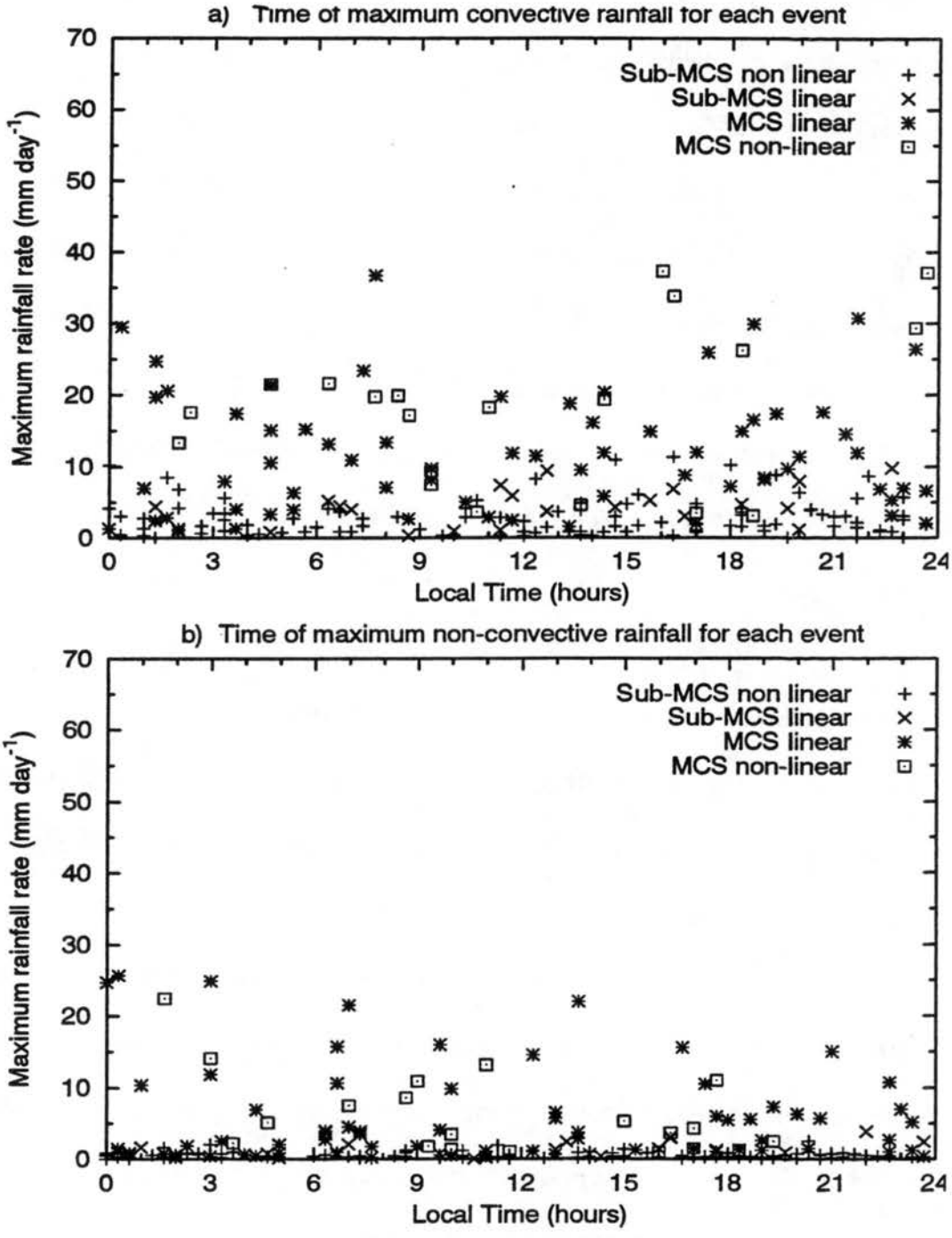

Figure 4.7. The time of day of the maximum a) convective, and b) non-convective rainrate for each event.

for the heaviest rain events. These figures suggested that the diurnal variation of rainfall was dominated by a few heavy rain events. Although the evidence for a mean phase lag was weak, it may have been a life cycle signature of these large events. To examine these points in detail, the diurnal composites and harmonic analyses of convective and non-convective rain for each organizational mode are presented in the next four subsections.

4.4 Sub-MCS scale non-linear events

The diurnal composite of total, convective, and non-convective rainfall along with the first two harmonics of convective and non-convective rain for sub-MCS scale non-linear events are given in Figs. 4.8 and 4.9. The semi-diurnal variation was clearly evident in the diurnal composites for total and convective rain, with the 16LT peak slightly greater than the 04LT peak. The non-convective variation was quite small by comparison. The convective rainfall had nearly the same variance in the first two harmonics (37% and 42%: Fig. 4.9), similar to that of total rainfall as discussed in Section 4.2. The non-convective semi-diurnal harmonic explained nearly the same variance and was in phase with the convective semi-diurnal harmonic, though it had a much weaker amplitude. As mentioned in Chapter 3, non-convective rain for these events results from settling ice particles within decaying convective cells following the collapse of the updraft. Individual convective cells had life cycle timescales of about an hour, so the population of convective cells at any given time was comprised of both

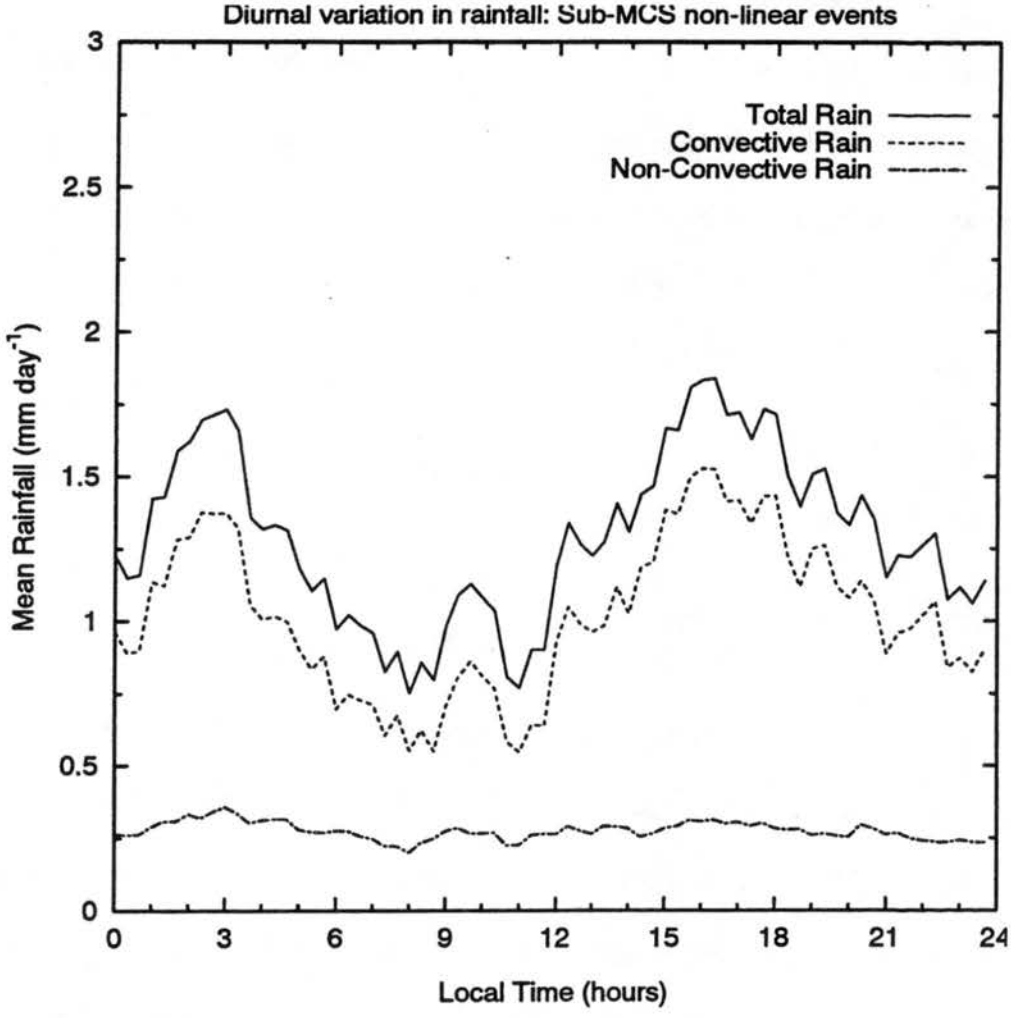

Figure 4.8. As in Figure 4.1, but for sub-MCS scale non-linear events.

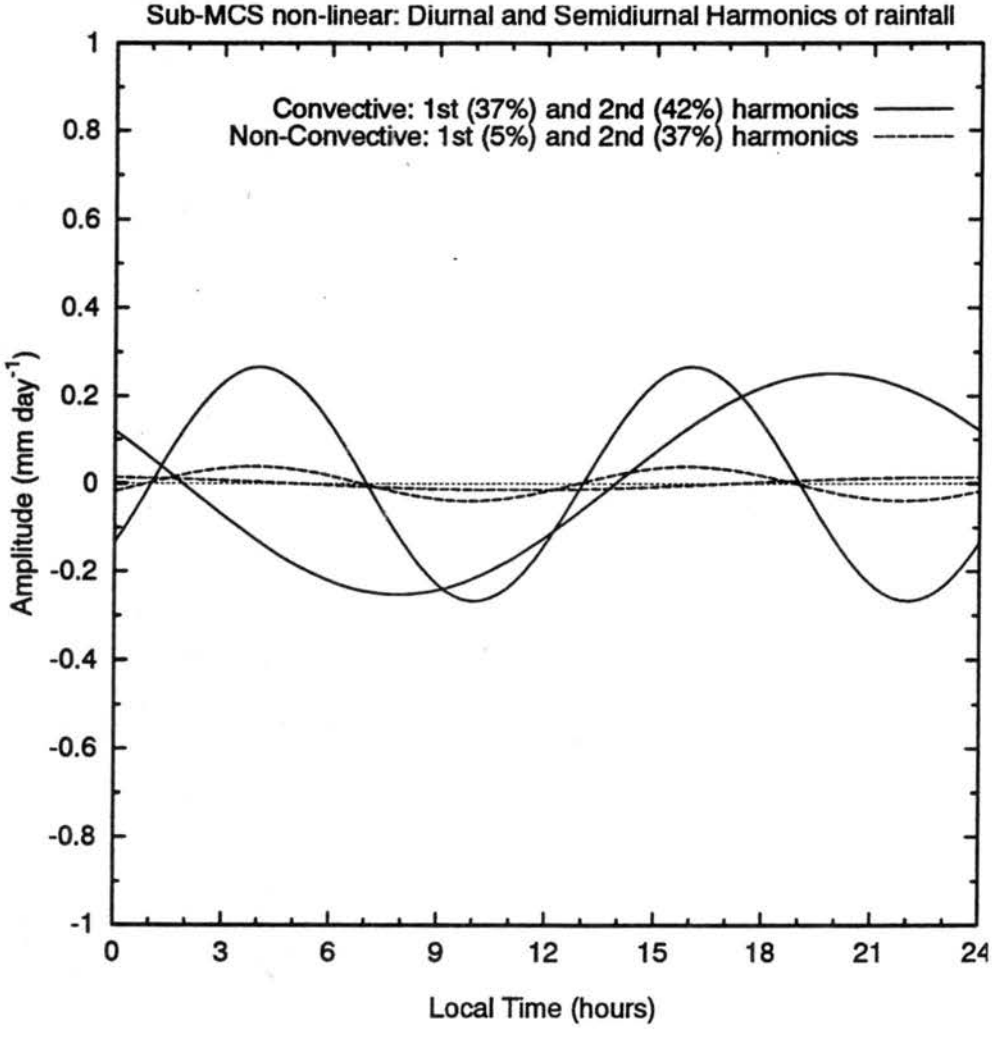

Figure 4.9. As in Figure 4.2, but for convective and non-convective rain of sub-MCS scale non-linear events.

active and decaying convection. This accounted for the similarity in the phase of convective and non-convective rain. The phase of the diurnal harmonic for convective rain suggested that early evening convection produced more rainfall, possibly related to boundary layer heating (see below). However, almost none of the non-convective variance was in the diurnal harmonic. These observations suggested that the semi-diurnal rain variation involved modulation of the ice phase of deep convection, while the diurnal rain variation involved warm rain processes. These latter processes may relate both to shallow clouds and to the portion of deep clouds which were below the melting level.

The sub-MCS scale non-linear event composite vertical profiles of vertical motion, temperature deviation, specific and relative humidity (Fig. 4.10a-d) provided insight to the physical mechanisms at work. The 16LT semi-diurnal rainfall maximum was associated with relatively strong upward motion at 4 km, a moistening boundary layer, and high boundary layer temperature associated with daytime solar heating. High values of low level specific humidity after sunset (22LT, Fig. 4.10c) may act to decrease evaporation below the melting level and enhance warm rain production, resulting in the diurnal rainfall harmonic peak at 20LT. Higher nocturnal relative humidity values occurred at all levels compared to daytime, though values are generally low (less than 60%) above 750 mb at all times of day. By the time of the 04LT semi-diurnal rainfall maximum, low level vertical motion was nearly absent, while the boundary layer had cooled and moistened considerably. This was coincident with weaker convection and lower rainfall rates at 04LT compared to 16LT.

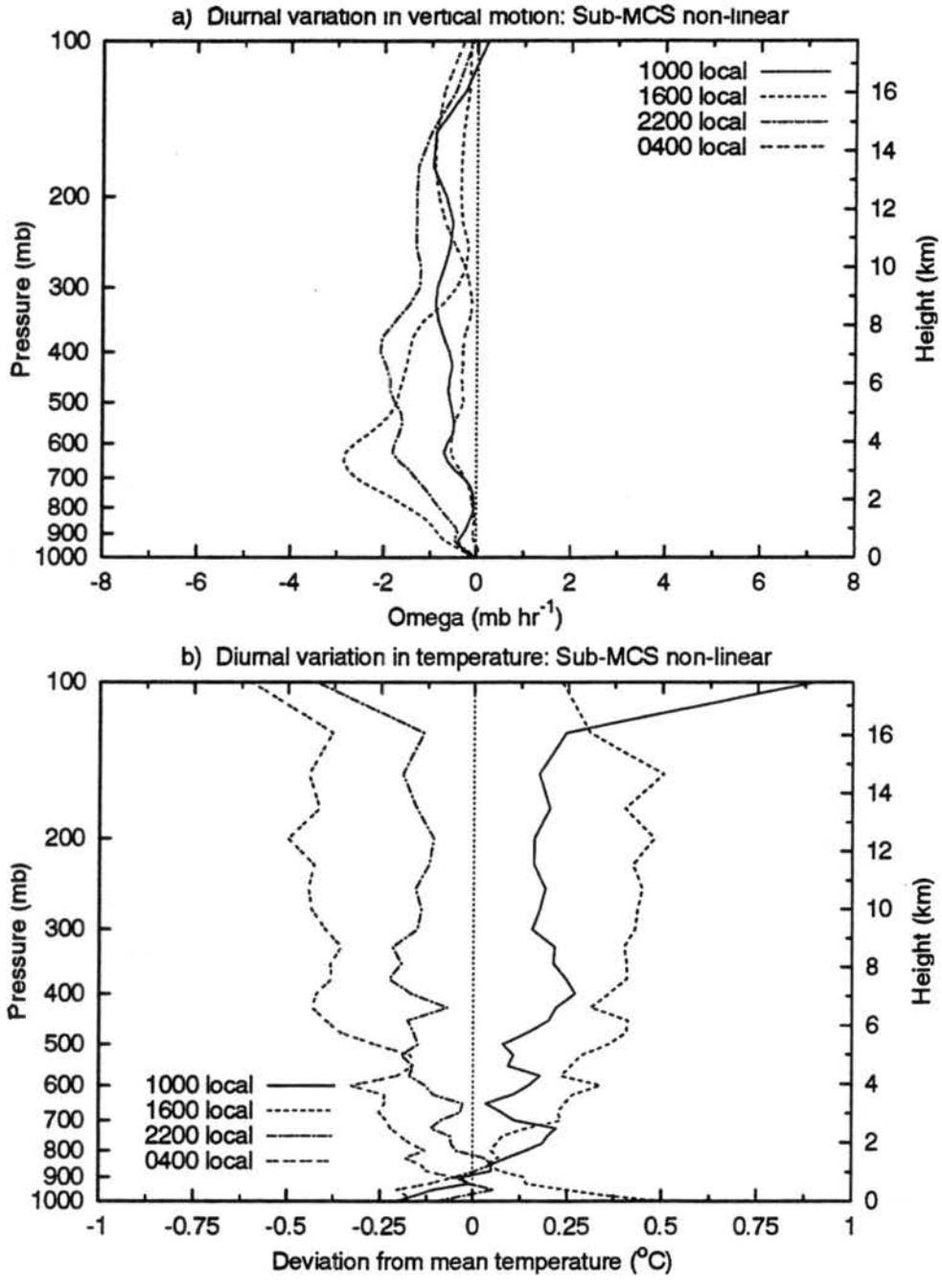

Figure 4.10. The diurnal variation of composited vertical profiles of a) vertical motion, and b) temperature from sounding data for sub-MCS scale non-linear events.

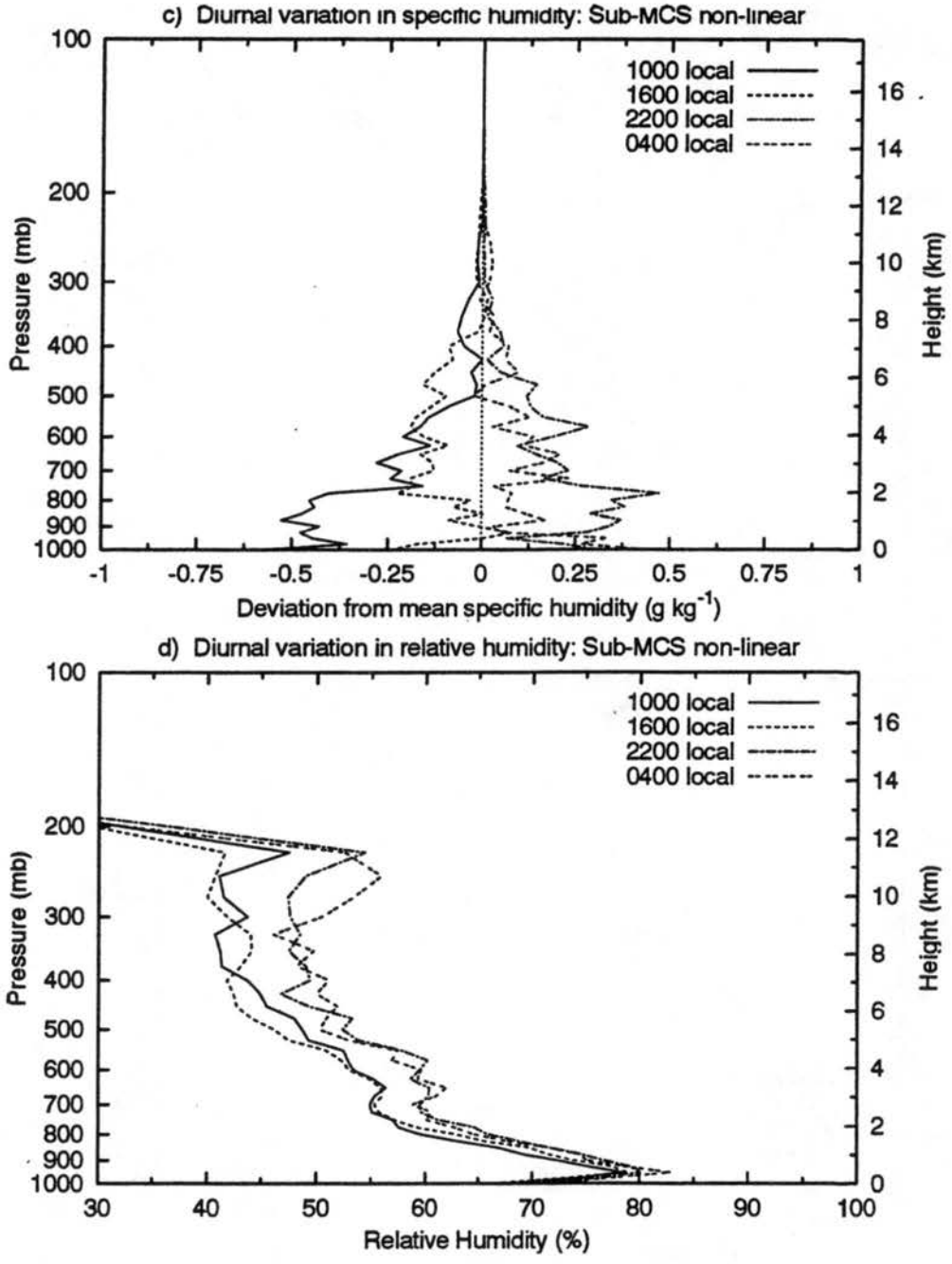

Figure 4.10. (continued) The diurnal variation of composited vertical profiles of c) specific humidity, and d) relative humidity from sounding data for sub-MCS scale non-linear events.

The phase of the semi-diurnal rainfall variation strongly suggested a link with the semi-diurnal surface pressure oscillation associated with the atmospheric tides, though the mechanism was not clear. This pressure wave has minima at 04LT and 16LT near the equator with a 1 mb amplitude (Haurwitz and Cowley 1973). Brier and Simpson (1969) have calculated that these pressure oscillations result in corresponding semi-diurnal surface convergence variations peaking several hours later (07LT and 19LT). They hypothesized that the small ($\sim 10^{-7}$ s^{-1}) amplitude of this convergence oscillation may slightly augment condensation rates in the cloud. Yet, typical convergence values in convective clouds are 10 to 100 times greater than this value. Furthermore, the observed semi-diurnal rainfall oscillations were in phase with the pressure oscillations. Using the TAO buoy array across the equatorial Pacific ocean, Deser (1994) observed semi-diurnal oscillations in surface zonal wind associated with the passage of the pressure wave. The westerly perturbation from the mean zonal wind (typical amplitude of 0.1 m s^{-1}) had maxima which lead that of surface pressure by one hour (03LT and 15LT). It was not readily apparent if or how these surface wind and convergence perturbations relate to the semi-diurnal rainfall oscillations of this event type, given the small magnitude of the perturbations. It is also possible that the mechanisms for the semi-diurnal rainfall oscillation are independent of the tides. Decreased column stability associated with higher nocturnal relative humidity values in the boundary layer and greater boundary layer temperatures in the afternoon may relate to the semi-diurnal rainfall variations.

4.5 Sub-MCS scale linear events

The diurnal composite of total, convective and non-convective rainfall for sub-MCS scale linear events along with the first two harmonics of convective and non-convective rain are shown in Figs. 4.11 and 4.12. Most of the variance was in the diurnal harmonic for both rain types (just over 40%), with very little variance explained by the semi-diurnal harmonic (around 15%). The similarity of the fraction of variance explained by both harmonics of convective and non-convective rain implied that both rain types were modulated together, as with the semi-diurnal variation in sub-MCS scale non-linear events. However, the peak in the non-convective rain diurnal harmonic (21LT) actually led that of convective rain (23LT) by two hours. This was likely related to the fact that generally several short lines were within the radar's view at any given time, each in an arbitrary state of evolution. It was therefore not appropriate to interpret the phase separation of the convective and non-convective diurnal harmonics in terms of the evolution of individual lines because the phase separation was random.

Upward vertical motion peaked at 22LT near 700 mb (Fig. 4.13a), consistent with the rainfall maximum near that time. Yet, at 22LT and 04LT very dry air existed at and below this level (Fig. 4.13b), while at 16LT the low level air was 3-4 g kg^{-1} more moist. This suggested that the nocturnal dry low level air may be a result of convective downdrafts, though the temperature profiles (not shown) were too noisy to support this inference. The high tropospheric specific humidity in the afternoon corresponded to the time of maximum increase in rainfall rate (Fig. 4.11). Specific humidity peaked at low

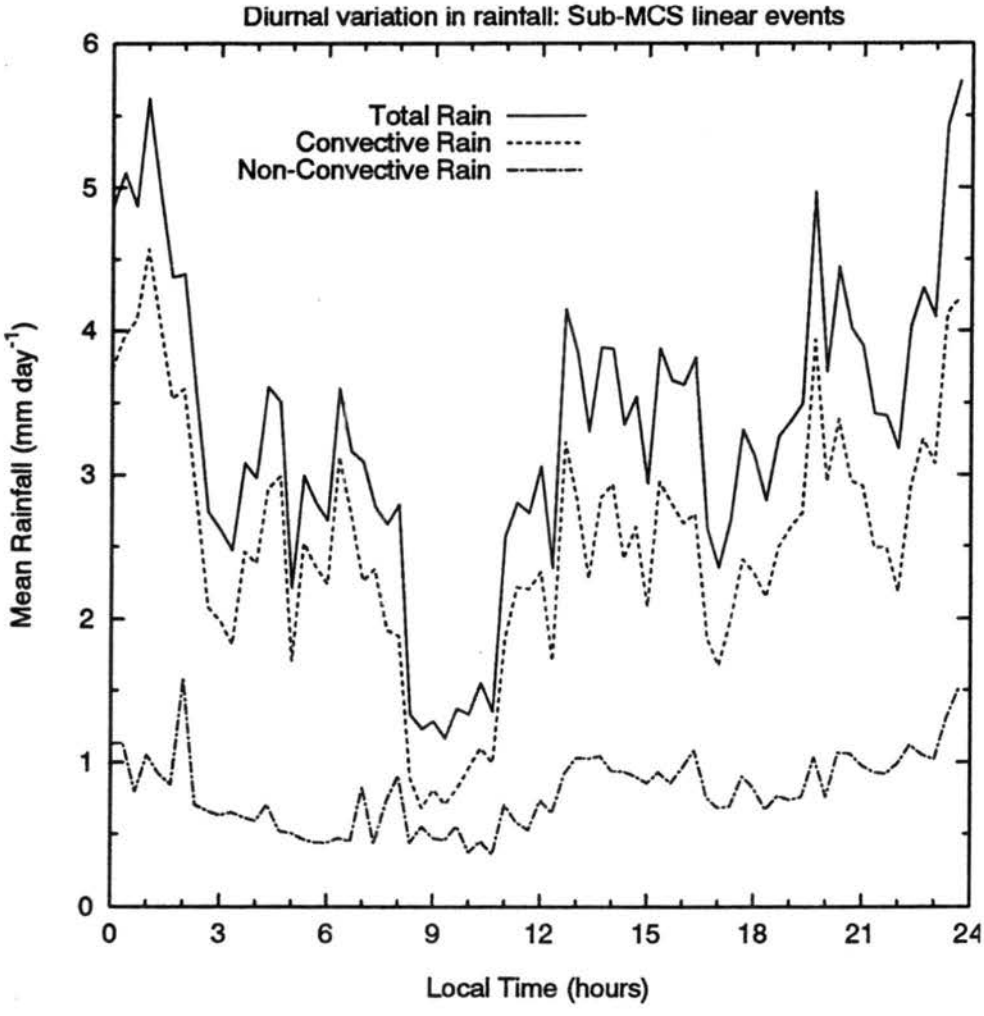

Figure 4.11. As in Figure 4.1, but for sub-MCS scale linear events.

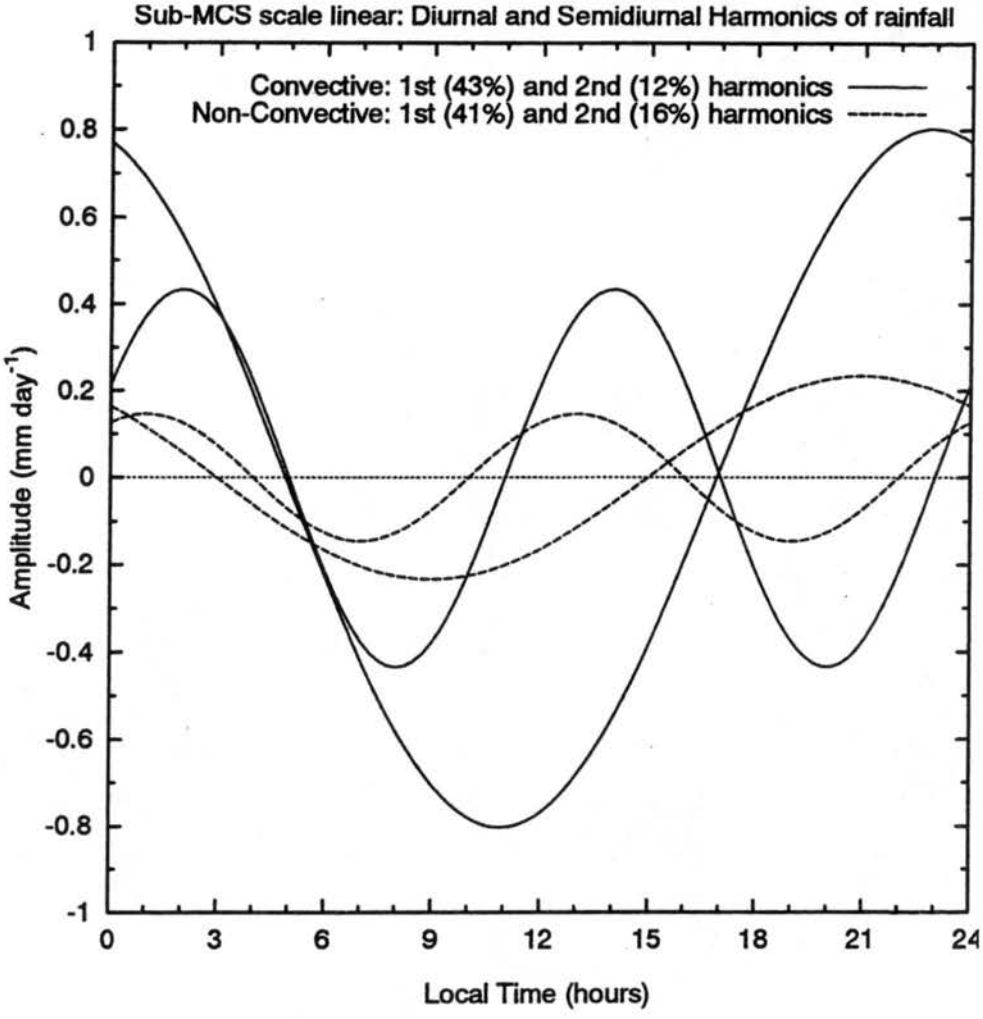

Figure 4.12. As in Figure 4.2, but for convective and non-convective rain of sub-MCS scale linear events.

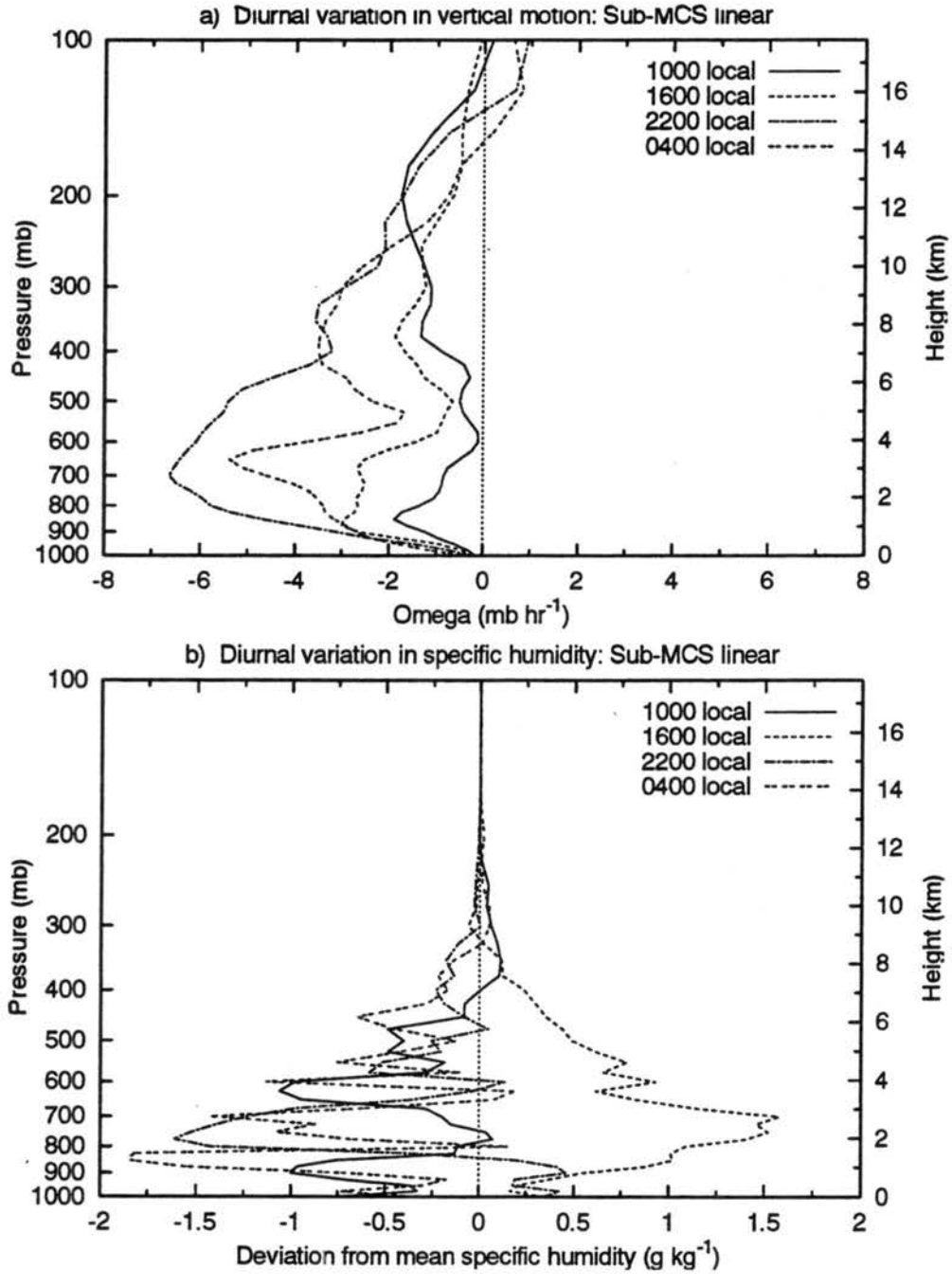

Figure 4.13. The diurnal variation of composited vertical profiles of a) vertical motion, and b) specific humidity from sounding data for sub-MCS scale linear events.

levels (3 km) at 16LT. This may be related to the presence of afternoon non-precipitating shallow cumulus clouds (Lin and Johnson 1996). The diurnal variation of rainfall in this organizational mode may therefore be related to intensification of afternoon sub-MCS scale linear events due to solar heating of the boundary layer and moistening by shallow cumulus.

4.6 MCS scale linear events

The diurnal rain composite for MCS scale linear events (Fig. 4.14) did not indicate a single well defined maximum. Nevertheless, the diurnal harmonic explained more than half of the variance in the convective rain diurnal composite (Fig. 4.15). The late afternoon convective rain diurnal harmonic maximum (1830LT) was consistent with the idea that afternoon heating augments convective intensity. The non-convective rainfall diurnal harmonic peak (21LT) lagged the convective peak by 2.5 hours. This time lag was consistent with non-convective rain forming from the detrainment of condensate from convective cells, as shown in many case studies of MCS scale squall lines. However, the fraction of the variance explained for each of the first two harmonics were very different between convective and non-convective rain. This suggested that the variation in convective rain was not necessarily tied to that of non-convective rain, even though the two rain types are physically linked. It was often observed in COARE that lines of convection propagated into pre-existing regions of non-convective rain, or formed on the edges of non-convective rain areas. As a result, at any given time the non-

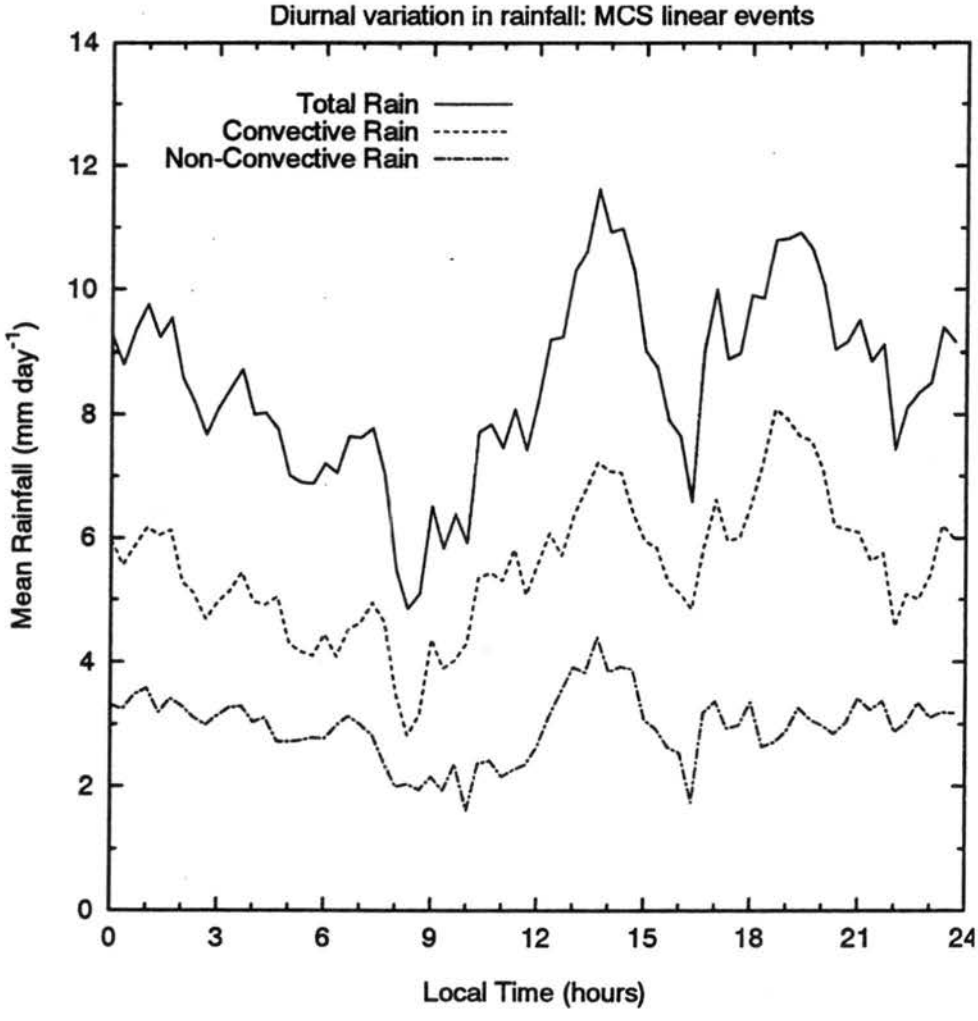

Figure 4.14. As in Figure 4.1, but for MCS scale linear events.

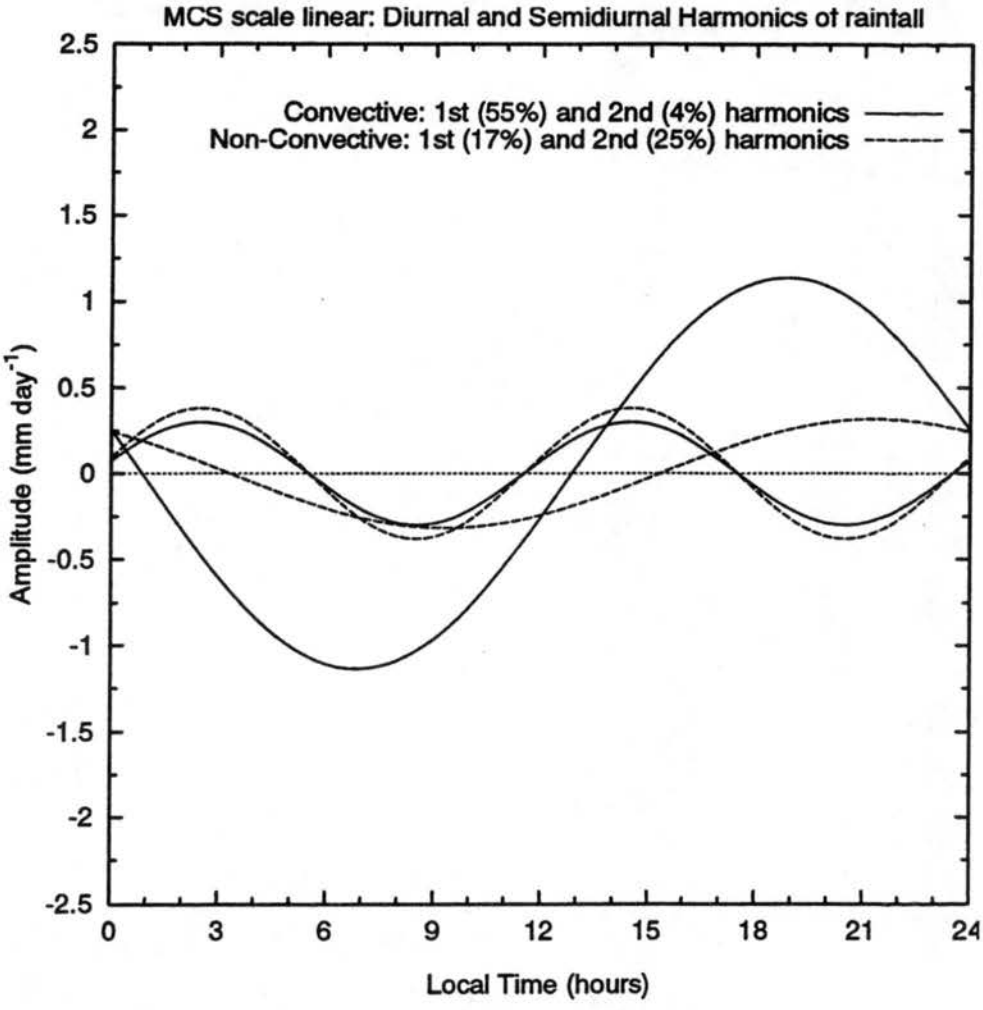

Figure 4.15. As in Figure 4.2, but for convective and non-convective rain of MCS scale non-linear events.

convective rain seen by the radar may not have been produced by the collocated convective region. Therefore, the phase lag between convective and non-convective rain did not necessarily illustrate system evolution. Keenan et al. (1989) found that over the Gulf of Carpenteria during the Australian Monsoon Experiment (AMEX), the diurnal peak in the number of convective and non-convective radar echoes were in phase, possibly for a similar reason.

The diurnal variation in profiles of vertical motion and relative humidity (Fig 4.16a-b) provided further evidence that the diurnal rainfall modulation was not an effect of system evolution, but instead represented intensity differences between day and night MCS scale linear events. The strongest ascent occurred at 22LT, with a deep layer of upward motion in the mid and upper troposphere. This was consistent with deep widespread convection with upper level ascent for this event type (Chapter 3). The peak upward vertical motion weakened and shifted downward by 10LT, yet at this time the upward motion was still deeper and stronger than the strongest sub-MCS scale non-linear event upward motion profile (16L; Fig.4.10a). If the diurnal rainfall variation of MCS scale linear events evolved from isolated convective cells in the afternoon to a nocturnal MCS, the composite afternoon vertical motion profile should have been similar to that of sub-MCS scale non-linear events. The same conclusion may be drawn from the relative humidity profiles. The driest MCS scale linear event profile (10LT) was much moister at all levels than the nocturnal sub-MCS non-linear composites, except in the boundary layer where the profiles were similar. The difference between the MCS scale linear event relative humidity composite at 22LT compared to 10LT at mid levels was greater

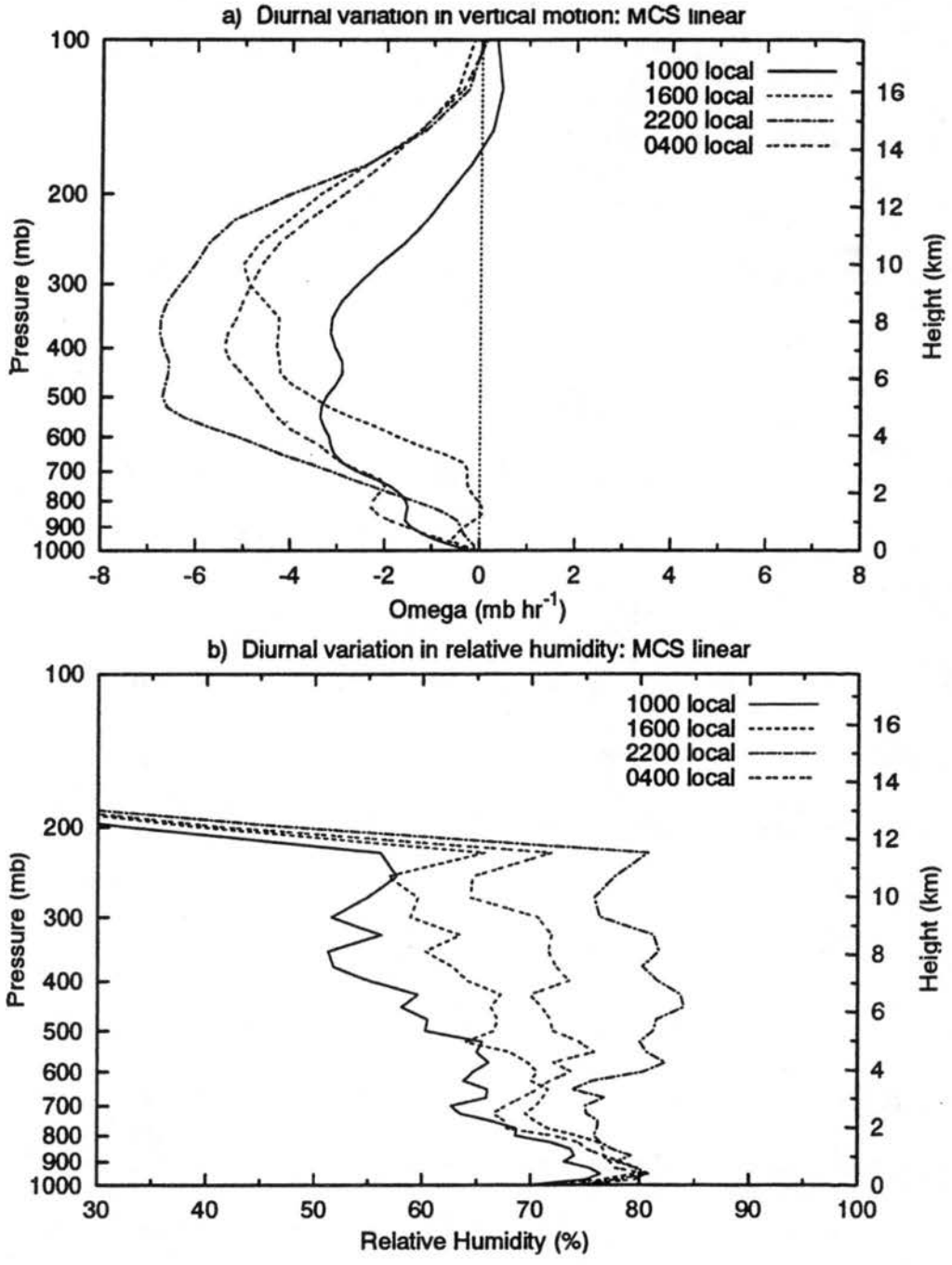

Figure 4.16. The diurnal variation of composited vertical profiles of a) vertical motion, and b) relative humidity from sounding data for MCS scale linear events.

than 20%. This suggested that there was less non-convective cloudiness and rainfall present in the late morning compared to the evening, consistent with Fig. 4.14.

4.7 MCS scale non-linear events

The daily total rainfall variation of MCS scale non-linear events had the highest amplitude and greatest diurnal variance of any organizational mode. Shown in Figs. 4.17 and 4.18 are the diurnal rainfall composites for MCS scale non-linear events and the harmonic analyses of these composites. Both convective and non-convective rain had a significant fraction of the variance of the diurnal composites explained by the first harmonic (43% and 60% respectively), and almost none in the second harmonic. The convective rain diurnal harmonic peak (01LT) lead the non-convective peak (0430LT) by 3.5 hours. This phase lag is consistent with the mechanism of enhanced condensate detrainment from the strong nocturnal convection[6] resulting in a maximum in non-convective surface rainfall several hours later. However, the larger fraction of the variance in the non-convective rainfall composite explained by the diurnal harmonic (compared to convective rainfall) suggested that radiative mechanisms may affect the precipitating anvil clouds directly. Results from cumulus ensemble model studies indicated that destabilization of anvil clouds at night by cloud top cooling and cloud base warming resulted in longer-lived anvil clouds (Fu et al. 1995, Guichard et al. 1996).

[6] The lightning observations of Petersen et al. (1996) suggested that convection was more vertically developed at night for the larger systems during COARE.

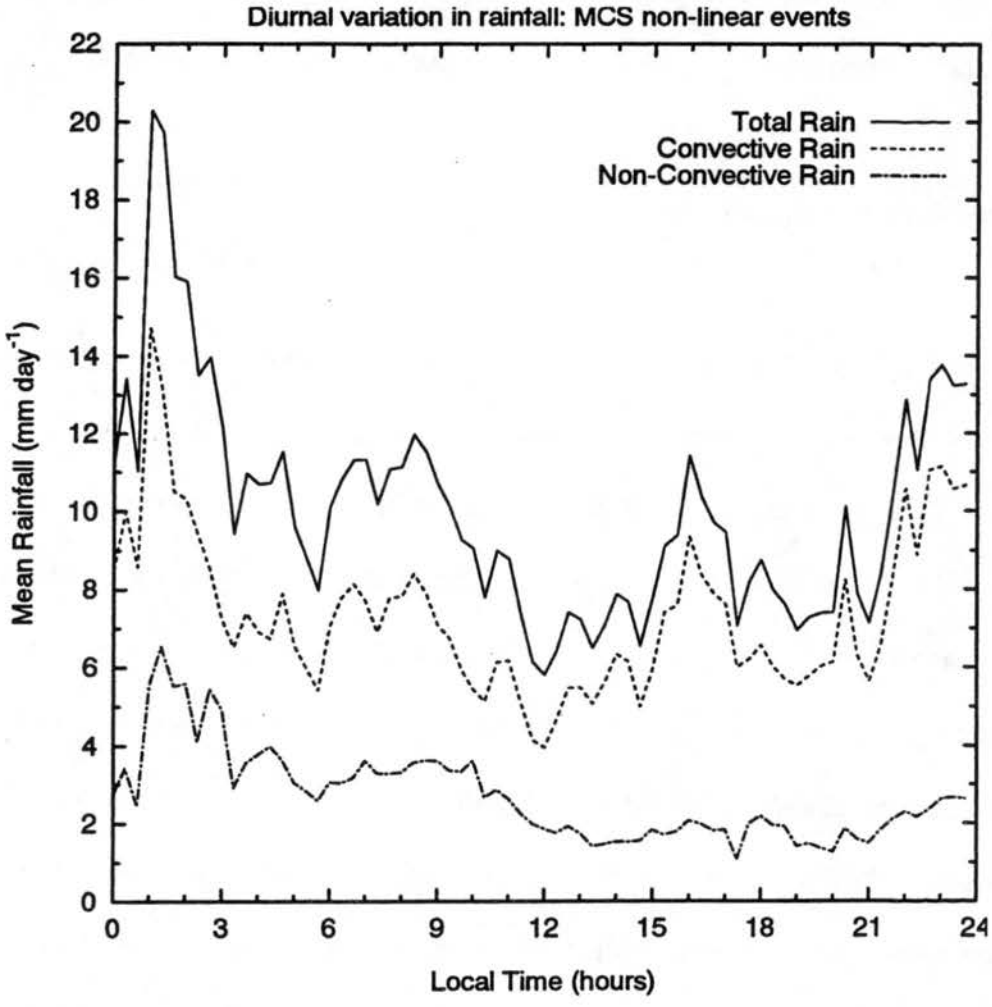

Figure 4.17. As in Figure 4.1, but for MCS scale non-linear events.

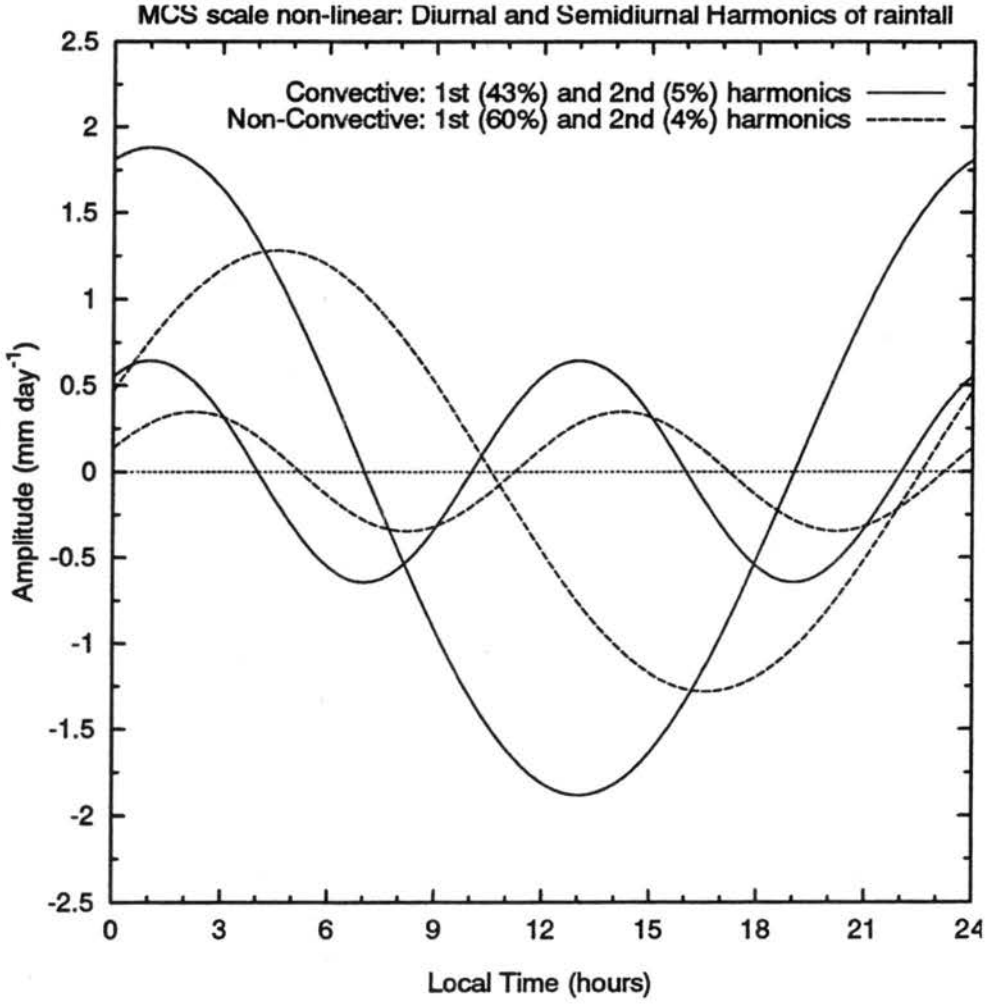

Figure 4.18. As in Figure 4.2, but for convective and non-convective rain of MCS scale non-linear events.

These two mechanisms may act together to produce the observed diurnal variation in non-convective rain.

MCS scale non-linear events were unique in that the total rain diurnal harmonic has a maximum several hours after midnight, rather than in the early evening. The profile of vertical motion (Fig. 4.19a) contained the strongest upward motion at 22LT, with maxima at 750 mb and 450 mb. By 04LT, the low level peak remained, while the upper level peak had weakened. This may have been attributable to a decrease in deep, vertically developed convection between the two times, consistent with the diurnal convective rain composite. Cloud to ground lightning flash rates were highest at 01LT for COARE systems (Petersen et al. 1996), consistent with the most vertically developed convection occurring between 22LT and 04LT. The low level peak in vertical motion was much weaker at 10LT, and was absent by 16LT. The divergence profile composite (Fig. 4.19b) showed a shallow layer of strong convergence ($< 10^{-5}$ s^{-1}) below 850 mb at 22LT and 04LT, which implied low level upward motion. This nocturnal enhancement of low level convergence was unique to MCS scale non-linear events. Although weakened, the upper level upward motion remained relatively strong throughout the day, suggesting the continued presence of widespread convection. The region of strong upper level divergence descended several kilometers from 22LT to 10LT, implying a transition to less vertically developed (though still strong) convection during that period. Again, these observations supported the notion that the nocturnal convection was enhanced relative to the daytime convection, rather than illustrating the life cycle of daily MCSs. The specific humidity below 800mb was enhanced at 04LT (Fig. 4.19c). This may

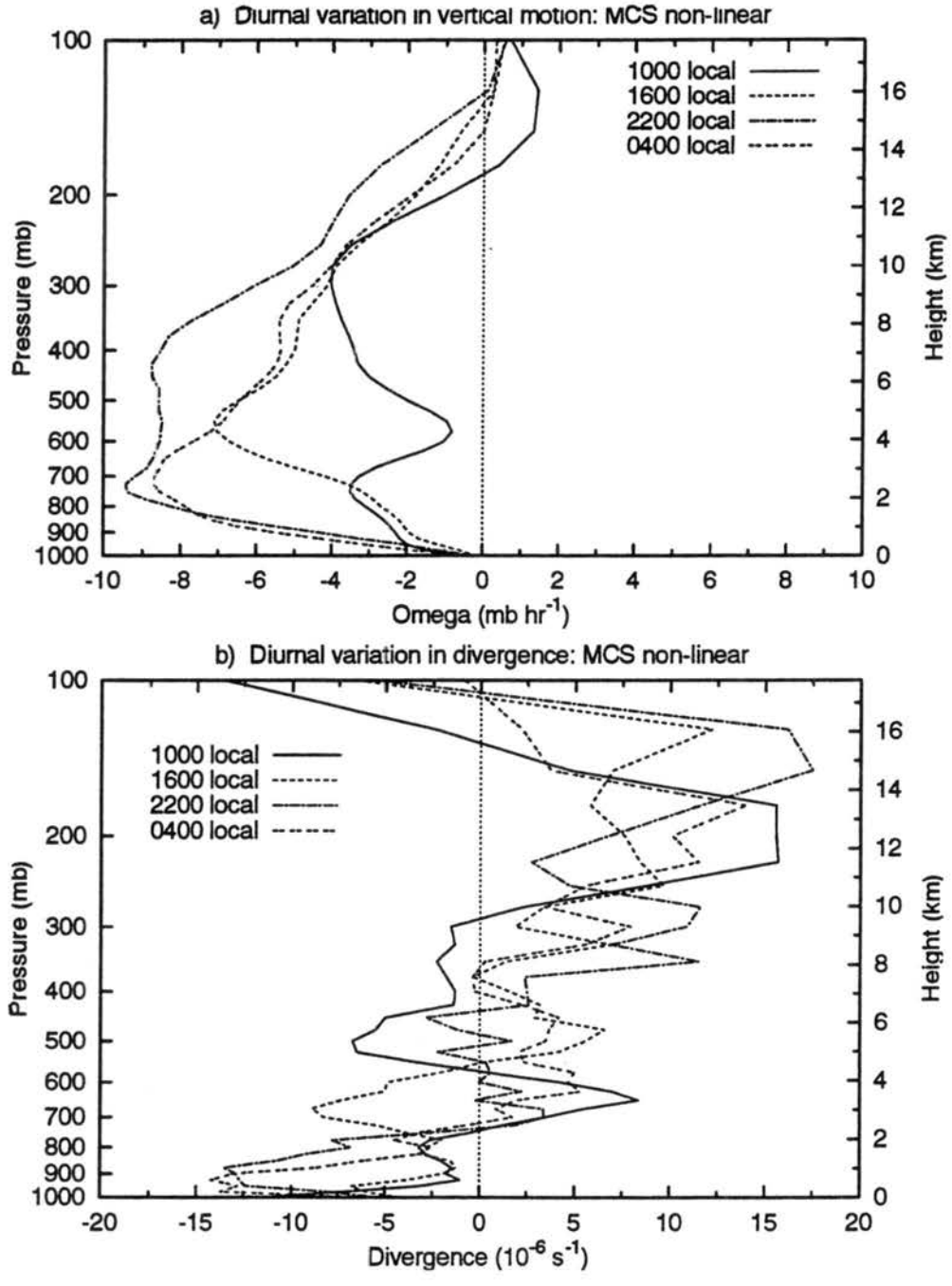

Figure 4.19. The diurnal variation of composited vertical profiles of a) vertical motion, and b) divergence from sounding data for MCS scale linear events.

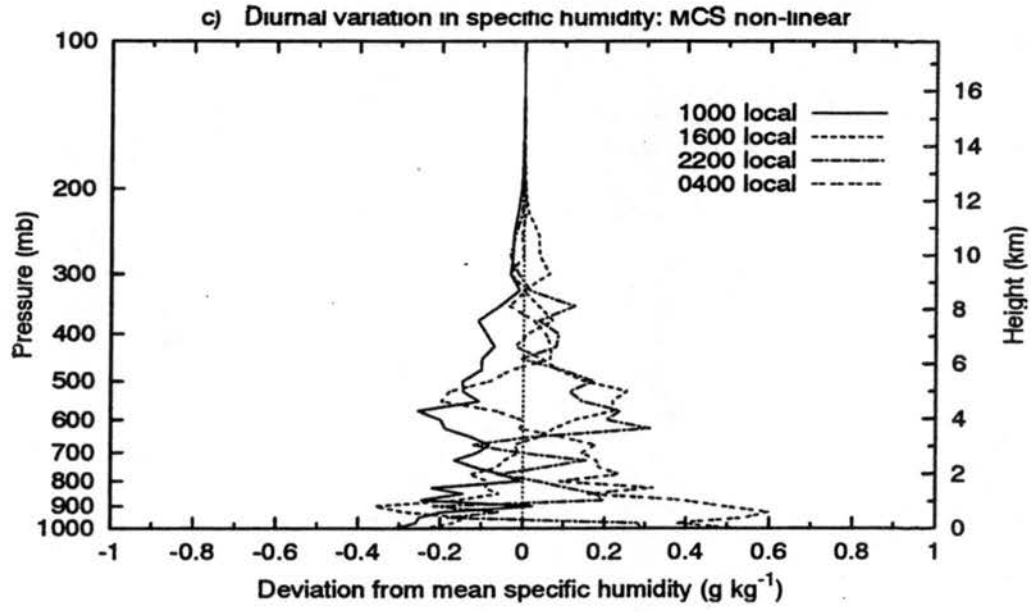

Figure 4.19. (continued) The diurnal variation of composited vertical profiles of c) specific humidity from sounding data for MCS scale linear events.

indicate widespread moistening from evaporation of non-convective rain, which had a peak in the diurnal harmonic around that time.

CHAPTER 5

INFLUENCE OF EQUATORIAL 4 - 5 DAY WIND OSCILLATIONS ON RAINFALL IN THE IFA

The goal of this chapter is to understand whether rainfall in the IFA during COARE has a variation corresponding to the strong 4-5 day oscillation in the low level wind field. The rainfall variability is interpreted based on the composite structure of the waves documented in previous studies, as discussed in Sec. 5.1.

5.1 Structure of 4 - 5 day waves: background

Westward propagating disturbances in the wind field of period 4 - 5 days and wavelength 4000 km - 8000 km are a common mode of wave activity in the tropical Pacific Ocean. Theoretical and observational studies have suggested that these waves occur with two basic structures.

The first type, mixed Rossby-gravity (MRG) waves, occur in the troposphere and stratosphere in the near equatorial regions of the central and western Pacific Ocean (Yanai et al. 1968), following their theoretical prediction by Matsuno (1966) in a quasi-

geostrophic framework. Theories for the generation of these waves focus on a tropospheric source. A wave-CISK unstable coupling of cumulus convection with free Rossby-gravity waves may produce the observed waves (Hayashi 1970, Itoh and Ghil 1988). Mak (1969) proposed that lateral forcing from extratropical regions could establish a resonant mode with a 4 day period. In the Pacific basin, Nitta and Takayabu (1985) showed that the 4-5 day low level wind oscillations originate near the dateline and propagate westward. Using outgoing longwave radiation data and ECMWF wind analysis, Hendon and Liebmann (1991) showed that positive convective anomalies associated with the 4-5 day oscillation are strongest near the dateline and in the boreal autumn. They hypothesized that the double ITCZ flanking the cold equatorial water near the dateline during that season was related to the generation of westward propagating equatorially trapped MRG waves there.

The second wave type is referred to as "tropical disturbance" (TD) wave structure, following Takayabu and Nitta (1993). That study discussed the change in low level wind structure from MRG waves near the dateline to TD waves in the western Pacific, in a nine year climatology. In their conceptual model (Fig. 5.1), equatorial MRG waves propagate westward, with a positive convective anomaly associated with the convergent region of the wave. As the wave moves to the west, it encounters higher tropospheric shear (stronger low level westerlies) and higher SSTs. They suggested that these environmental changes may result in shorter wavelength closed circulations displaced north of the equator (TD wave structure). The mechanisms leading to the transition of MRG waves near the dateline to TD waves in the western Pacific however were not

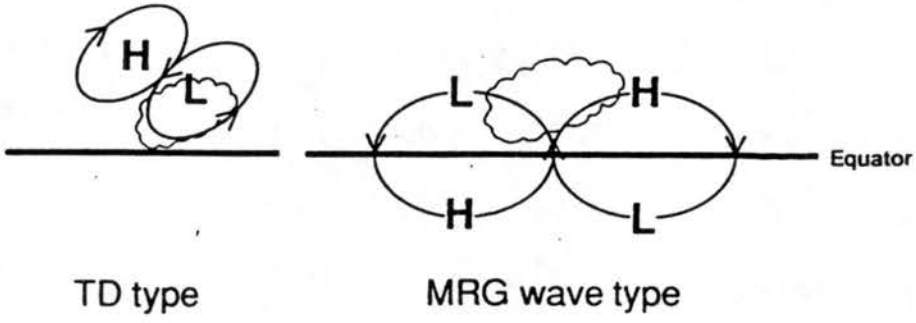

Figure 5.1. Schematic of TD disturbances (western Pacific) and MRG wave disturbances (central Pacific). Solid lines with arrows indicate the lower tropospheric wind pattern. Letters H/L represent high/low pressure anomaly centers. Cloud shaped figures represent regions where convection is observed. Adapted from Takayabu and Nitta (1993).

known. Another hypothesis was that TD waves were generated directly from a convective source, without transitioning from MRG waves. Nakazawa (1988) hypothesized that westward moving Rossby waves are generated in association with the heating from eastward propagating super cloud clusters (i.e. Gill 1980). Most of the convection was associated with the closed cyclonic vortices. On occasion, the cyclonic vortices associated with the TD waves may lead to tropical cyclogenesis in the western Pacific north of the equator (Numaguti 1995).

The composite structure of TD waves in the western Pacific Ocean were studied by Reed and Recker (1971) from sounding data (5°N - 20°N) between 130°E and the dateline. They found that precipitation amounts were higher in the vicinity of the wave trough (cyclonic low level circulation in the northern hemisphere). Rainfall was shown to be concentrated just east of the trough axis near the dateline, and west of the axis in the western Pacific. Furthermore, the vertical wave axis transitions from an eastward tilt with height in the central Pacific to a westward tilt in the western Pacific. These east to west differences were hypothesized to be associated with meridional changes in the basic state vertical shear. Time-averaged tropospheric shear was typically stronger in the western Pacific because of the influence of low level westerly wind bursts.

During TOGA COARE, Numaguti (1995) observed strong 4-5 day variation of the 850 mb meridional wind within 2° of the equator (Fig. 5.2). The waves were most active near the longitude of the IFA (150°E - 160°E) during November. Group propagation was to the east, which resulted in strong 4-5 day wave activity shifting to near the dateline in early December. In the dateline region, the frequency and structure of the oscillation was

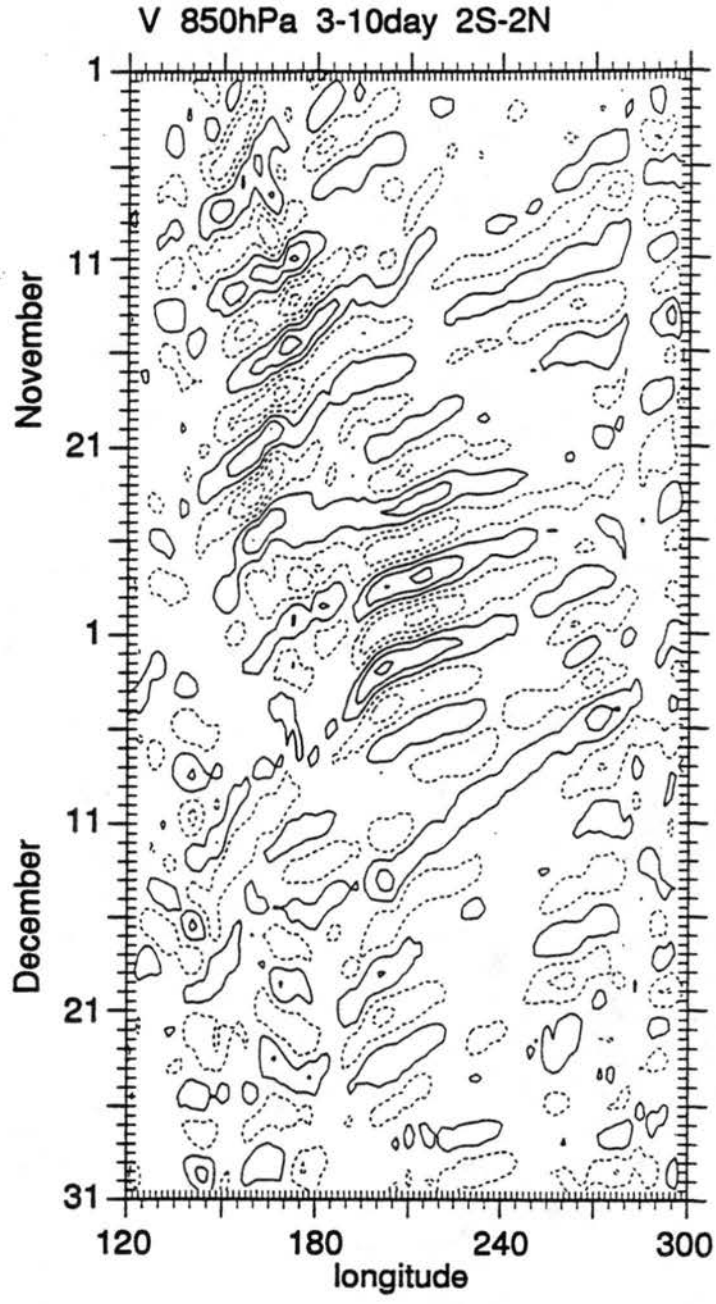

Figure 5.2. Time-longitude section of the 850 mb meridional wind at the equator for November - December 1992 using a 3-10 day bandpass filter, from the Japanese Meteorological Agency Global Analysis (GANAL). The contouring begins at ± 1.5 m s^{-1} with ± 3 m s^{-1} increments. Northerly winds indicated by the dotted lines, southerly winds by the solid lines. Adapted from Numaguti (1995).

consistent with the presence of MRG waves centered on the equator. In the vicinity of the IFA however, the wind oscillation structure resembled the TD wave type discussed by Takayabu and Nitta (1993). Fig. 5.3 shows the Japanese Meteorological Agency Global Analysis (GANAL) low level winds and brightness temperature during the month of November at the nominal IFA longitude (156°E), from Numaguti et al. (1995). The clockwise low level circulation associated with the waves (anticyclonic in the northern hemisphere) straddled the equator, while the counterclockwise circulation centers (cyclonic in the northern hemisphere) were displaced 8° - 12° northward of the equator. Most of the low brightness temperatures (used as a proxy for convection) were associated with the regions of counterclockwise circulation well north of the equator. However, note the small areas of convection just south of the equatorial clockwise circulation centers, in the region of the IFA (c.f. Fig. 5.3). These findings of Numaguti et al. (1995) are important to keep in mind when interpreting the 4-5 day variability from shipboard radar in COARE, which is located near 2°S latitude.

5.2 Wind and rain oscillations in the IFA

Regular oscillations in the 850 mb wind field were detected in the vicinity of the R/V Vickers during the month of November. Time series of the zonal and meridional wind components at that level (Fig. 5.4a) revealed this variation for the period (13 November - 1 December) during which the oscillation was most apparent. Regular variations in the

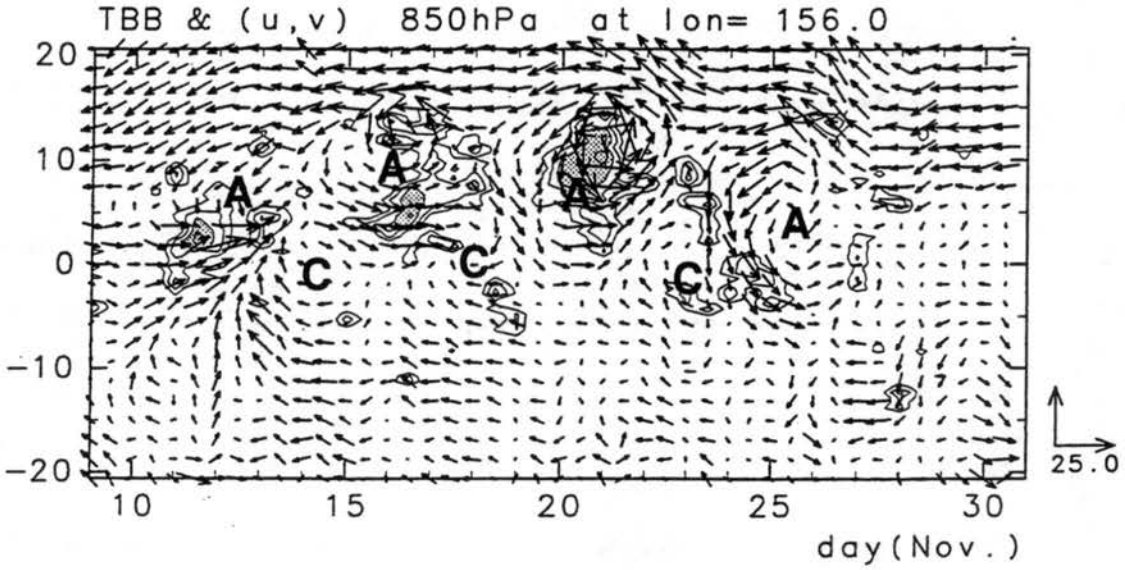

Figure 5.3. Time-latitude section of the 850 mb wind and equivalent black-body temperature at 156°E longitude for 10 November - 30 November 1992. The brightness temperature contour interval is 20° K, with areas less than 215° K shaded. The letters A and C represent the centers of anti-clockwise and clockwise vortices, respectively. Adapted from Numaguti et al. (1995).

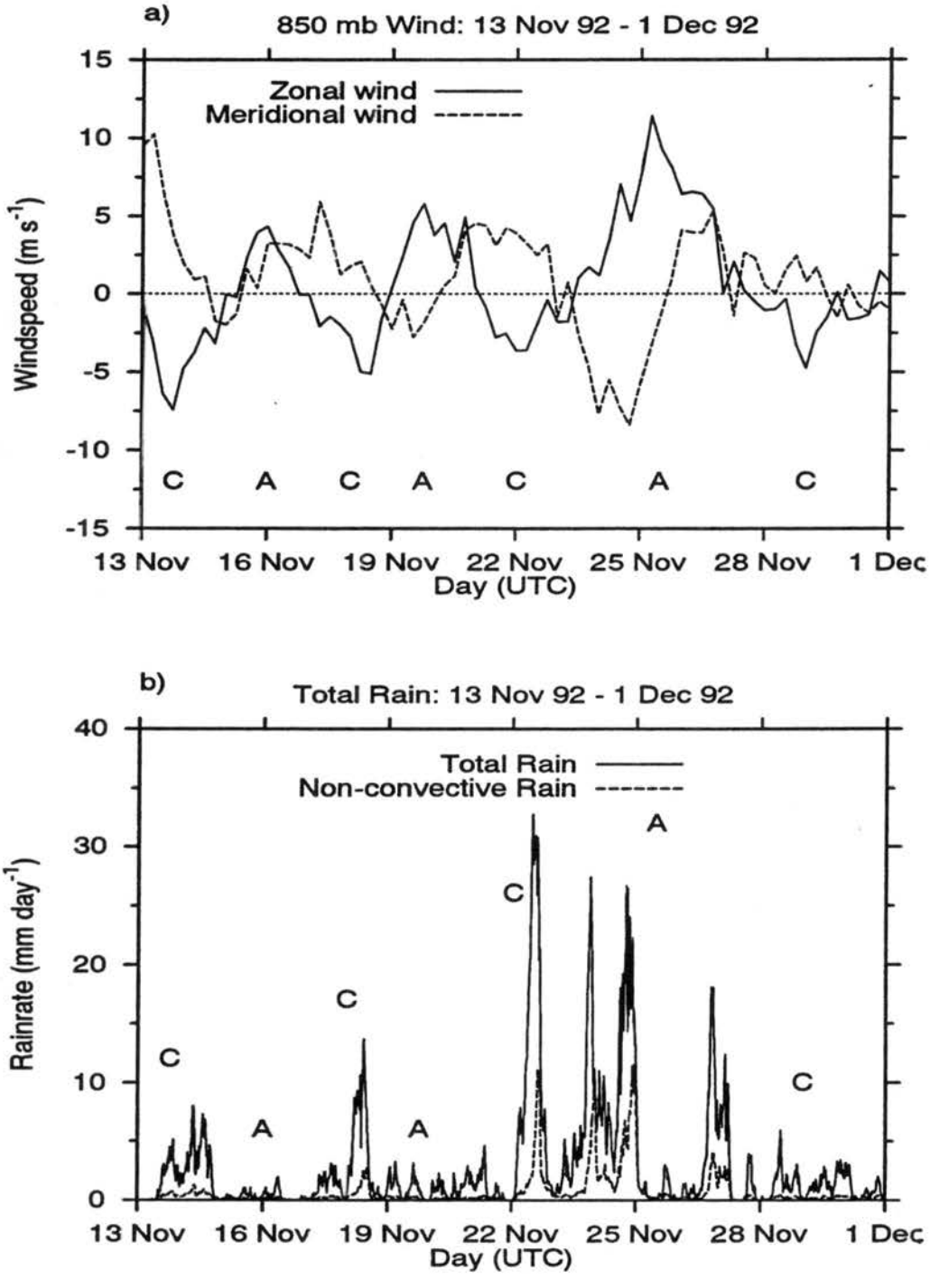

Figure 5.4. Time series (13 November 1992 - 1 December 1992) of a) zonal and meridional wind component, and b) total and non-convective rain, representative of the nominal position of the R/V Vickers (2°S, 156°E). The letters C and A indicate the time that the centers of clockwise and anti-clockwise circulation centers (respectiviely) were situated at the longitude of the ship.

rainfall time series (Fig. 5.4b) on the other hand were much less apparent, but were in fact present as discussed below.

Before presenting analyses of these time series, it is useful to discuss qualitatively the relationship between features of both time series to the larger scale wave patterns discussed in Numaguti et al. (1995). The time at which the center of clockwise circulation associated with the 4 -5 day low level wind oscillations passed the ship's longitude is shown in Fig. 5.4 to be associated with southeasterly winds, consistent with Fig. 5.3. This suggests that the low level wind oscillations observed near the ship were directly linked to the waves documented in that study. However, the relationship of the wind variation to the rainfall at 2°S was complex. For the first three cycles of the wind oscillation (13 November - 23 November, c.f. Fig. 5.4), peaks in the total rainfall rate of at least 10 mm day^{-1} occurred following the passage to the north of the clockwise circulation center. This corresponded to a rotation of the wind vector from southeasterly to northeasterly. Following 23 November, a high wind event occurred which appeared to originate from the northwest (Fig. 5.3), associated with heavy rainfall. Following this event through 1 December, the wind oscillations weakened while the rainfall rate diminished.

These general rainfall tendencies observed from ship radar were remarkably consistent with low brightness temperatures associated with high clouds shown in Fig. 5.3 between the equator and 4°S. Although these brightness temperature features were small compared to those north of the equator, they corresponded well in space and time with the radar observed rainfall events on 14 November, 18 November, and 22-24

November. Furthermore, each of these events contained MCS scale organization (c.f. Fig. 3.1a) even though the corresponding brightness temperature signatures did not reveal extensive cold cloudiness. The rainfall time series in Fig. 5.4b shows that non-convective rainfall was associated with each of the three events, consistent with MCS scale organization. An example of the horizontal reflectivity patterns of the 18 November event is given in Fig. 5.5, revealing a weakly organized line 100 km in length with a large associated region of stratiform rain in its wake.

These observations suggest that significant rainfall organized on the MCS scale occurred on the southern portion of the wave train associated with the clockwise circulation features. Though far removed from the main locus of convective activity associated with the cyclonic vortices in the northern hemisphere, the rainfall variations at 2° S may be linked to the 4 -5 day variation in the low level winds. This possibility is explored in the remainder of this chapter.

5.3 Analysis of the wind and rainfall time series

Shown in Fig. 5.6 are power spectra of the 850 mb zonal wind, meridional wind, and total rain time series given in Fig. 5.4, encompassing the period of the regular wind oscillations. The time series of the wind components contained strong power at a period of 4.5 days, with little higher frequency variability. In contrast, most of the variability in the rainfall time series was concentrated at the higher frequencies, between one and two days. Nevertheless, a weak spectral peak in the rainfall time series was present at 4.5

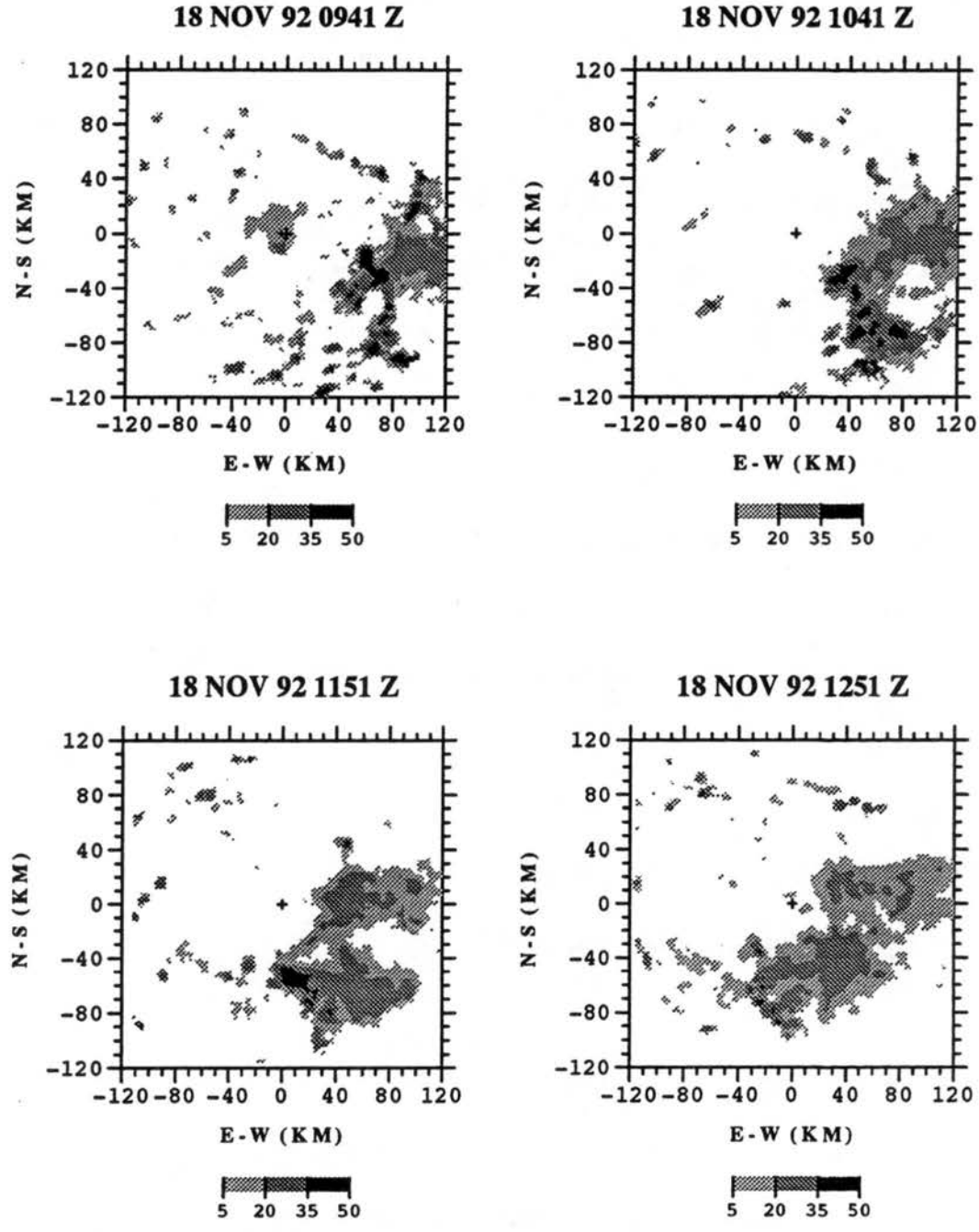

Figure 5.5. Hourly maps of radar reflectivity at a height of 2 km for an MCS scale linear event on 18 November 1992. Values are expressed in dBZ.

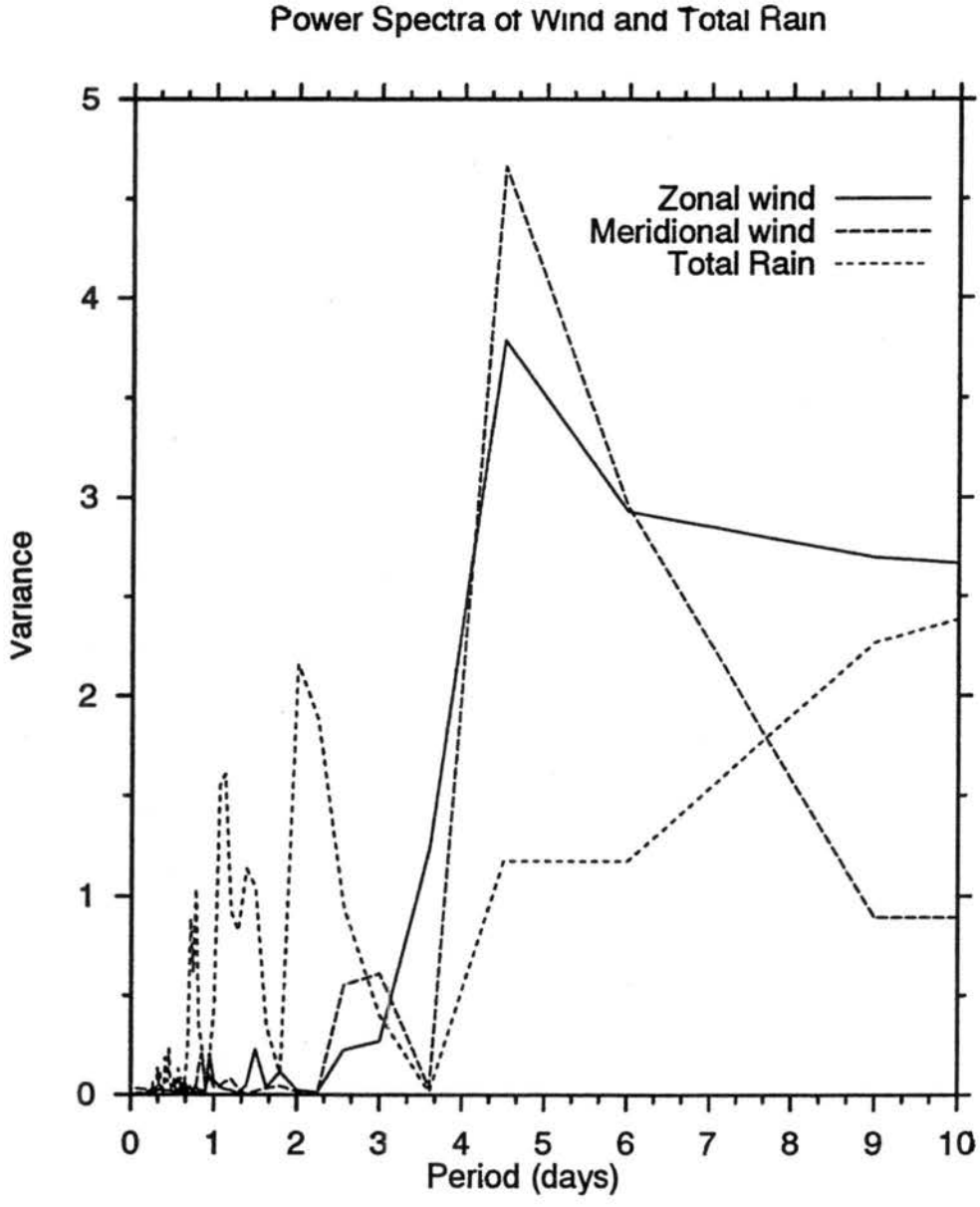

Figure 5.6. Power spectra of the zonal and meridional wind components and total rainfall for the time series shown in Fig. 4 (13 November 1992 - 1 December 1992).

days. Therefore, the 4.5 day oscillation in the 850 mb winds was quite evident at the location of the ship radar, while a similar variation in rainfall was much less apparent.

In order to illustrate the phase relationship between each wind component and the rainfall, a 4.5 day composite of the time series is given in Fig. 5.7. The zonal wind oscillation led that of the meridional wind by about 1.25 days, or one-quarter of a wavelength (Fig. 5.7a). This was consistent with studies of the composite 4.5 day wave structure of the low level winds for the western Pacific (Reed and Recker 1971, Liebmann and Hendon 1990, Numaguti 1995). There was no clear phase relationship between the wind composites and the rainfall (Fig. 5.7b). More rainfall occurred during low level easterly winds at the latitude of the IFA, associated with the passage to the north of the clockwise circulation center. However, the higher frequency variability dominates the 4.5 day rainfall composite, consistent with the spectral analyses.

To understand the significance of the 4.5 day variability relative to higher frequency modes, a harmonic analysis was performed on the 4.5 day composites shown in Fig. 5.7. More than 90% of the variance of the composite wind components was explained by the first (4.5 day) harmonic (Fig. 5.8a), consistent with the strong spectral peak at that frequency. The quarter wavelength phase lag in the first harmonics of the meridional wind relative to the zonal wind confirmed a similar inference drawn from the composites. Fig. 5.8b shows the first four harmonics of the 4.5 day rainfall composite. Over 80% of the variance was explained by the first four harmonics combined (1.1 day to 4.5 day period). The 4.5 day harmonic accounted for 16% of the variance, with the maximum rainfall nearly collocated with the peak in the zonal wind first harmonic

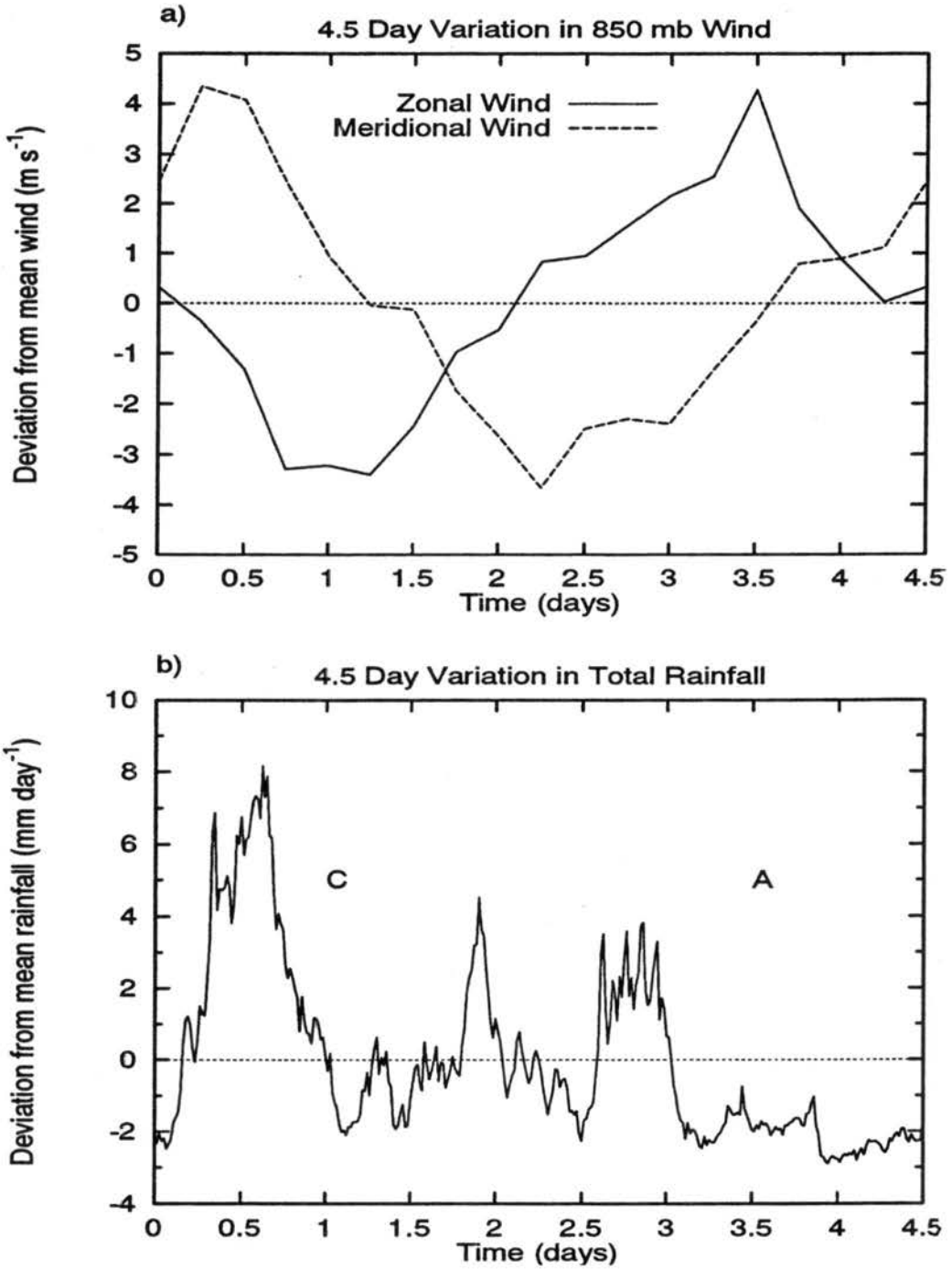

Figure 5.7. 4.5 day composites for the period 13 November 1992 - 1 December 1992 of a) zonal and meridional wind, and b) total rainfall. The letters C and A represent the composite location of the clockwise and anti-clockwise circulation centers north of the ship's location.

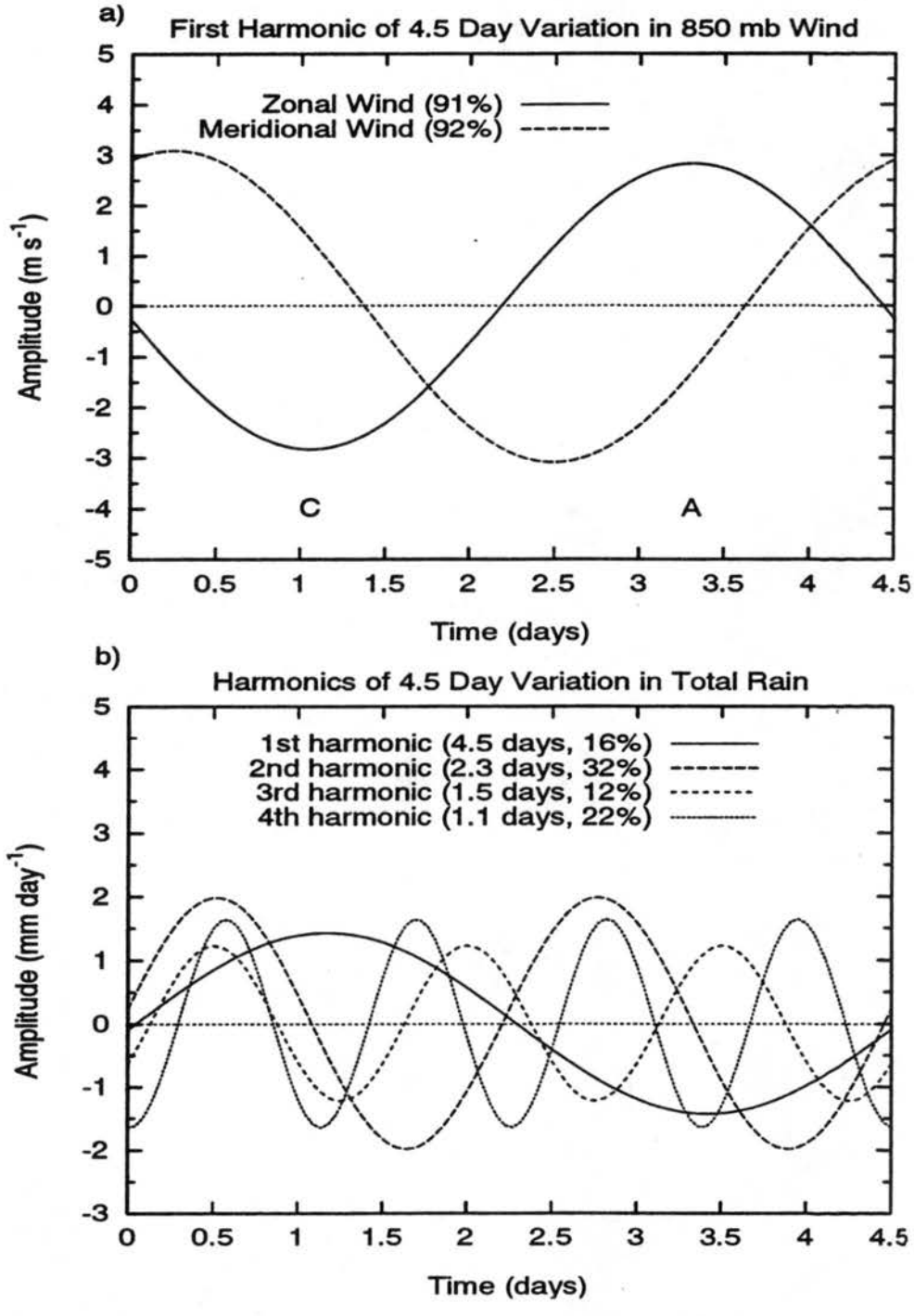

Figure 5.8. Harmonic analyses of the 4.5 day composites (Fig. 7): a) first (4.5 day) harmonic of zonal and meridional wind components, and b) first four harmonics (4.5 day, 2.3 day, 1.5 day, 1.1 day) of the total rainfall. The fraction of the total variance of the 4.5 day composites explained by each harmonic is indicated in the legends.

associated with easterly winds. *These observations indicate that there was weak 4.5 day rainfall variability present in the IFA at the southern portion of the clockwise circulation associated with the strong 4.5 day low level wind oscillation.* However, individual higher frequency modes explained higher fractions of the variance of the rainfall composite. Nearly one-third of the variance was in the 2.3 day mode. A strong two day variability was seen in outgoing longwave radiation data during the convective phase of the ISO by Chen et al. (1996) and Takayabu et al. (1996) during COARE. However, since the convection associated with the ISO was far removed from the IFA in mid-to-late November, it was not likely that the 2.3 day rainfall variability shown here was related to that observed in the aforementioned studies. Finally, the diurnal mode explained 22% of the rainfall variance (see Chapter 4).

5.4 Possible mechanisms for 4.5 day rainfall variation in the IFA

Takayabu and Nitta (1993) discussed the existence of TD type near equatorial waves in the western Pacific, with the cyclonic circulation displaced northward relative to the clockwise equatorial eddies. This basic structure of 4 - 5 day waves was confirmed for the longitude of the IFA by Numaguti et al. (1995). Those studies suggested that convection was concentrated within the anticyclonic circulation regions near 10° N, and therefore displayed a tight coupling with the 4 - 5 day waves. The shipboard radar measurements did not sample convection in the cyclonic gyres; rather, the rainfall sample was limited to a 240 km diameter region centered at 2°S. Nevertheless, evidence was

presented that supported a weak 4.5 day rainfall variation, south of the center of the equatorial clockwise eddies and away from the cyclonic circulation centers. The mechanism for the coupling of convection to the 4 - 5 day circulation in the IFA is therefore likely not related directly to low level convergence in the cyclonic circulation. Instead, *the advection of dry low level air from the subtropics by the meridional winds associated with the 4 - 5 day circulation may prevent convection from organizing on the scale of an MCS*, as discussed below.

Numaguti et al. (1995) documented intrusions of low level dry air (at ~ 3km) into the IFA region during November 1992. They documented two major events of dry air advection: near 13-14 November in low level southerlies, and near 25-26 November in low level northerlies. A less intense dry air advection event occurred southerly winds from 19-21 November (see their Fig. 18). The spacing of these dry air intrusion events was approximately 4 - 5 days. Thesee events correspond well to maxima in the meridional wind components associated with the 4 - 5 day waves, and with minima in the radar-estimated rainfall (c.f. Fig. 5.4). The presence of dry air may limit the vertical development of convection by entrainment of this dry air into ascending moist parcels, and by increasing parcel stability at the base of the dry air intrusion by radiative cooling of the underlying moist air[1] (Mapes and Zuidema 1996). These effects may also act to hinder the organization of convective clouds into mesoscale systems. It may therefore be more instructive to consider the 4 - 5 day wind oscillations in the IFA region as modulating conditions which suppress rather than enhance organized convection. It must

[1] This latter effect actually dominates over the effect of destabilization due to boundary layer solar heating when averaged over a day.

be pointed out that intrusions of subtropical dry air into the IFA region were not limited to periods of 4 - 5 day wave activity (Yoneyama and Fujitani 1995, Mapes and Zuidema 1996).

CHAPTER 6

SUMMARY AND CONCLUSIONS

A ninety day sample of convection was obtained from shipboard radar reflectivity data during TOGA COARE. This unprecedented view of oceanic convection over the warm pool region of the western Pacific Ocean allowed the study of rainfall associated with a broad spectrum of convective organization. Convective events were characterized by horizontal organization with respect to the scale of an MCS, and morphology in terms of linear organization. For the first time, the occurrence frequency and rainfall production of MCS scale convective events have been compared systematically with those on the sub-MCS scale. It was found that four fifths of the total rainfall was associated with MCS scale events, consistent with the observation that the largest tropospheric heating occurred with these events. However, since sub-MCS scale non-linear events (isolated convective cells) were present more than half of the time, the net heating from these groups of isolated clouds were at times an important component of the heating. This event type produced about 15% of the total rainfall, a result which must be considered in satellite retrievals of rainfall from cloud top outgoing longwave radiation measurements since these events did not produce extensive cloud shields. Cloud height

populations were distinct between MCS and sub-MCS scale modes of organization. Most of the rainfall associated with sub-MCS scale non-linear convection was produced by shallower convection compared to MCS scale events. However, convection on both scales of organization contained a distinct peak in rainfall production from convective features of 8-9 km height, which may be related to the presence of inversions at the 0°C level (Johnson et al. 1996).

Differences in the large scale environment (of which the sampled convection is an inseparable part) were associated with distinct occurrence and rainfall characteristics of convective events. The mean profiles of divergence (and thus vertical motion) and relative humidity varied significantly with the scale and morphology of precipitation events. The magnitude of the composite relative humidity profile increased at all levels with the spatial scale of convective organization. On the MCS scale, mid level convergence vs. divergence was tied to the relative amount of non-convective precipitation. It was hypothesized that the observed mid level convergence is a meso-α scale signature of convergent flow features associated with MCS scale linear events, which may augment non-convective rainfall in those systems. However, vertical heating profiles suggest the presence of upper-level mesoscale ascent in *both* MCS scale event types. Mesoscale ascent in MCS scale non-linear events may be related more to widespread residual upward momentum associated with extensive embedded convection rather than to convergent horizontal flow features as in MCS scale linear events. Detailed kinematic studies of these MCS scale events are needed to verify this hypothesis. In contrast, heating and vertical motion associated with sub-MCS scale

events was weak and confined to lower levels.

Strong surface winds and associated tropospheric shear characterized the occurrence of sub-MCS scale linear events. All other organizational modes occurred in both strong and weak wind regimes, illustrating that wind speed was not an indicator of the level of convective organization. Although MCS scale linear events were as common during all wind and moisture regimes, non-convective rainfall amounts from that mode were much lower during dry air and weak wind periods as well as during periods of low level easterly winds. These observations suggest that for these events, high mid-level moisture and strong low level shear were important signatures of widespread non-convective rainfall. Furthermore, rainfall from mid-level convective features on the sub-MCS scale was enhanced for weak wind and dry air periods relative to deeper features. The lack of mesoscale system circulations in sub-MCS scale events may cause the characteristics of the cloud population to be more sensitive to these environmental differences.

The diurnal variation of rainfall over the western Pacific Ocean warm pool region has been examined in detail in the context of the categories of scale and morphology. A harmonic analysis of the diurnal "all event" rainfall composite revealed that a weak amplitude (0.37 mm day^{-1}) diurnal variation exists, with a 01LT maximum. The diurnal harmonic explained only one-third of the total variance in the rainfall composite which, while significant, was not dominant. In addition, the semi-diurnal variation was as significant as the diurnal variation.

The diurnal variation of rainfall was distinct between the scale and morphology of convective organization. The weak ninety day weak diurnal rainfall variation resulted

from the superposition of the stronger individual rainfall variations associated with the separate organizational modes, which were out of phase. Moreover, the physical mechanisms behind the diurnal rainfall variation for each mode appeared to be distinct. The evolution of precipitation events did not appear to play a role in the timing of the diurnal rainfall maxima of each mode, since individual events could reach maximum rainfall production at all times of day. Rather, the diurnal rainfall modulation was related to the occurrence of conditions augmenting the intensity of systems at preferred times of day.

The most significant diurnal rainfall variance and the highest amplitude was found with MCS scale non-linear events, with a maximum at 0230LT. Strong nocturnal low level convergence and large areal coverage were associated with these events. These observations were consistent with the Gray-Jacobsen mechanism of the enhancement of rainfall by the circulations induced by nocturnal radiative cooling in the cloud-free regions surrounding a spatially large system. Furthermore, these events lack propagating linear convective features, whose longevity and intensity may be tied closely to the interaction of a propagating gust front with the environmental shear (Rotunno et al. 1988). In the absence of this interaction, nocturnal radiative destabilization may play a dominant role in the modulation of MCS scale non-linear event rainfall. Linear events on both scales showed a weaker diurnal rainfall variation, with maxima in the early evening. The timing of the diurnal maxima in these event types may be related to the intensification of late afternoon convection by the enhanced entropy flux associated with solar heating of the boundary layer. The resulting strong late afternoon downdrafts may

lead to a vorticity balance with the strong low level shear observed in COARE which was more favorable for afternoon squall line maintainance compared to morning squall lines.

Sub-MCS scale non-linear event rainfall displayed significant diurnal and semi-diurnal variations. The diurnal rainfall variation may be linked to a late afternoon enhancement of warm rain processes, since non-convective rain did not undergo diurnal variability. Moreover, the semi-diurnal rainfall maxima coincided in time with pressure minima associated with the semi-diurnal atmospheric tides (04LT and 16LT). The weak surface convergence oscillations implied by the pressure wave (Brier and Simpson 1969) did not appear strong enough to affect convection. However, if there was a link between the pressure wave and semi-diurnal convective intensity, it is reasonable to expect a manifestation in the weaker, isolated convection associated with sub-MCS scale non-linear events.

An important finding of this study was that non-convective rainfall had a considerable fraction (60%) of the variance explained by the diurnal harmonic for the heaviest rainfall producing events (MCS scale non-linear). This implied that the widespread light rain associated with MCS scale non-linear events may be particularly "vulnerable" to nocturnal radiative destabilization of the associated broad cloud tops. This mechanism, if operative, likely acted in parallel with the detrainment of condensate from more vertically developed nocturnal convection (lightning observations of Petersen et al. 1996) to produce the observed variance.

Weak rainfall variability was present on the 4 - 5 day timescale of westward propagating disturbances in the low level wind field. The interpretation of this

variability was linked to the horizontal structure of the waves in the COARE region. Since cyclonic (northern hemisphere) gyres associated with these waves were situated well north of the IFA, the ship radar only sampled rainfall in the southern portion of the equatorial clockwise circulation in between the cyclonic gyres. Therefore, the 4 - 5 day rainfall variation in the IFA was not associated with convergence in the cyclonic gyres. Rather, this variability appeared to be linked to the advection of dry subtropical air by the meridional flow associated with the waves.

The philosophy guiding this study has been to view the complex organization of convection in terms of simple but dynamically significant modes, relating to the bulk heating and moistening (MCS vs. sub-MCS scale) and bulk transport properties (linear vs. non-linear)of convection. The long term goal of this type of study is to help bridge the gap between a meso-α scale characterization of the environment (as in a GCM grid box), and the heating and transport properties of "sub-grid scale" convection. The results presented herein are intimately tied to the spatial and temporal scales of the radar and sounding measurement arrays. Detailed case studies of each organizational mode are needed to confirm inferences made with the larger scale statistical approach used in this study.

REFERENCES

Albright, M. D., D. R. Mock, E. E. Recker, and R. J. Reed, 1981: A diagnostic study of the diurnal rainfall variation in the GATE B-scale area. *J. Atmos. Sci.*, **38**, 1429-1445.

Biggerstaff, M. I. and R. A. Houze, 1991: Kinematic and precipitation structure of the 10-11 June 1985 squall line. *Mon. Wea. Rev.*, **119**, 3034-3065.

Brier, G. W., and J. Simpson, 1968: Tropical cloudiness and rainfall related to pressure and tidal variations. *Quart. J. Roy. Meteor. Soc.*, **95**, 120-147.

Bluestein, H. B. and M. H. Jain, 1985: Formation of mesoscale lines of precipitation: severe squall lines in Oklahoma during the spring. *J. Atmos. Sci.*, **42**, 1711-1732.

Chen, S., and W. R. Cotton, 1988: The sensitivity of a simulated extratropical mesoscale convective system to longwave radiation and ice-phase microphysics. *J. Atmos. Sci.*, **45**, 3897-3910.

Chen, S. S., R. A. Houze, and B. E. Mapes, 1996: Multiscale variability of deep convection in

relation to large-scale circulation in TOGA COARE. *J. Atmos. Sci.*, **53**, 1380-1409.

___, and R. A. Houze, 1996: Diurnal variation and lifecycle of deep convective systems over the tropical Pacific warm pool. *Quart. J. Roy. Meteor. Soc.*, in press.

Cheng, C. and R. A. Houze, 1979: The distribution of convective and mesoscale precipitation in GATE radar echo patterns. *Mon. Wea. Rev.*, **107**, 1370-1381.

Churchill, D. D., and R. A. Houze, Jr., 1984: Development and structure of winter monsoon cloud clusters on 10 December 1978. *J. Atmos. Sci.*, **41**, 933-960.

Cotton W. R., M. Lin, R. L. McAnelly, C. J. Tremback, 1989: A composite model of mesoscale convective complexes. *Mon. Wea. Rev.*, **117**, 765-783.

___, and R. Anthes, 1991: *Cloud and Storm Dynamics*. Academic Press, 883 pp.

Deser, C., 1994: Daily surface wind variations over the equatorial Pacific ocean. *J. Geophys. Res.*, **99**, 23,071-23,078.

Emanuel, K. A., 1987: An air-sea interaction model of intraseasonal oscillations in the tropics. *J. Atmos. Sci.*, **44**, 2324-2340.

___, J. D. Neelin, and C. S. Bretherton, 1994: On large-scale circulations in convecting atmospheres. *Quart. J. Roy. Meteor. Soc.*, **120**, 1111-1143.

Finkelstein, J., 1964: Diurnal variation of rainfall amount on tropical Pacific islands. Proceedings, *Symposium on Tropical Meteorology*, New Zealand Meteorological Service, Wellington, N.Z., 286-294.

Fu, Q., S. K. Krueger, and K. N. Liou, 1995: Interactions of radiation and convection in simulated tropical cloud clusters. *J. Atmos. Sci.*, **45**, 3897-3910.

Gamache, J. F., and R. A. Houze, 1983: Water budget of a mesoscale convective system in the tropics. *J. Atmos. Sci.*, **40**, 1835-1850.

Gill, A. E., 1980: Some simple solutions for heat-induced tropical circulation. *Quart. J. Roy. Meteor. Soc.*, **106**, 447-462.

Gray, W. M., and R. W. Jacobsen, 1977: Diurnal variation of deep cumulus. *Mon. Wea. Rev.*, **105**, 1171-1188.

Greco, S., R. Swap, M. Garstang, S. Ulanski, M. Shipham, R. C. Harriss, R. Talbot, M. O. Andreae, and P. Artaxo, 1990: Rainfall and surface kinematic conditions over central Amazonia during ABLE 2B. *J. Geophys. Res.*, **95**, 17,001-17,014.

Guichard, F., J.-L. Redelsperger, and J.-P. LaFore, 1996: The behaviour of a cloud ensemble in response to external forcings. *Quart. J. Roy. Meteor. Soc.*, **122**, 1043-1073.

Hartmann, D. L., H. H. Hendon, and R. A. Houze, 1984: Some implications of the mesoscale circulations in tropical cloud clusters for large-scale dynamics and climate. *J. Atmos. Sci.*, **41**, 113-121.

Haurwitz, B., and A. D. Cowley, 1973: The diurnal and semidiurnal barometric pressure oscillations: Global distribution and annual variation.*Pure Appl. Geophys.*, **102**, 193-202.

Hayashi, Y., 1970: A theory of large-scale equatorial waves generated by condensation heat and accelerating the zonal wind. *J. Meteorol. Soc. Jap.*, **48**, 140-160.

Hendon, H. H., and B. Liebmann, 1991: The structure and annual variation of antisymmetric fluctuations of tropical convection and their association with Rossby-gravity waves. *J. Atmos. Sci.*, **48**, 2127-2140.

___, and K. Woodberry, 1993: The diurnal cycle of tropical convection. *J. Geophys. Res.*, **98**, 16,623-16,637.

Holle, R., 1968: Some aspects of tropical oceanic cloud populations. *J. Appl. Meteor.*, **7**, 173-

183.

Houze, R. A., 1977: Structure and dynamics of a tropical squall-line system. *Mon. Wea. Rev.*, **105**, 1540-1567.

___, and C. Cheng, 1977: Radar characteristics of tropical convection observed during GATE: mean properties and trends over the summer season. *Mon. Wea. Rev.*, **105**, 964-980.

___, and A. K. Betts, 1981: Convection in GATE. *Rev. Geophys. Sp. Phys.*, **19**, 541-576.

___, R. A., S. G. Geotis, F. D. Marks, and A. K. West, 1981: Winter monsoon convection in the vicinity of north Borneo. Part I: Structure and time variation of the clouds and precipitation. *Mon. Wea. Rev.*, **109**, 1595-1614.

___, 1982: Cloud clusters and large-scale vertical motions in the tropics. *J. Meteorol. Soc. Jap.*, **60**, 396-410.

___, and E. N. Rappaport, 1984: Air motions and precipitation structure of an early summer squall line over the eastern tropical Atlantic. *J. Atmos. Sci.*, **41**, 553-574.

___, 1989: Observed structure of mesoscale convective systems and implications for large scale heating. *Quart. J. Roy. Meteor. Soc.*, **115**, 425-461.

___, B. F. Smull, and P. Dodge, 1990: Mesoscale organization of springtime rainstorms in Oklahoma. *Mon. Wea. Rev.*, **118**, 613-654.

___, 1993: *Cloud Dynamics*. Academic Press, 573 pp.

Itoh, H., and M. Ghil, 1988: The generation mechanism of mixed Rossby-gravity waves in the equatorial troposphere. *J. Atmos. Sci.*, **45**, 585-604.

Janowiak, J. E., P. A. Arkin, and M. Morrissey, 1994: An examination of the diurnal cycle in oceanic tropical rainfall using satellite and in-situ data. *Mon. Wea. Rev.*, **122**, 2296-2311.

Johnson, R. H., 1984: Partitioning tropical heat and moisture budgets into cumulus and mesoscale components: Implications for cumulus parameterization. *Mon. Wea. Rev.*, **112**, 1590-1601.

___, P. E. Ciesielski, and K. A. Hart, 1996: Tropical inversions near the 0°C level. *J. Atmos. Sci.*, **53**, 1838-1855.

Keenan, T. D., J. McBride, G. Holland, N. Davidson, and B. Gunn, 1989: Diurnal variations during the Australian monsoon experiment (AMEX) Phase II. *Mon. Wea. Rev.*, **117**, 2535-2552.

___, T. D., and R. E. Carbone, 1992: A preliminary morphology of precipitation systems in tropical northern Australia. *Quart. J. Roy. Meteor. Soc.*, **118**, 283-326.

Kraus, E. B., 1963: The diurnal precipitation change over the sea. *J. Atmos. Sci.*, **20**, 551-556.

Lau, K. M., L. Peng, C. H. Sui, and T. Nakazawa, 1989: Dynamics of super cloud clusters, westerly wind bursts, 30-60 day oscillations and ENSO: An unified view. *J. Meteorol. Soc. Jap.*, **67**, 205-219.

Leary, C. A., 1984: Precipitation structure of the cloud clusters in a tropical easterly wave. *Mon. Wea. Rev.*, **112**, 313-325.

___, and R. A. Houze, 1979: The structure and evolution of convection in a tropical cloud cluster. *J. Atmos. Sci.*, **36**, 437-457.

LeMone, M. A., 1983: Momentum transport by a line of cumulonimbus. *J. Atmos. Sci.*, **40**, 1815-1834.

___, G. M. Barnes and E. J. Zipser, 1984: Momentum flux by lines of cumulonimbus over the tropical ocean. *J. Atmos. Sci.*, **41**, 1914-1932.

Liebmann, B., and H. H. Hendon, 1990: Synoptic-scale disturbances near the equator. *J. Atmos. Sci.*, **47**, 1463-1479.

Lin, X., and R. H. Johnson, 1996a: Kinematic and thermodynamic characteristics of the flow over the western Pacific warm pool during TOGA COARE. *J. Atmos. Sci.*, **53**, 695-715.

___, and ___, 1996b: Heating, moistening and rainfall analysis over the western Pacific warm pool during TOGA COARE. *J. Atmos. Sci.*, in press.

Loehrer, S. M. and R. H. Johnson, 1995: Surface pressure and precipitation life cycle characteristics of PRE-STORM mesoscale convective systems. *Mon. Wea. Rev.*, **123**, 600-621.

Machado, L. A. Toledo, J-Ph. Duvel, and M. Desbois, 1993: Diurnal variations and modulation by easterly waves of the size distribution of convective cloud clusters over West Africa and the Atlantic Ocean. *Mon. Wea. Rev.*, **121**, 37-49.

Madden, R. A., and P. R Julian, 1994: Observations of the 40-50-day tropical oscillation - a review. *Mon. Wea. Rev.*, **122**, 814-837.

Mak, M. K., 1969: Laterally driven stochastic motions in the tropics. *J. Atmos. Sci.*, **26**, 4-64.

Mapes, B. E., 1993: Gregarious tropical convection. *J. Atmos. Sci.*, **50**, 2026-2037.

___, and R. A. Houze, 1993: Cloud clusters and superclusters over the oceanic warm pool. *Mon. Wea. Rev.*, **121**, 1398-1415.

___, and P. Zuidema, 1996: Radiative-dynamical consequences of dry tongues in the tropical troposphere. *J. Atmos. Sci.*, **53**, 620-638.

Matsuno, T., 1966: Quasi-geostrophic motions in the equatorial area. *J. Meteorol. Soc. Jap.*, **44**, 25-42.

McAnelly R. L., and W. R. Cotton, 1989: The precipitation life cycle of mesoscale convective complexes over the central United States. *Mon. Wea. Rev.*, **117**, 784-807.

McGarry, M. M., and R. J. Reed, 1978: Diurnal variations in convective activity and precipitation during phases II and III of GATE. *Mon. Wea. Rev.*, **106**, 101-113.

Nakazawa, T., 1988: Tropical super clusters within intraseasonal variations over the western Pacific. *J. Meteorol. Soc. Jap.*, **66**, 823-839.

Nitta, T., and Y. Takayabu, 1985: Global analysis of the lower troposphere disturbances in the tropics during the the northern summer of the FGGE year. Part II: Regional characteristics

of the disturbances. *Pure and Appl. Geophysics*, **123**, 272-292.

Numaguti, A., 1995: Characteristics of 4 - 20 day-period disturbances observed in the equatorial Pacific during the TOGA COARE IOP. *J. Meteorol. Soc. Jap.*, **73**, 353-377.

___, R. Oki, K. Nakamura, K. Tsuboki, N. Misawa, T. Asai, Y-M. Kodama, 1995: 4 - 5 day-period variation and low-level dry air observed in the equatorial western Pacific during the TOGA-COARE IOP. *J. Meteorol. Soc. Jap.*, **73**, 267-290.

Orlanski, I., 1975: A rational subdivision of scales for atmospheric processes. *Bull. Amer. Meteor. Soc.*, **56**, 527-530.

Panofsky, H. A., and G. W. Brier, 1968: *Some applications of statistics to meteorology*. The Pennsylvania State University, University Park, PA.

Patterson, V. L., M. D. Hudlow, P. J. Pytlowany, F. P. Richards, and J. D. Hoff, 1979: GATE radar rainfall processing system. NOAA Technical Memorandum EDIS 26, Washington, D.C.

Peixoto, J. P., and A. H. Oort, 1992: *Physics of climate*. American Institute of Physics, 520 pp.

Petersen, W. A., S. A. Rutledge, and R. E. Orville, 1996: Cloud-to-ground lightning

observations from TOGA COARE: Selected results and lightning location algorithms. *Mon. Wea. Rev.*, **124**, 602-620.

Randall, D. A., Harshvardhan, and D. A. Dazlich, 1991: Diurnal variability of the hydrologic cycle in a general circulation model. *J. Atmos. Sci.*, **48**, 40-62.

Reed, R. J., and E. E. Recker, 1971: Structure and properties of synoptic-scale wave disturbances in the equatorial western Pacific. *J. Atmos. Sci.*, **28**, 1117-1133.

Riehl, H. and J. S. Malkus, 1958: On the heat balance in the equatorial trough zone. *Geophysica*, **6**, 503-538.

Rosenfeld, D., E. Amitai, and D. B. Wolff, 1995: Classification of rain regimes by the three-dimensional properties of reflectivity fields. *J. Appl. Meteor.*, **34**, 198-211.

Rotunno, R., J. B. Klemp, and M. L. Weismann, 1988: A theory for strong, long-lived squall lines. *J. Atmos. Sci.*, **45**, 463-484.

Rutledge, S. A. and R. A. Houze, 1987: A diagnostic modeling study of the trailing stratiform region of a midlatitude squall line. *J. Atmos. Sci.*, **44**, 2640-2656.

___, R. A. Houze, M. I. Biggerstaff, and T. Matejka, 1988: The Oklahoma-Kansas Mesoscale

Convective System of 10-11 June 1985: Precipitation structure and single-Doppler radar analysis. *Mon. Wea. Rev.*, **116**, 1409-1430.

___, R. Cifelli, C. DeMott, W. Petersen, T. Rickenbach, J. Lutz, R. Bowie, M. Strong, E. Williams, 1993: The shipboard deployment of the MIT C-band radar during TOGA COARE. Preprints, *26th International Conference on Radar Meteorology*, Norman, OK, Amer. Meteor. Soc., 371-373.

Schmidt, J. M. and W. R. Cotton, 1989: A high plains squall line associated with severe surface winds. *J. Atmos. Sci.*, **46**, 281-301.

Short, D. A., P. A. Kucera, and O. W. Theile, 1995: Patterns of rainfall from shipborne radar data for the COARE intensive observing period. Preprints, *21st Conference on Hurricanes and Tropical Meteorology*, Miami, FL, Amer. Meteor. Soc., 273-276.

Simpson, J., T. D. Keenan, B. Ferrier, R. H. Simpson, and G. J. Holland, 1993: Cumulus mergers in the maritime continent region. *Meteorol. Atmos. Phys.*, **51**, 73-99.

Smull, B. F., and R. A. Houze, 1987: Rear inflow in squall lines with trailing-stratiform precipitation. *Mon. Wea. Rev.*, **115**, 2869-2889.

Steiner, M., and R. A. Houze, 1993: Three-dimensional validation at TRMM ground truth sites:

Some early results from Darwin, Australia. Preprints, *26th International Conference on Radar Meteorology*, Norman, OK., Amer. Meteor. Soc., 417-420.

___, R. A. Houze and S. E. Yuter, 1995: Climatological characteristics of three-dimensional storm structure from operational radar and raingauge data. *J. Appl. Meteor.*, **34**, 1978-2007.

Takayabu, Y. N., and T. Nitta, 1993: 3 - 5 day-period disturbances coupled with convection over the tropical Pacific ocean. *J. Meteorol. Soc. Jap.*, **71**, 221-246.

___, K.-M. Lau, and C.-H. Sui, 1996: Observation of a quasi-2-day wave during TOGA COARE. *Mon. Wea. Rev.*, **124**, 1892-1913.

Tokay, A. and D. A. Short, 1996: Evidence from tropical raindrop spectra of the origin of rain from stratiform versus convective clouds. *J. Appl. Meteor.*, **35**, 355-371.

Velden, C. S., and J. A. Young, 1994: Satellite observations during TOGA COARE: Large-scale descriptive overview. *Mon. Wea. Rev.*, **122**, 2426-2441.

Waldvogel, A., 1974: The N_o jump of raindrop spectra. *J. Atmos. Sci.*, **31**, 1068-1078.

Webster, P. J. and R. Lukas, 1992: TOGA COARE: The coupled ocean-atmosphere response experiment. *Bull. Amer. Meteor. Soc.*, **73**, 1377-1416.

Wielicki, B. A. and R. M. Welch, 1986: Cumulus cloud properties derived using Lansat satellite data. *J. Clim. and Appl. Meteor.*, **25**, 261-276.

Willis, P., R. A. Black, F. D. Marks, and D. Baumgardner, 1995. Airborne rain drop size distributions in TOGA COARE. Preprints, *21st Conference on Hurricanes and Tropical Meteorology*, Miami, FL, Amer. Meteor. Soc., 431-433.

Xu, K., and D. A. Randall, 1995: Impact on interactive radiative transfer on the macroscopic behavior of cumulus ensembles. Part II: Mechanisms for cloud-radiative interactions. *J. Atmos. Sci.*, **52**, 800-817.

Yanai, M., T. Maruyama, T. Nitta, and Y. Hayashi, 1968: Power spectra of large-scale disturbances over the tropical Pacific. *J. Meteorol. Soc. Jap.*, **46**, 308-323.

___, S. Esbensen, and J.-H. Chu., 1973: Determination of bulk properties of tropical cloud clusters from large-scale heat and moisture budgets. *J. Atmos. Sci.*, **30**, 611-627.

Yoneyama, K., and T. Fujitani, 1995: The behavior of dry westerly air associated with convection observed during the TOGA-COARE R/V Natsushima cruise. *J. Meteorol. Soc. Jap.*, **73**, 291-304.

Zipser, E. J., 1977: Mesoscale and convective-scale downdrafts as distinct components of squall-line circulation. *Mon. Wea. Rev.*, **105**, 1568-1589.

___, R. J. Meitin and M. A. LeMone, 1981. Mesoscale motion fields associated with a slowly moving GATE convective band. *J. Atmos. Sci.*, **38**, 1725-1750.

APPENDIX A

MODIFICATION TO CONVECTIVE - NON-CONVECTIVE PARTITIONING ALGORITHM

Steiner et al. (1995) discuss the need to "tune" the peakedness criterion in their convective - non-convective partitioning technique for a particular geographic region and radar. The tuning involves modulating the threshold value which the point in question must exceed the background reflectivity area by to be considered convective with the value of the background area (the "tuning curve", Fig. 7 of Steiner et al. 1995). However, details of the tuning procedure are not discussed (ibid.) and appear to be somewhat subjective. In order to minimize the subjectivity inherent in the technique, the effect of the tuning on the ninety day rainfall, convective fractions, and rainfall distribution by height were examined. A comparison was made of these parameters using the tuning curve for Darwin (ibid.) versus using a constant threshold value (4.5 db; Steiner and Houze 1993). The difference in both the mean rainfall rate and the convective rain fraction is about 3-4% lower for the constant threshold case (Table A1). This difference is smaller than errors introduced by subjective (visual inspection) determination of the algorithm's performance. Such a subjective analysis would be

Table A1. Comparison of ninety day mean rainfall rate (mm day^{-1}) and convective rain fraction for two assumptions of the peakedness criterion for convective reflectivity identification (Steiner et al. 1995, their Fig. 7).

	Constant Threshold ("control")	**Variable Threshold ("tuned")**
Rainrate (mm/day)	4.5	4.4
Convective rain fraction (%)	69	66

required to tune the algorithm. Moreover, the TOGA C-band radar used in Darwin has nearly identical specifications as the MIT radar. Therefore, the tuning procedure was not performed for the present study.